Guidelines for small scale biochar production system to optimise carbon sequestration outcome

A thesis presented in partial fulfilment of the requirements for the degree of

Master of Engineering

In

Bioprocessing Engineering

At Massey University, Palmerston North

New Zealand

Arthur Cortez Pires de Campos

2019

Abstract

Biochar is made in a 60 kg batch pyrolysis reactor developed by Massey University in both prior work and during this project. This thesis details the design and control features necessary to produce biochar (charcoal) at temperatures ranging from 400-700°C. It also examines the emissions abatement necessary to achieve the best possible carbon footprint by combusting the gases to avoid release to the atmosphere. The feedstock for this work was *Pinus radiata* without bark.

The biochar reactor is a vertical drum mounted on top of a combustion chamber containing two forced draft LPG burners. The combustion gases pass through an outer annular drum and so heat the biomass through the external wall. Evolving pyrolysis gases then move toward a central perforated core inside the drum, then descend into the combustion chamber where they are partially combusted. The range of highest treatment temperatures (400-700°C) was extended by controlling the partial combustion by varying a secondary air supply into the combustion chamber (previously only 700°C was achievable).

Effective emissions abatement requires complete combustion. This work reveals that the flammability of the pyrolysis gases is not high enough to self-combust and so does not remove soot and other products of incomplete combustion, such as CO and CH4. Therefore, supplementary fuel is always needed. Here, this was achieved using modulated LPG burners at the flare. This system has the problem of batch pyrolysis reactors, where the release of volatiles from the reactor is uncontrolled, making the design of a variable rate flare system a non-trivial matter. Modifications made to the reactor design in this project include insulating the flare chimney, extending it to provide sufficient residence time, and installing adjustable vents to ensure sufficient air entrainment for complete combustion. This achieved emissions of CO and CxHy (hydrocarbon, mostly CH4) of 32 and 51 ppm respectively, which were well within the US EPA limits for both suspension and fluidised bed biomass burners(2.400 and 240 ppm respectively).

The net environmental impact was determined for char made at 700°C, through carbon footprint analysis. An efficient system is needed to achieve a net sequestration

benefit. Here, even with emissions abatement and the above mentioned very low CO and CxHy emissions, no net benefit was achieved. With the flare working, the net fractional sequestration was -0,14 (kg C sequestered)/(kg C in biomass). Then, when the flare is turned OFF, the net fractional sequestration was -1,240[1] (kg C sequestered)/(kg C in biomass). Therefore, another frame of reference for well-operated systems is that the permissible emission should be less than 0.001 (kg C emitted as CO)/(kg C biomass), without considering methane or other GHGs.

[1] The thesis uses European number nomenclature. 1,1 is one point one, and 1.100 is one thousand one hundred.

Acknowledgements

First of all, I would like to express my deep gratitude to the New Zealand government, which, through the NZAid Development Scholarship, has selected me for the opportunity to carry out this international master's project. Special thanks to Jamie Hooper and Logan Tate, NZAid officials, who supported me all the time during my academic journey in New Zealand.

I would like to give a special thanks to Professor Jim Jones, who believed in my potential to deliver a high-level project and supervised me throughout this work with great engagement, dedication, affection, patience and helpful criticism. Also, I have an immense gratitude for having given me the opportunity to internationalize my career, presenting this project at ANZBC2018 (Australian New Zealand Biochar Conference).

I would like to thank my secondary supervisors, Dr. Georg Ripberger and Dr. Jim Q. Chen, and also to Nadeem Caco, who were always available to help me throughout this project, even when long-period assistance was needed for running the experiments. Furthermore, thanks to the technical team in Massey University, who have supported me with all practical engineering issues, mainly related to software configuration and fixing the pyrolyser and its apparatus.

Last but not least, long distance support from my family and girl-friend was extremely important to successfully pursued this project.

This work has been very beneficial to my personal and professional growth, which allowed me to put together theory and practice. I have been constantly encouraged to deal with interdisciplinary topics, improving my knowledge in different areas of expertise, with emphasis to applied engineering technologies.

"Now that we are aware of the effects of pollution on the environment it is important to mitigate these effects and produce biochar in a way that is sustainable and renewable (Blackwell, et al., 2009).

Table of Contents

List of figures

List of tables

Chapter 1 – Introduction

Since the mid-20th century, the world has been facing a wide range of undesirable disturbances in the environment caused mainly by the increase of global warming, which is aggravated by the uncontrollable greenhouses gases (GHG) emission into the atmosphere (IPCC, 2014). The stricter emission targets set up by the Paris Agreement, in 2015, created worldwide an urgent need for more investment in advanced technologies, which provides for greater sustainable development. Bioenergy´s negative emission technologies (NETs), such as biochar, which is the focus of this research, play a key role for climate change mitigation in the future, because they offer the potential of long-term carbon sequestration (Borba et al., 2012; Creutzig et al., 2015; Fuss et al., 2016; Krey et al., 2013; Smith, P., 2016; Suzuki et al., 2016).

The impact on the climate by biochar production mainly comes from emissions of products of incomplete combustion (PICs). Carbon monoxide (CO), methane (CH4), other hydrocarbons and particulate, which compose the principals PICs, have a global warming potential significantly higher than CO2 on a molecular basis. Hence, a process that is seemingly sequestering carbon having a negative C footprint can easily turn into a net positive C footprint if not precisely controlled. This problem is particularly true for small-scale production facilities, which are often mooted in the literature as offering communities a method of local production of biochar for amendment to soils. Large-stationary units have more capability to measure and control emissions due to the possibility of applying scrubbers and electrostatic precipitators, for example. When pyrolysis is undertaken on a small-scale unit, PIC emissions need to be mitigated by the complete combustion of the off-gases (Camps, et al., 2016).

Pyrolysis is the combustion of woody biomass in absence of oxygen at temperatures around 400 – 700°C. Gases are driven off with the final product being biochar (or charcoal). The gases can be utilised for energy application and the biochar, with a high carbon content, can be incorporated into soils with the potential to increase crop productivity.

The CO2 is taken from the atmosphere during the growth of the biomass fuel and the fixed carbon in the biochar is locked up in the soil to give a negative carbon footprint.

In summary, polluting charcoal making systems can have a high net global warming potential. To eliminate this, the off-gases must be properly combusted. It is the objective of this research to determine how well this can be achieved in small-scale biochar production. The Massey 60 kg reactor was modified and used as a model system to analyze this problem. A methodology has been developed to account for emissions and, by using the net global warming potential of all emissions, to determine the net sequestration carbon footprint of biochar manufacture.

Chapter 2 - Literature Review

This chapter contextualizes the project by discussing the global need for sequestration to mitigate climate change, then focuses on biochar as a mechanism for achieving this. It then discusses the role of biochar in sequestration and its use in soils, before going on to discuss its production. The review then discusses the various factors that influence the yield and quality of biochar production, and the kinetics of pyrolysis, which is the mechanism by which biomass decomposes in the absence of oxygen. Pyrolysis occurs in a pilot-scale systems, and so the effects of mass and heat transfer are then discussed and how they affect the pyrolysis outcomes. The review concludes with a discussion on emissions abatement.

2.1. Climate change global policy scene and the NETs role

The United Nations Framework Convention on Climate Change (UNFCCC) is an international organization initially composed by 175 different countries responsible for the majority of global GHG emissions, aims to debate and develop international policies for tackling the climate change issues. However, there are several challenges related to the complexity of building a globally reliable strategy for mitigating the consequences of climate change (Creutzig et al., 2015; Key et al., 2013; Suzuki et al., 2016).

Since the Kyoto Protocol, which was internationally agreed in 2005, wide efforts by governments have been undertaken through negotiated agreements via the annual Conferences of the Parties (COP) (Borba et al., 2012). In 2015, due to the failure to meet the goals agreed in the Kyoto Protocol, the 21st COP assigned international emissions targets, known as the “Paris Agreement”. This accordance limits the increase of global temperature well below 2°C in 2100 and requires pursuing efforts to keep it above 1.5°C (Fuss et al., 2016; Suzuki et al., 2016), which means that the concentration of CO2eq (carbon dioxide equivalent is a measure used to compare the emissions from various greenhouse gases based upon their global warming potential) in the atmosphere must not be higher than 550 ppmv

(parts per million volume) (Creutzig et al., 2015). Therefore, a lot of research has been commissioned to simulate the best scenario of policies and investments that should be undertaken by governments to guarantee the reaching of the targets set by the country members.

According to Krey et al. (2013), Integrated Assessment Models (IAMs) have been used to build up climate change mitigation scenarios. Suzuki (2015) and Borba et al. (2012) concluded that the energy system plays a fundamental role in this context and global efforts must be improved to reduce fossil fuel demand, support the sustainable economic development and provide energy security. Krey et al. (2013) explore the feasibility of innovation energy technology toward climate steadiness, based on the analyses of the cost-benefits of energy sector transformation, considering the application of low-carbon sources and efficient use of energy.

Creutzig et al. (2015) and Krey et al. (2013) assume a significant importance for bioenergy in all IAM scenarios to achieve the global CO2eq stricter emissions targets. Results rely on bioenergy intensification and modernization, with models projecting 35% of total energy production from bioenergy in 2050, and more than 50% in 2100. Low-carbon energy sources, such as nuclear, wind and solar, have less impact on the mitigation cost when compared with bioenergy. Nevertheless, negative emission technologies (NETs) appear in the majority of <2°C scenarios as a determinant option for successful achievement (Creutzig et al., 2015). Hence, bioenergy and NETs, such as biochar and BECCS (Bioenergy with Carbon Capture and Storage), for example, have significant importance for climate change mitigation future scenarios due to their potential for long-term carbon sequestration (Borba et al., 2012; Creutzig et al., 2015; Fuss et al., 2016; Krey et al., 2013; Smith et al., 2015; Suzuki, 2015; Suzuki et al., 2016).

2.2. Biochar and the climate change

The two issues that link biochar to climate change are its production and its use. For production, current charcoal technologies are not efficient, highlighted by the contrast between actual experimental and expected theoretical yields (Antal et al., 1990). The low efficiency of traditional kilns for biochar production ranges from 8-

36%, exacerbating deforestation in tropical countries which contributes to global warming (Pennise et al., 2001). Hence, many environmentalists think that charcoal manufacture should be banished (Van der Plas, 1995). The low efficiency of conventional kilns can be explained by the quick escape of tarry vapors from the heated zone without reaching equilibrium and thus not helping to form charcoal. The emissions are produced at temperatures ranging from 250 to 400 °C and, in addition to the tars, contain non-condensable gases, such as CO2, CO, H2, CH4 and other hydrocarbons. When operating efficiently, the tars crack to condense more char, increase yield, and produce more non-condensable gases. Considering that the cost of the wood feedstock is around 50% of the total charcoal production cost, there is a high interest to improve the process efficiency and convert the tarry vapors into charcoal (Antal, 1996). Hence, a high carbonization efficiency decreases the quantity of feedstock needed and the release of these tarry vapors into the atmosphere (FAO, 1985).

The use of biochar is amendment to soil where, due to its high stable form of carbon, it can have a C-residence time in soils of hundreds to thousands of years. This is compared to crop waste which decays within decades (Lehmann et al., 2006). Hence, the manufacture of biochar and its incorporation into soils has potential to reduce the CO2 to be emitted back to the atmosphere. According to Roberts et al., 2010, if the biochar applied into the soil does not increase the emission of other greenhouse gases, and if the GHG emissions from the transport and production of the biochar and biomass don´t offset the C already sequestered, then the overall carbon balance will be positive, providing a real abatement effect. The carbon retention in biochar (ratio of the C sequestered in the biochar over the C in the original dry biomass feedstock) depends critically on the initial characteristics of the feedstock and the different factors of thermal-degradation (pyrolysis) process (Lehmann & Joseph, 2009). Woolf et al., 2010, state that up to 49% of C retention has been acknowledged in the literature, suggesting that higher carbon retention ratio lead to less stable biochar, ranging from 4-29 years its residence time in soils. So far, some research on biochar field trials, despite the majority being short-term experiments, reveal interesting results, suggesting that biochar can also reduce N2O

and CH4 emissions from soils. However, it is well known that further studies are needed to understand with more detail the interaction between biochar and the different types of soils, and its truly potential of reducing emissions, enhance fertility and stock carbon (Arkinson et al., 2010). A recent meta-analysis of field trials indicates that biochar boosts tropical but not temperate climate crop yields (Jeffery et al.,2017).

2.3. Biochar characteristics and uses

Biochar is a bio-product originating from sustainably produced biomass that has been converted into charcoal through the process of pyrolysis, which degrades the biomass thermally in the absence of oxygen. Due to its mild exothermicity, this process co-produces of bioenergy and biochar. The bioenergy has a great potential for reducing emission due to the generation of energy from a renewable source and the biochar offers long-term sequestration of carbon when tilled into the soil (Field, 2013; Smith, 2016). Biochar also has uses as a source of carbon in industrial processes where it is generally described as charcoal, such as steel and iron production, as well as widely used for power generation.

Conventionally, biochar or charcoal is produced by burning wood biomass in pits or brick kilns, which has significant impact on the environment due to its inefficient conversion in the carbonization process. Furthermore, these kilns have little or no GHG emission control. Current increasing awareness of climate change consequences has highlighted the need for more sustainable and environmental friendly technologies of charcoal production. Therefore, to emphasize this aspect, the IBI (International Biochar Initiative, 2012) have specified that to meet the requirements for biochar qualification, the feedstock must not only come from sustainable source (e.g. agricultural waste), but the production process must also minimize undesirable emissions, and it needs to reach some quality standard. These quality standards have been determined by the IBI (International Biochar Initiative) and EBC (European Biochar Certificate), which principally consider the characteristics of biochar stability in the soil. Because of its porosity, biochar has the capability of retain water, nutrients and pollutants. Therefore, biochar can be used for soil remediation, protecting water cycling,

increasing crop growth, saving fertilizer, carbon sequestration and clean energy generation (Lehmann and Joseph, 2009).

2.4. Biochar and soils

The Earth´s soils store almost four times more organic C than the atmosphere, and the total atmospheric CO2 is cycled through the biosphere every 14 years (Lehmann & Joseph, 2009). However, using biomass to produce biochar can impact the ecosystem services that this biomass develops. Concerns about ecosystem services has led to the development of scenarios which analyze the conflicts of food versus biochar and energy production, when considering a vast adoption of biochar and bioenergy production (Müller et al, 2008). Moreover, Lehmann and Joseph (2009) also highlight the importance of maintain "the minimum residue cover required to protect soils surfaces" when considering biochar production from crop residues; this is important to avoid the increase of water and wind erosion, as well as to keep the minimum of soil organic matter required for plant growth in no-till farming.

The "Terra Preta" (TP) soils in the Amazon Basin were formed by the application of charcoal into soils during the Pre-Columbian era. They suggest that the permanency of biochar varies from hundreds to thousands of years. However, as TP soils formed over hundreds of years under unknown conditions, this raises questions about the success of modern biochar application (Lehmann, 2007).

According to Blackwell et al., 2009, biochar applied into soils can likely alter its physical characteristics, such as the structure, porosity and density, and thus providing a higher water retention capacity, cation exchange capacity (CEC) and decrease soil acidity. If so, a better environment for plant growth is provided, enabling the development of deeper and stronger root structures, as well as the increase of microbiological activity (Lenmann & Rondon, 2006).

However, the broad variety of soils and different biochar properties produce a wide range of complex interactions which make it harder to define the outcome, especially so because most studies by necessity use short-time analyses. Different

results can be found in the literature, showing that biochar can affect positively or negatively on crop productivity, varying from -28% to +39%, depending mainly on the biochar production methods, feed stocks and soil nature (Jeffery et al., 2011).

Nevertheless, the evidence from TP soils, which is naturally an extensive leached soil akin to those found in deserts, confirm that adding carbon directly influences the soil quality and provides a fertile environment capable of sustaining for thousands of years the millenary agriculture of indigenous population in the Brazilian Amazon region (Glaser et al, 2001).

As shown by Rondon et al., 2007, biochar intensifies the microbiological activity in soils and consequently increases the N2 fixation by bacteria. Considering that nitrogen (N) is a limiting element of crop production, it is possible to associate the higher crop productivity in some studies of biochar application in soils with the increase of N fixation by microorganisms, providing more nitrogen for plant growth. The increase in N fixation and consequent improvement in crop growth and microbiological activity from biochar in soils can be linked to further decreases in NO2 emission. In contrast, some studies suggest that it can also controversially increase CO2 emission, due to the higher metabolic activity from the increased quantity of microorganism in the soil.

Jeffery et al., 2016, suggest that biochar has also the potential of mitigate methane (CH4) emission from soils, especially when applied into flooded fields or acid soils, where the crop management requires periods of flooding, such as rice. On the other hand, they also argue that a decrease in CH4 sink has been observed when biochar is applied in normal or neutral soils without periods of flooding. An experiment in Finland conducted by Karhu et al. (2011), which analyzed the fluxes of CH4, CO2 and NO2 emission from biochar application of 9 t/ha in a clover–wheat–bean–oat agricultural rotation system over a silt soil, showed that the addition of biochar provided 96% increase in CH4 uptake, while no significant influence was detected in the NO2 and CO2 emission.

According to Dari et al. (2016), phosphorous (P) sorption and release from soils is not significantly influenced by hardwood or poultry litter biochar application in two different types of soils. Hence, this study suggests that the safely amount of P that can be applied in soils with biochar depends more on the original soils characteristics of P

retention than the biochar potential of enhancing such sorption. The manufacture of biochar from phosphorus-rich sources, e.g., biosolids, does not affect P bio-availability (Wang et al.,, 2014.)

2.5. Biochar production via pyrolysis

Biochar is the carbonized product of biomass pyrolysis, which is the thermal degradation of the organic material in the absence of oxygen. The process temperature usually ranges from 200°C up to 700°C. Degradation of the organic material results in the cleavage and rearrangement of the carbon bonds. Carbon-containing gas and tar are produced alongside the biochar. The gas can be combusted for producing energy or flared to avoid direct emission into the atmosphere of the more harmful PICs of carbon monoxide, methane and particulate. Doing this ensures a positive environmental impact of the process.

Figure 2.1: Biomass pyrolysis products (A Brownsort, P., 2009. UKBRC Working Paper 5)

The process of pyrolysis of biomass is mainly undertaken in different types of kilns (traditional method) or reactors (modern method), which allow the heat to be transferred through the biomass efficiently. For starting the process, an external heat source is required to elevate the temperature to around 280°C, where the primary reactions usually start. During this heating phase, all free moisture in the biomass is evaporated. Once primary reactions begin, gas, volatiles and char are produced. According to Neves et al., 2011, secondary reactions occur in higher temperatures. For that, the volatiles from the primary reactions interact with the

char already produced, forming secondary char and further gas, which is also known as syngas (Antal Jr. & Grønli, 2003). Primary reactions are endothermic, requiring heat input to drive them, whereas secondary reactions are mildly exothermic. While the existence of secondary reactions is well-known, the mechanisms are only partially understood.

During pyrolysis, mainly O (oxygen), H (hydrogen) and N (nitrogen) are driven off into the volatile phase in different ways. Depending on the highest treatment temperature (HTT), the biomass structure reorganizes, from long-chain molecules rearrange to form ring structures of 6 carbon atoms, which are more stable and consequently more resistant to decomposition (Demirbas & Arin, 2002).

Demirbas and Arin (2002) have divided the pyrolysis process into 4 different zones, which make it simple to analyze. Zone A occurs up to the temperature of 200°C, and zone B between temperatures of 200 – 260°C. Both zones A and B are endothermic, and at this point the biomass is becoming charred and any volatile products are basically non-condensable. Zone C is where the pyrolysis essentially starts. Between the temperatures of 260-500°C, this zone is responsible for the exothermic reactions, with a rapid temperature rise. The formation of combustible gases, such as carbon monoxide, take place from the cleaving of acetic and formic acid, and the carbonyl group. Methane, formaldehyde, methanol and hydrogen, are all produced. Above 500°C, secondary reactions begin to occur, classified as zone D. It results in the formation of a “layer of charcoal”, and the pyrolysis process should be completely finalized at 600°C.

Pyrolysis is also classified into three different categories: slow (conventional) pyrolysis, fast pyrolysis and flash pyrolysis. The difference between them are mostly related to temperature range, heating rate and residence times. The focus of this work is slow pyrolysis.

Slow pyrolysis is characterized by a slow heating rate, generating a significant amount of solid (biochar), liquid (tar) and gases (syngas). The process can be divided in two main stages. The first one, known as “pre-pyrolysis”, which occur between 120 and 200°C, is responsible for the first internal rearrangement, taking place from water evaporation, bond breakage, emergence of free radicals, and formation of carboxyl

and carbonyl groups. Extractives are also removed in this stage. The second stage is defined as the most important phase, because it is where the creation of the pyrolysis product occurs. The char is formed at rates as slow as 0,1 – 1 °C/s and carbon-rich products are produced (Demirbas & Arin, 2002).

Fast pyrolysis is recommended to produce mainly liquid and/or gaseous products. Dry biomass can yield 75% liquid, 12% char and 13% gas (Bridgwater, 2003). The char yield from this method does not exceed 17 wt% (Demirbas & Arin, 2002). It is well known that due to the heat transfer limitations of fast pyrolysis, it is highly important to use small particles of biomass. The heating rate can range from 10-200 °C/s (Mohan, et al., 2006). Therefore, this method is widely used in renewable energy since bio-oil is produced in a greater quantity. Bio-oil is a liquid fuel with a high calorific value and less sulphur and aromatic elements than conventional fuels (Bridges, 2014) and is suitable for burning in boilers, although not in engines due to its oxygen content.

2.5.1. Wood pyrolysis

So far, wood is the most common feedstock for biochar production. However, the quantity of cellulose, hemicellulose, lignin, organic and inorganic material varies considerably among different types of wood. A schematic for the decomposition products is shown in Figure 2.2.

The first components to be degraded in wood pyrolysis are the hemicelluloses through “torrefaction”, which occurs between temperatures from 200-280°C (Antal Jr. & Mok, 1990). According to Mohan et al., 2006, the hemicellulose is a branched polymer with small chains and amorphous structure, comprising around 30% of the biomass and is the most reactive component of the wood.

Cellulose is the principal component of the wood fibers, comprising up to 50% of the wood structure. It is characterized by long polymers chains associated through sequences of networks, situated in the cell walls which provides the plant strength. Its degradation occurs at temperatures ranging from 240-350°C (Bridges, 2014).

Lignin is more difficult to decompose compared to hemicellulose and cellulose, requiring a broad range of temperatures from 280-500°C. Its structure is a branched element which generates phenols during decomposition (Mohan, et al., 2006). Lignin represents between 16-33% of the wood mass. Antal Jr. et al. (1996) state that high yields charcoal is likely to be generated by high lignin wood content. Lignin has three times more methoxyl than wood, and the cleavage of the aromatic C:O bond and the methyl C:O bond lead to the production of compounds one and two oxygen atoms, respectively, at 325-375°C. At the end of pyrolysis, a small amount of inorganic minerals and organic elements remain, which represent the ash content of the wood.

Figure 2.2: Thermal degradation of hemicellulose, cellulose and lignin (Brownsort, 2009)

The biochar production process directly affects its product properties. Influencing factors are the heating rate, highest treatment temperature (HTT) reached, soak time at the HTT, and feedstock and vapour residence time (Antal Jr & Grønli, 2003; Lehmann & Joseph, 2009). Therefore, it is highly important to determine how these relate to biochar properties in a modern biochar production system. Together they assure consistent quality of biochar produced and minimize the environmental impacts.

2.5.2. Principal factors which affect pyrolysis

Because production of biochar is the objective here, the pyrolysis process must be designed and tuned to achieve this outcome. Thus, as discussed above, slow pyrolysis is the preferred method. The following sub-sections describe the many factors that affect the process and influence the yield.

2.5.2.1. Moisture

It is widely described in the literature that using biomass with high moisture content in the process results in an inferior final energy balance. This is because more heat is required for drying the biomass using auxiliary fuel, either more biomass or fossil fuel. Also, the drying process means the pyrolysis reaction takes more time to initiate. At high temperatures, water vapour has an important role in the process of producing biochar, facilitated by water released as a product of the decomposition. However, complete drying of the biomass is expensive. Therefore, Mok et al. (1992) recommend that biomass should has around 10% moisture content.

2.5.2.2. Temperature

Temperature is considered the principal coefficient which influences the characteristic of the final product obtained from pyrolysis. As shown previously, the optimum temperature range for producing biochar is ~300-600°C. Temperature affects significantly the carbon content, aromaticity and cation exchange capacity (CEC) of the biochar.

Figure 2.3: Changes of aromaticity of biomass in pyrolysis (Cimò, 2014).

Baldock and Smernik (2002) have stated that increasing the temperature of pyrolysis results in a higher aromaticity of biochar, indicated schematically in Figure 2.3. Brewer, Unger, Schmidt-Rohr, and Brown (2011) supported this statement by NMR analyses, showing that the changes in the solid structure are responsible for increasing aromaticity, which also makes the biochar more stable in soils (Lehmann et al., 2009).

Figure 2.4 highlights the influence of temperature on some of the principal elements of wood pyrolysis. Higher peak temperature results in greater carbon content in the charcoal, but also means a higher loss of carbon, oxygen, hydrogen and water, resulting in a smaller charcoal yield.

Figure 2.4: The effects of temperature on charcoal properties (Antal & Grønli, 2003).

2.5.2.3. Pressure

Increasing pressure provides a higher biochar yield. The reason is the greater interaction between the char and the primary vapours generated from the increased pressure, enhancing secondary reactions (Antal et al., 1996; Antal & Grønli, 2003; Mok, et al., 1992). Moreover, Mok et al. (1983) shows that higher flow rates through a bed of biomass undergoing pyrolysis, which reduces the residence time, results in a higher overall heat of reaction. The heat of reaction is positive for the primary endothermic reactions and negative for the secondary exothermic reactions. Thus, the overall heat of reactions is a reflection of the degree to which secondary reactions occur. This is because less secondary reactions occur, resulting in more formation of volatiles and tar. In contrast, lower gas flow combined with pressurizing the vessel to increase the residence time of volatiles, enhances the secondary reactions, consequently producing char with higher yields (Antal et al., 2003).

2.5.2.4. Heating rate and residence time

As reported previously, depending on the type of pyrolysis, different heating rates and residence times of the vapor phase are employed. In general, slow pyrolysis has heating rate <1°C/s and residence time of gases in the range of minutes (typically 2-30 min), while fast pyrolysis involves heating rates higher than 10°C/s and residence time of seconds (normally 1-5 s).

As the machine used in this project is a slow pyrolysis reactor (Bridges et al., 2013), slower rates are adopted, aimed at producing greater amounts of biochar. Residence time is somewhat a function of the system design, which here ensures that mass and heat transfer occur in the same direction. Thus, the condensable fractions essentially go through cycles of volatilisation, condensation and re-volatilisation, which means that they have a long residence time in the reactor, and when re-volatilised can undergo secondary reactions to increase the amount of biochar produced.

2.5.2.5. Particle size

Particle size also has an important influence in the yield, as the mass and heat transfer dynamics are determined by the internal resistance within particles. Mass and heat transfer are in opposite directions in particles; heat must get in to overcome the activation energy necessary for reaction and mass transfer of volatiles is out. The outflowing volatiles then inhibit heat transfer in, which means large particles (bigger than 2,5 cm^3) take some time to pyrolyse. However, larger particles also facilitate more secondary reactions. Thus, more char formation is achieved with larger particle sizes (Ripberger et al., in preparation). The heat transfer within particles is discussed further in Section 2.10.

2.6. Charcoal yields

In summary, to produce a high charcoal yield, it is necessary to have a slow heating rate in order to decrease the vapour formation rate in order to increase its residence time in the reaction zone. This enhances the contact between the char and the volatiles, increasing the secondary reactions and maximizing the char formation. As can be seen in Figure 2.5, doing this results in higher char yields.

Table 2.1: Type of pyrolysis and yields (Brownsort, 2009).

		Slow Pyrolysis	Intermediate Pyrolysis	Fast Pyrolysis
Feed		Scores of feeds reported		
Temperature, °C	Range	250 - 750	320 - 500	400 - 750
	Typical	350 - 400	350 - 450	450 - 550
Time	Range	mins - days	1 - 15 mins	ms - s
	Typical	2 - 30 mins	4 mins	1 - 5 s
Yields, % wt on dry				
Char	Range	2 - 60	19 - 73	0 - 50
	Typical	25 - 35	30 - 40	10 - 25
Liquid	Range	0 - 60	18 - 60	10 - 80
	Typical	20 - 50	35 - 45	50 - 70
Gas	Range	0 - 60	9 - 32	5 - 60
	Typical	20 - 50	20 - 30	10 - 30

2.7. Biochar stability and reactivity

Cation exchange capacity (CEC) is a function that indicates the fertility of soils, representing the capability of the particles in the soil to retain nutrients. Gaskin et al. (2008) state that biochars produced from lower temperatures are more likely to have higher CEC due to the lower losses of acidic carbonyl (C=O) groups, resulting in more cations on the biochar surface and consequently more nutrient retention. Hence, less oxygen loss, which is reflected in a lower C/O ratio, is indicative of a less stable and more reactive biochar. Therefore, biochar produced at lower temperatures and a less prolonged carbonization process is consequently more reactive and has a higher concentration of unstable carbon. This results in faster decomposition, converting the unstable carbon into CO2 when consumed by the microorganisms in the soil.

The acknowledged measure of the stability of biochar is the widely used elemental ratios, O/C and H/C. The H/C ratio indicates the aromaticity of the biochar (molecular stability), while O/C ratio shows the reactiveness of the biochar (polarity), as shown in Figure 2.6. The reactivity of biochar decreases with pyrolysis temperature, while the aromacity increases.

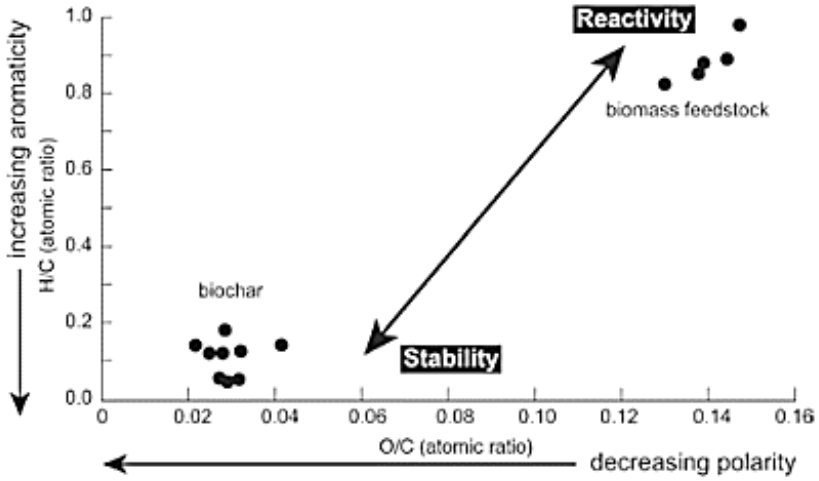

Figure 2.5: Reactivity and stability of biochar (H.-Y. Cai, 1996).

2.8. Pyrolysis kinetics models

Several kinetics models of pyrolysis have been developed by different authors, and a summary of some of the most related to wood pyrolysis, and consequently more relevant to this study, are given below.

Probably the simplified model of Shafizadeh and Chin (1977) is the most common in the literature, involving a mechanism of primary reactions for the basic cleavage of the bonds in the wood constituents, then secondary reactions as the tarry volatiles are further decomposed to produce more gas and char (Figure 2.7). Fantozzi et al. (2007), in studying pyrolysis in a continuous rolling drum applied the Shafizadeh and Chin model to system to predict the heat flows for slow pyrolysis.

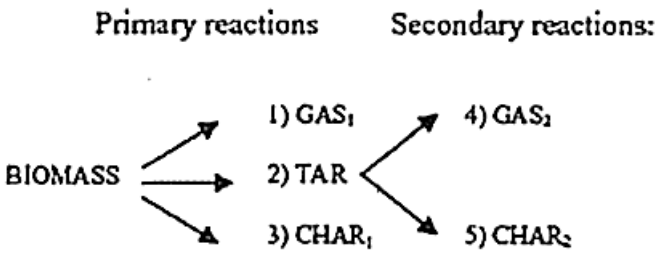

Figure 2.6: Basic pyrolysis kinetics Shafizadeh and Chin, 1977 (Fantozzi, et. al., 2007b).

In the model of Shafizadeh and Chin (ibid.), gas, tar and char are produced from the primary endothermic reaction, and the secondary reaction occur from the further degradation of tar, which are exothermic producing secondary char and gas. Moreover, Fantozzi et al (ibid.) showed how density, moisture content and rotational speeds of the drum influence the proportion of gas, tar and char.

A more specific model about wood pyrolysis, by Mok and Antal (1983) is also widely used in the literature. As wood is composed by hemicellulose, cellulose and lignin, this model follows the degradation of each of these components. Cellulose represents around 50% of the mass of dry wood (Mohan, et al. 2006), so on, this model details how devolatilization occurs in cellulose thermal degradation. The cellulose decomposition model is shown in Figure 2.8. The main elements analyzed by this study were the influence of gas flow rate and pressure in the reaction products. Under a high

flow rate and atmospheric pressure, the volatiles are driven off quickly, not favoring further secondary reactions. However, once they occur, the net enthalpic heat of reaction increases significantly as they are exothermic. Elevating the pressure enhances the exothermic phase, producing more char.

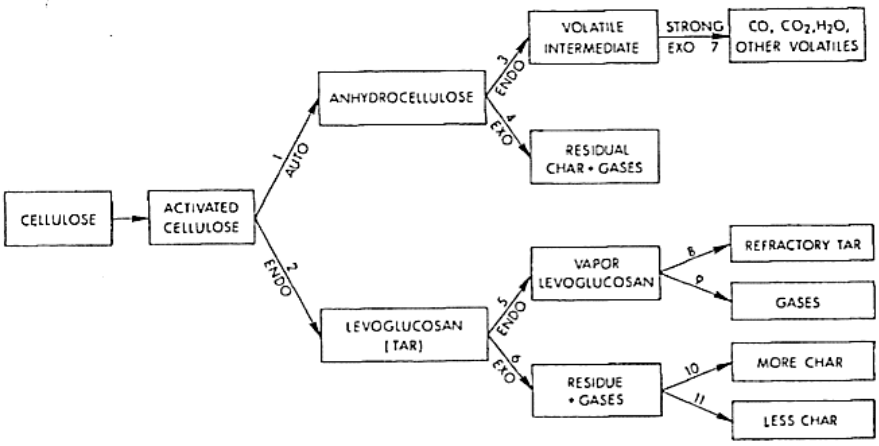

Figure 2.7: Decomposition of cellulose during pyrolysis (Mok & Antal, 1983)

Figure 2.8 shows that two pathways were proposed, both for the primary endothermic reaction. Anhydrocellulose is recognized as a “co-product” from the endothermic reaction from the activated cellulose which produces levoglucosan (tar). Anhydrocellulose can suffer both endo- and exothermic reactions, producing intermediate volatiles and residual char plus gases, respectively. The volatiles evolved suffer further exothermic degradation, producing further gases and other volatiles. The levoglucosan pathway go through two different reactions, vaporization or decomposition. The vaporization is the endothermic reaction, which produces tar and gas. The exothermic reaction, decomposition, can produce more or less char depending on the extent of interaction between the volatiles and tar.

Another relevant kinetics model of wood pyrolysis is described by Neves et al. (2011), which is developed by results from other studies. This study tries to simplify the very complex interactions between feedstock characteristics, reaction conditions and product composition. Effectively, it reduces pyrolysis to a correlated

input-output model. Important to highlight is the interaction of tar and gas in the primary pyrolysis for producing more char in the secondary pyrolysis. The model is showed in figure 2.9.

Figure 2.8: Primary and secondary reactions of pyrolysis (Neves et al., 2011).

In conclusion, the model adopted for designing the machine which this project is using was the model developed by Shafizadeh and Chin (1977), and applied by Fantozzi et al. (2007b) to a continuous slow pyrolysis system, because it describes adequately the products of biomass pyrolysis, and includes heat and mass transfer limitation (Bridges, 2014)

2.9. Mass balance of pyrolysis

As reported previously, from the start of the pyrolysis process, the biomass begins to lose components, such as water and organic elements, and gradually decreases its weight. The greatest and fastest decrease in weight occurs between the temperatures of 200 and 400°C, after which the rate slows considerably from 400 to 700°C. The yield, or quantity of solid material produced (biochar), decreases as the highest treatment temperature (HTT) increases, but countered by the carbon concentration increasing in the biochar as shown in Figure 2.10.

Figure 2.9: (a) effects of temperature on char yields; and (b) CHO contents for chars made at different temperatures (Antal & Gronli, 2003).

The kinetics interactions between the endothermic and exothermic reactions are highly complex and are affected by the engineering design of the system, the particle size, and the density and ash content of the wood. In some situations, mass and heat transfer occur by diffusion and in other parts of the system by convection, where the latter is driven by an evolved or forced pressure difference. These effects have been analyzed by Fantozzi et al. (2007b) for a continuous rolling drum pyrolyser and Bridges (2014) and Caco (2017) for the design of reactor used in this work. The next two sections discuss the heat and mass transfer resistances during pyrolysis.

2.10. Heat transfer during pyrolysis

Heat transfer occurs mainly by 3 different mechanisms: conduction within the particles, convection through the interstitial pores within particles and between the particles of the biomass bed, and radiation from particle surfaces to other nearby surfaces. Heat travels along the temperature gradient. In the reactor, the metal wall is heated up by the primary heat source, and then conduction and radiation transfer the heat from the metal to the touching or nearby biomass particles. Depending on the stage of the process, different mechanisms have more influence

on the heat transfer. For example, after all moisture has evaporated and before reaching the temperature of the first gases and volatiles being produced, which is around 280°C, conduction is predominant. Once the gases start to be generated, they transport heat as they travel through the pores of the particles and through the void spaces between particles in the bed, transferring their heat by convection, which is faster than conduction.

Particle size is a key and limiting factor of heat transfer. Heat travels between particles largely by radiation or by convection from gases travelling through the bed. Within particles, heat transfer is shown in Figure 2.11. The bigger particle size, the more difficult it is to transfer heat into the internal area of the particles, simply because heat must transport in by conduction, which opposes the convective mass transport out of the particle. Reaction occur within the particle when the local heat exceeds the activation energy of decomposition. The generated volatiles generate a local pressure which drives their transport by convection out of the particle, against the resistance of the travel path. As they travel secondary reactions occur (Neves, et al., 2011). These are exothermic so, depending, on the distance of travel and the temperature, they can cause local heating. This heat then conducts inward to the cooler regions and so the cycle repeats itself. The soak time of the biomass is directly related to the efficiency of the heat transfer. A longer soak time is needed when bigger particles are used, due to the longer time that it takes to equilibrate the temperature inside and at the surface of the particles (Kockar et al., 2000).

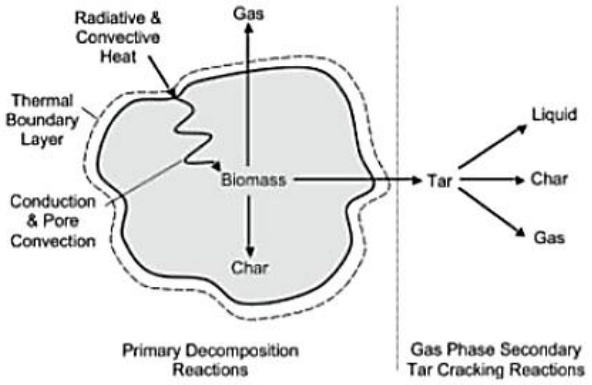

Figure 2.10: Heat and mass transfer over a biomass single particle during pyrolysis (Bezanson, n.d.).

2.11. Mass transfer during pyrolysis

Within particles, after the local temperature exceeds the activation energy, devolatilization occurs, producing gases which move towards the particle surface before been released. It means that the biomass simultaneously loses mass and shrinks, but not in proportion to the weight loss, and so increases in local porosity. There appears to be a maximum size of particle beyond which fracturing occurs (Ripberger et al., personal communication and in preparation). The volatilized mass travels out of the particles along the pressure gradient. As explained above, there is a complex interaction between mass and heat transfer, which is widely investigated by researchers (Babu & Chaurasia, 2004; Fantozzi, et al., 2007). Mass transfer in pyrolysis is generally one-way and convective.

2.12. Reactors

Charcoal production is first recorded in the archeological record at Chauvet Cave in France, dated to 30-32 ky BP (1000 years before present), for the purpose of rock art. The next need for charcoal was the smelting of metals, ca. 12 ky BP in Turkey, which required both the existence of ceramics (pottery) able to hold molten metals and charcoal able to generate the temperatures required for smelting (ca. 1000°C).

The use of charcoal as an additive to soil may well have happened accidentally at first as a char byproduct of pot making, which itself pre-dates agriculture. The Terra Preta soils contain many pot shards and charcoal (Woods & Devenan, 2010). Into the modern era, charcoal making was and still is a common forest activity.

Pit kilns are one of the principal traditional charcoal making techniques, which just requires a small fire to ignite the wood in an air restricted environment. Mound and earth kilns, where soil is used to cover the wood above and under the ground, respectively, employ the same process. These types of kiln account for most of the charcoal produced in Africa (FAO, 2017), typical producing low yields with inconsistent quality of the products, as well as no control over emissions.

The first progress towards more efficient production is seen with the construction of kilns using bricks, providing greater heat isolation. Three holes were added to fire up the wood, discharge the smoke and remove the char. Some of them also contain vents on the base to control the air intake. The archetypal examples of these are beehive kilns, which process most of the charcoal in Brazil. The large concrete Missouri kiln is another within the same class of kiln. These are large batch kilns which effectively work on the same principle as the earth mound, where a small amount of wood is lit and kept burning until enough heat has been built up after which the kiln is sealed. The pyrolysis reaction spreads gradually across the kiln over several days to weeks, until the conversion to charcoal is complete, after which it is given more time, days to weeks to cool down before it is opened.

Later on, metal kilns were developed, allowing better control of air input and gas output, providing higher yields and slight reduction of emissions.

However, the greatest advance in charcoal making came from the development of the retort technique, where the off-gases are recirculated to an external combustion zone to deliver heat back to the process. Hence, the efficiency of the retort reactors is significantly higher than for traditional ones. Due to the higher temperatures achieved and the complete exclusion of air from the pyrolysis chamber, better control over emission could be attained to deliver higher yields and higher fixed carbon content charcoal.

Further progresses had led to newer advanced types of reactors, such as the converters, allowing recovery and refining not only of the char, but also products from the volatile fraction, as the liquid condensable elements and syngas.

2.13. Emissions on pyrolysis

Traditional charcoal production systems are well known to be polluting and inefficient. The uncontrolled emission of harmful off-gases is considered the major issue of a charcoal making process. These gases are mainly composed by nitric oxides (NOx) and PICs, represented by carbon monoxide (CO), methane (CH4), non-methane volatile organic components (NMVOC) and total suspended particles (TSP) (Sparrevik et al., 2015).

Pennise, M. (2001) measured the off-gases emission of wood pyrolysis from different types of traditional kilns in Kenya and Brazil, reporting in the literature the off-gases factor on grams of pollutant (g) per kilogram of charcoal (kg) formed. They also showed the total global warming potential (GWP) of each system when considering the different values of GWP of each off-gases component relative to CO2 on a carbon atom basis. Emission factors from all the kilns studied ranged from 543 to 3027 for CO2, 32 to 62 for CH4, 143-373 for CO, 24-124 for NMVOC, 0.011 to 0.3 for N2O, and 0.0054 to 0.13 for NO (g/kg of charcoal). In relation to the total global warming impact of the charcoal production systems studied in his work, it was considered the GWPs values used on the IPCC (1995) reports, representing CO2, CH4, CO and N2O, as 1, 23, 4.5 and 290, respectively (CO2e; carbon as carbon dioxide equivalents). Hence, a range of 0.77 to 1.63 kg C emitted as CO2e was stated to be emitted per kilogram of charcoal produced.

A similar project was conducted by Sparrevik, M., et al., (2015), where the emissions of non-retort traditional kilns and retort kilns were analyzed and compared. Retorts kiln emission values ranged, in g per kg of charcoal, 1950 ± 64 for CO2, 157 ± 64 for CO, 6.1 ± 3.4 for NMVOC, 24 ± 17 for CH4, 12 ± 18 for TSP, and 1.8 ± 1.0 for NOx. For non-retorts kilns, emissions were consistently higher at 2380 ±

973 for CO2, 480 ± 141 for CO, 13 ± 3.8 for NMVOC, 54 ± 9 for CH4, 7.9 ± 2.6 for TSP, and 4.3 ± 1.6 for NOx.

Chapter 3 - Methodology and Equipment

This chapter describes the methodology adopted to investigate the problem mentioned above, to determine the carbon footprint in terms of net C-sequestration in small-scale biochar production. It then describes the Massey 60 kg reactor and the modification made as part of this project to provide effective flaring of the off-gases. Chapter 4 then goes on to discuss the control strategy to ensure effective flare combustion.

3.1 Methodology

In order to evaluate the sustainability of small-scale biochar making systems upon the production and emission scene, this work collected and analyzed data from 7 experiments on a 60 kg batch slow-pyrolysis reactor. LPG gas was used for reactor heating and augmentation of the flare. The original reactor was designed and constructed in the project by Bridges (2014) and subsequently mathematically modelled by Caco (2017) at Massey University, in Palmerston North. Figure 3.1 shows the principal information of the experiments, and gives an overview of the performance on each run. Important to note that different strategies were adopted for each run, so outputs are not directly related.

Table 3.1: Sum of runs showing the amount of biomass loaded, pyrolysis residence time and temperature, and char yield of each experiment.

Run	Wood chips (Kg)	Residence time (min)	Temperature (°C)	Char yield (%)
1	20,8	60	250	Test run
2	57,2	210	400	36,45
3	60,89	240	450	34,69
4	56,83	270	600	34,14
5	56,7	295	600	32
6	54,6	240	700	29,7
7	51,8	240	700	30,53

Some modifications were made to the Massey University 60 kg pyrolysis reactor before and during experiments to improve the control of the system. The goals of these modifications were to; (i), increase the understanding of pyrolysis in this specific machine; (ii), to enhance its capability to produce charcoal at different temperatures; (iii), to optimize the combustion chamber operation; and (iv), to optimize the flare afterburner to mitigate emissions as much as possible. The reactor is described in Section 3.2.

Measurements were temperature, load and gas composition. The reactor was equipped with thermocouples to monitor the temperature over time in different strategic points. Also, the system was weighed using high-accuracy load cells to record the mass loss both of the reactor and the LPG cylinders. A TESTO 350 gas analyzer capable of measuring CO2, CO, CxHy and NOx was utilized to detect the main components of the off-gases after burning. These measurements gave a precise temporal knowledge of the system during experiments which informed the operation and control decision-making.

All experiments were carried out with air-dried pine (*Pinus radiata)* wood chips without any bark. Wood composition has been determined in other work (Ripberger 2016). Char yield attained in each experiment was calculated on an oven-dry basis, following the definition given in Antal Jr. and Gronli (2003). Char composition was determined from proximate and ultimate analysis for selected experiments. Proximate analysis followed the international ASTM E 871 and 872 for Chemical Analysis of Wood Charcoal, carried out on a simultaneous thermal

analyser (STA F1) which combines a thermogravimetric analyser (TGA) and differential scanning calorimeter (DSC), SDT Q600 from Netzsch (Germany). Samples were ground in a ring mill from Rocklabs (Auckland, New Zealand). Moisture content was determined as loss in weight in a drying oven at 105°C. Volatile matter was determined from the weight loss at 950°C under anoxic conditions, and ash was determined as the residue after burning in air to constant weight at 750°C. The ultimate analysis was conducted on the Elementar Analysensysteme GmbH (Hanau, Germany) vario MACRO cube, using the procedure detailed in Ripberger (2016). The method determined the carbon, hydrogen, nitrogen and sulphur content of the char, with oxygen determined by difference.

Carbon balance calculations were developed and applied to the best-case experiment, resulting in a detailed footprint of emissions (run 7). It determined the theoretical carbon footprint and conversion efficiency from biomass carbon to sequestered carbon, as well as three operational scenarios; [1], production with emissions abated by after-burning; [2], production with no abatement of emissions; and [3], the required abatement to achieve zero net carbon sequestration. It must be noted that all operational scenarios have reduced footprints compared to the theoretical because of the need for additional fuel for heat up and augmentation of the flare to destroy the products of incomplete combustion.

In doing these carbon net-balance calculations, the impact of the harmful off-gases was converted into their global warming potential (GWP). The most conservative values from the AR5 IPCC report (2014) were used, that is, a 20-year horizon for CO and CH4, which are 18.9 and 84 respectively. The twenty-year horizon was chosen rather than the 100-year horizon because twenty years is within the life-time of those who are affecting emissions.

The results from the carbon footprint analysis were compared to literature reports of GWP for other retorts and kilns. This exercise sheds light on the real impact on climate change of emissions from different small-scale biochar production systems.

The following sub-section describes the reactor and the modifications to ensure good flaring of the off-gases to minimize the products of incomplete combustion.

3.2 The reactor

The pyrolyser shown in Figure 3.1 has a cylindrical geometry. The chamber which holds the wood chips to be pyrolysed has height of 1000 mm and internal diameter of 750 mm. At the centre of the reactor, there is a perforated core 900 mm in height and 100 mm in diameter, which allows the release of the pyrolysis gases from the reaction zone. This geometry ensures that mass and heat transfer occur in the same direction, from the outer heated wall towards the core. Gases leave through the core and exit into the bottom combustion chamber, where two forced draft burners provide heat to drive the process.

Figure 3.1: Massey 60 kg reactor front and side view

The reactor system was designed to be safe, operating very close to, but just below, atmospheric pressure, drawn by the stack updraft and the flare burners

which together draw away the flammable gases, tarry aerosols and particulate. As these products are first drawn through the bottom combustion zone, a portion are ignited. However, the portion ignited in this zone is limited in order to mitigate any operational risk of overheating the reactor and compromising it; nevertheless, some combustion is helpful for energy efficiency. The flammable gases, tar aerosols, particulates and combustion products from the combustion zone are then drawn up through the 20 mm annular zone between the inner and outer drums (Figure 3.2). Heat transfer occurs from the hot gas, through the reactor wall and into the wood-chips. The outer annulus wall is insulated. Finally, the gases are drawn up the flue stack by the forced draft from the top flare burners, where three forced draft burners augment their combustion, and ensure that the flue reaches at least 750°C for at least 1.5 seconds. In principle, this provides complete combustion of the flammable gases, tarry aerosols and particulate. They are then discharged to atmosphere (Bridges, 2014) as a smokeless flue.

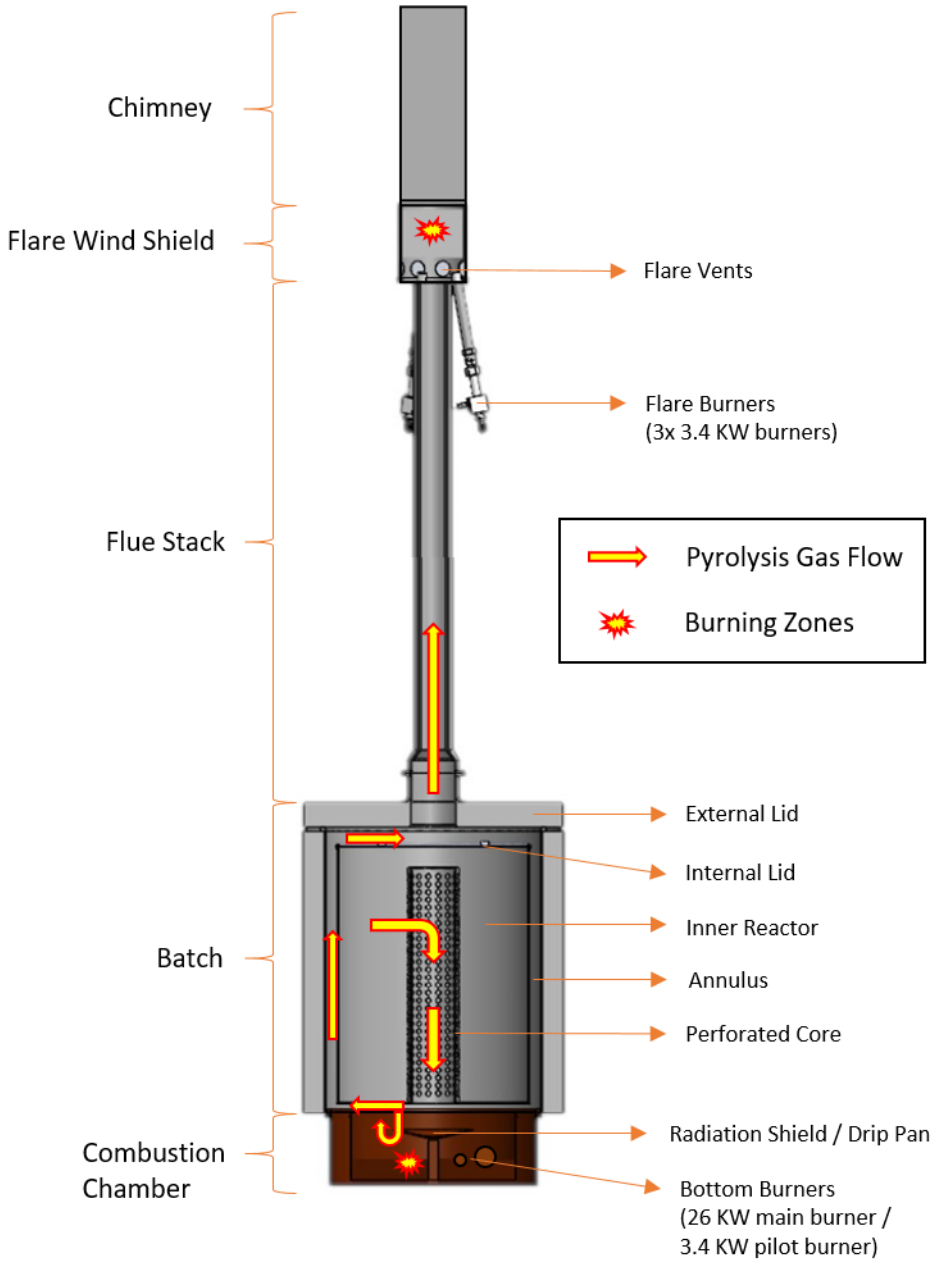

Figure 3.2: Schematic of the reactor

Inside the reactor, after biomass drying has occurred and pyrolysis reactions begin, these gases and volatiles flow, driven by a pressure gradient, towards the perforated inner core at the centre of the reactor. In the early stages of reactor operation, as they do so, the tarry vapours condense onto cooler wood chips nearer the centre. Later, as the heat spreads inwards, these tars re-volatilize and so the cycle of volatilization and condensation repeats.

The flue combustion system was designed to be satisfactorily high to generate a natural draft and consequently a slightly negative pressure, where $P_{System} < P_{atm}$. For safety, these prevent fugitive egress of flammable gases (from between the reactor and the combustion chamber on which it sits, and the lid which sits atop the reactor), carbon monoxide of which is an asphyxiant. The positioning of three forced draft burners in the flare, directed upwards into a central high-temperature zone creates an updraft necessary to draw in tertiary air through a ring-vent in the flare guard. This is necessary for oxidation of the particulate soot and tarry aerosols, which require a lot of oxygen. The amount of air needed is a compromise between enough for combustion and too much, which cools the zone.

In summary, the system is designed to provide two opportunities for product of incomplete combustion to be destroyed, firstly, in the base chamber combustion zone, then in the flue stack flare system.

3.3 Modifications

The pyrolysis reactor design and construction were developed by Bridges (2014), who also tested the production of biochar from pine wood chips. Her work then recommended several improvements on the machine. Later, Caco (2017) mathematically modelled the reactor to predict the biochar quality and yield, the carbon foot-print and the process duration to achieve complete pyrolysis, as well as designing and commissioning some modifications on the reactor in order to improve operational conditions and emissions compliance based on the EPA air quality standards.

However, Caco (2017) stated that even with these modifications, emission standard was still far from being met, and better control was needed over the reactions to maximize the recycling of heat from pyrolysis gases burning, their complete combustion in the flare system and the consequently saving on LPG usage. LPG is a fossil fuel used to augment the process, but detracts from the net carbon footprint.

Therefore, several further modifications on the reactor were made during different periods of this project. Essential ones, regarding physical redesign, were made in the

very beginning. Further adaptations to improve the control of the system were made throughout the experiments, as different control strategies were tested. The detailed modifications applied in the reactor are presented in the following section.

3.3.1. Combustion chamber

The combustion chamber initially had nine ventilation holes at its bottom to permit secondary air access into the bottom burning zone to drive further pyrolysis gases combustion, as shown in Figure 3.3. The flow of secondary air is dependent on the updraft and so, for safety the stack height and diameter were carefully designed to ensure that the amount of secondary air drawn in could never cause high combustion temperatures to exceed the working temperature of the stainless steel, out of which the reactor is made. However, there were several problems. First, apart from being safe, attempts to modulate the secondary air inflow failed due to the expansion and warping of the metal disc placed under the combustion chamber to carry this out. Second, during the cool-down phase, undesirable ingress of oxygen occurred into the reactor resulting in some percentage of the char turning to ash as oxidation continued. Third, if the draft had not fully developed, fugitive emissions could be released from these holes, presenting a health risk to operators. A fourth problem not directly related to the secondary air holes, but with the combustion chamber, was the seal between it and the reactor drum, which was achieved using a square silica rope (Bridges, 2014). This insulation rope acted as a gasket but tended to compress and needed to be inspected between each run to ensure a good seal was maintained. The integrity of the seal was also reliant on the drum being exactly vertical above the combustion drum before the drum was lifted up against it. This fourth point was addressed by adding a new wider insulation rope. To address the three significant concerns, the secondary air holes were sealed with fire cement. Secondary air supplied was modulated as discussed in Section 3.3.6 below.

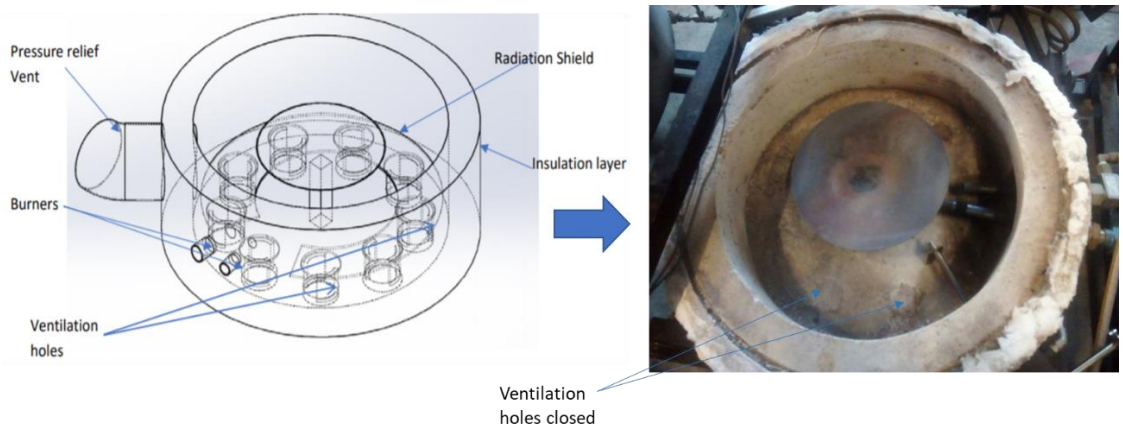

Figure 3.3: Original and modified combustion chamber.

3.3.2 External lid

The initial steel lid expanded and warped when it got hot during pyrolysis, allowing gases to escape. Caco (2017) redesigned and commissioned a new ceramic lid using fire bricks mounted inside a frame that can expand without warping. The lid with internal frame is shown in Figure 3.4.

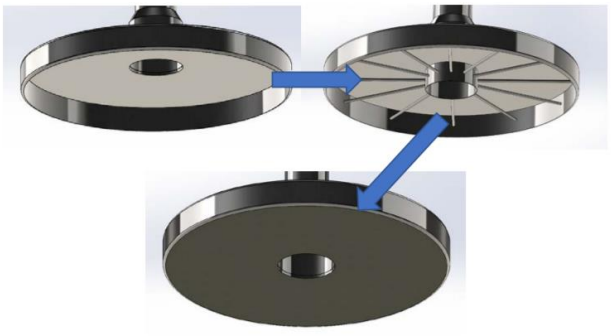

Figure 3.4: Lid modification (extracted from Caco, 2017)

3.3.4 Loading system

The previous loading mechanism of the reactor had the flue stack on a hinge system which allowed the reactor to tilt forward while the flue pivots backwards towards the ground. However, due to the new heavier ceramic lid and new flare system, both designed and commissioned within the project of Caco (2017), the hinge system was no longer capable of supporting the higher weight. Hence, a new loading system was designed and commissioned in this project, where the lid hangs on two steel cables and lifts up vertically via a pulley system and guided by a steel sheath around the flue stack and attached to the frame. When lifted clear, the reactor is able to be tilted forward by a manual gearbox. The current loading system is shown in figure 3.5.

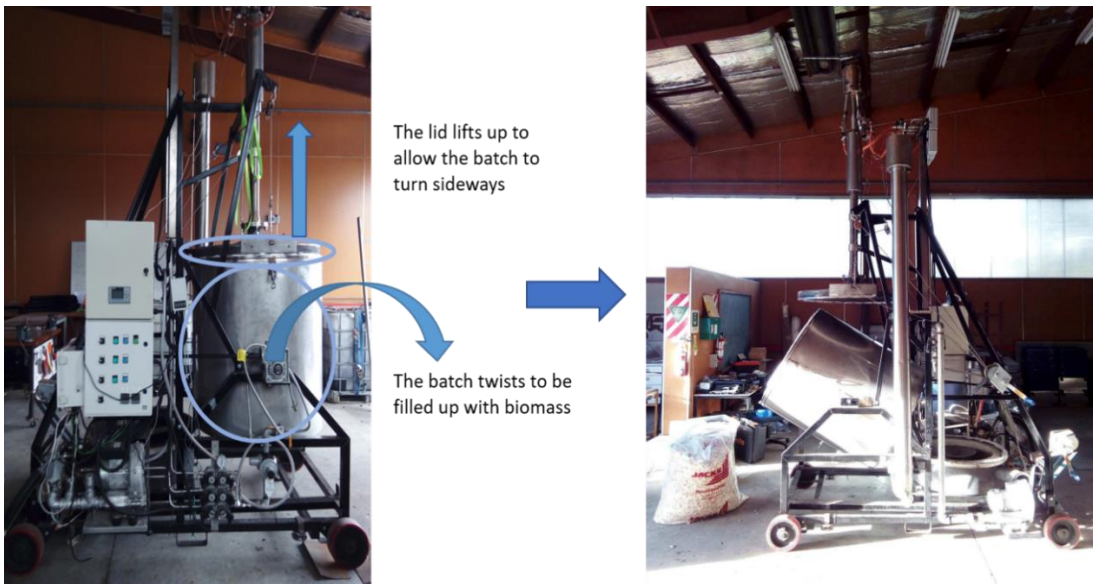

Figure 3.5: New reactor loading system.

3.3.5. Flare system

The original stack flare system was designed without accounting for the poor flammability of the pyrolysis gases, and the need for significant tertiary oxygen to combust the tarry aerosols and particulate. Thus, it was incapable of fully

combusting them (Jones et al., 2016). The new system, designed and constructed in the project of Caco (2017), added two new burners of 3.4 kw each to the single 3.4 kw burner firstly installed, for a total of 10.2 Kw total power to the stack flare, estimated to be reasonably enough to provide the complete combustion of the pyrolysis gases before going to the atmosphere. These burners were supplied with air from a dedicated fan separate to that which supplies the combustion chamber burners, where previously one fan had supplied all burners. The LPG supply from two 80 kg LPG tanks, however, remained common to all burners. Also, the redesigned system was changed geometrically to provide an adjustable ring-vent to draw more tertiary air, while still achieving the target temperature of 750°C. Figure 3.6 shows the old and new flare designs.

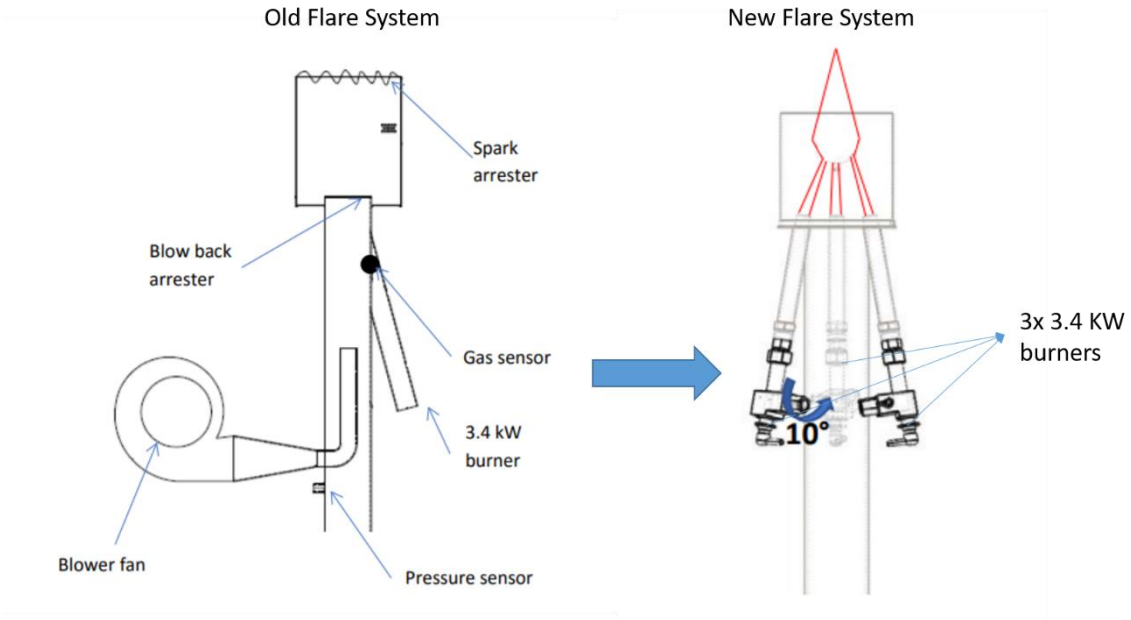

Figure 3.6: Changes on the flare design.

3.3.5. Flare system and chimney adjustments

The new flare system and new lid lifting arrangement were commissioned as part of this project. However, emissions were still over the US EPA standard considered in this

work (US EPA stack emissions limit of 2400 ppm of CO for > 1 hour sampling time, for biomass suspension burners exceeding ~3 MW heat generation), mainly because the flare burners had been working in a low part of their range, from 20 to 40% of capacity. After doing several tests, it was possible to find out that the mixing ratio of air and gas wasn´t set up right. Adjustments were made, and the flare burners started working over 70% efficiency. Even so, during the peak production of volatiles, it was still possible to observe some dark smoke, indicate incomplete combustion of the particulate. It was suspected that not enough oxygen was being supplied.

Consequently, eight (8) new holes were made around the windshield of the flare to provide extra air to the top burning zone. It was expected that more air being supplied to the flare during the greatest production of pyrolysis gases, should results on a higher combustion efficiency of the gases. The downside of providing more air is that, if it doesn't result in additional combustion, it can cool the flue, and if too cool, can result in insufficient temperature being reached. Also, during the last two experiments of this work, a chicken wire cage was putted inside the chimney to provide some turbulence for mixing and to act as a heat reservoir, and the chimney was thermally insulated with Superwool^{TM} to decrease the heat loss. From that, it was expected that afterburning of the pyrolysis gases should be improved significantly. The chicken-wire did not have the desired effect, adding too much resistance, but the additional insulation favorably added about 100°C to the flare zone temperature. These outcomes are discussed later in Section 5.4.

As part of these improvements, a thermocouple was placed at the top of the chimney to monitor its temperature, in order to understand the feedback between flaring conditions, control variables and the stage of the pyrolysis reaction. Figure 3.7 shows the additional modifications made to the flare system.

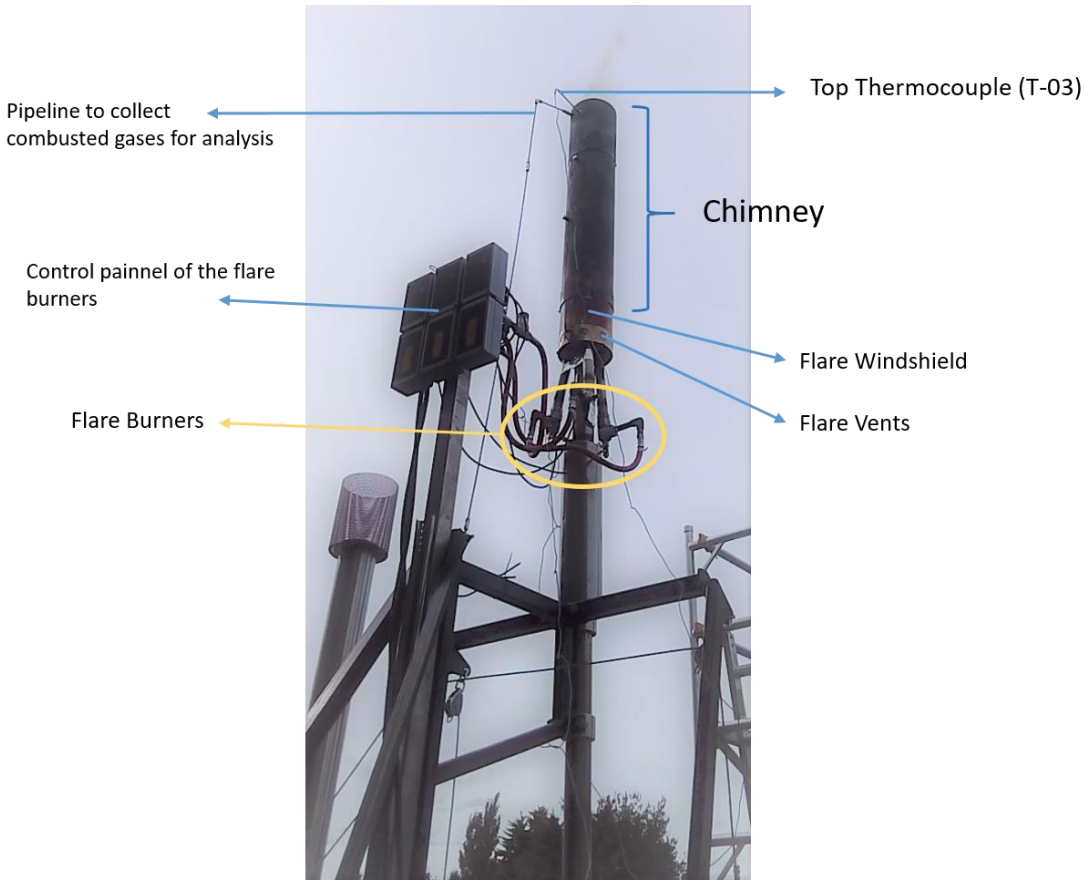

Figure 3.7: New flare system adaptations

3.3.6. Secondary air supply

As mentioned before, the original vent holes at the bottom of the chamber were sealed with fire cement. However, doing this blocked any extra air intake to the bottom combustion zone, which decreased significantly the beneficial burning of volatiles in the chamber. The consequence was that it was just possible to reach highest treatment temperatures (HTT) between 400-500°C during pyrolysis, as shown in the first three experiments of this work, when following the strategy of turning the main burner off at specified temperatures below 400°C. Previously, in the reactor of Bridges (2014), temperatures of ca. 700°C had been achieved in this operating mode. Here, the ability to produce relatively low temperature chars is an important finding. Now, however, the challenge was to work out how to operate the reactor in order to produce higher temperature chars without burning too much LPG. Therefore, extra air

was injected into the chamber during periods of significant gas VOC's (volatile organic compounds) production, to burn as much of the pyrolysis gases as possible at the bottom of the reactor, and so create the heat needed to drive up the pyrolysis chamber temperature into the exothermic reaction range, where it would supply enough heat internally to increase the temperature further.

Different ways of supplying extra air were tested during experiments. Firstly, the main burner was adjusted so that when it was turned OFF when the pyrolysis chamber reaches 350°C (400°C was also tried), the associated forced air supply, which had been dumped externally, now continued to be delivered into the combustion chamber. The pilot burner remained on. This provided oxygen for secondary combustion of the pyrolysis gases, tarry aerosol and particulate. By doing this, it was possible to reach temperatures around 600°C. In further experiments, extra air was also introduced into the chamber through the former over-pressure vent. A number of arrangements were tried. Injecting air directly from a blower into the chamber had the undesirable effect of reversing the slight negative pressure from the natural draft to a positive pressure, resulting in fugitive emissions through gaps between the combustion chamber and reactor, and at the reactor lid. The best arrangement was to remove the pressure relief vent and instead use this as an open port to the combustion chamber. This allowed the natural draft to work as intended, with a slight negative system pressure. Inflow to the open port was then assisted by air gently blown from towards the port. This flow was provided by the blower, greatly modulated, and the pipe was mounted some distance from the port to ensure that air entry was essentially at atmospheric pressure to avoid affecting the natural draft within the system. Another handy aspect of this arrangement was that the internal part of the chamber could be seen from outside. It was then possible to monitor the flammability of the pyro gases during different stages of reaction and find out the right time to have the blower on and the optimal air velocity, without cooling down the system or changing significantly the pressure.

3.3.7 Workplace safety

Aspects of workplace safety were addressed in this work. The unit was operated outside to ensure good dispersal of flue gases. An environmental CO monitor was used to ensure that CO concentrations were well within Worksafe limits, of 50 ppm for 1-hour exposure (Worksafe, 2013). In setting up experiments, the unit needed to be wheeled outside and the flare shroud needed to be placed on top of the stack, and the gas sampling tubing needed to be screwed together. A 3.4 m high mobile scaffold was purchased for this task from Total Site Supplies Ltd, Timaru. This also made it easy to readjust the tertiary air supply while running the reactor.

Chapter 4 - Control objectives and strategy

One of the objectives in this project is to define 'good control' for the pyrolysis of biochar in batch reactors. For this reason, and because the unit is an experimental apparatus, control was kept relatively manual, but with a focus on recording temperatures, loads and the flue composition in order to ascertain where actions are required. From these, recommendations can be made about operating parameters for more automated control to be incorporated into later advances of the pyrolyser.

4.1. Strategy of design

'Good control' means ensuring safe operation of the reactor, combusting all products from incomplete combustion, minimizing polycyclic aromatic hydrocarbons (PAH's) formation, limiting CO, NOx and particulate emissions to within Air Quality Standards, and to ensure the char quality meets the international standards, both for the char properties and for the process from which it is made.

The first design developed in the project of Bridges (2014) highlighted several issues. One was air contacting the hot char during the cool-down phase, which caused ash formation. A second was the inadequate design of the flue stack flare system, where the flame often went out and was insufficient to destroy the particulate or combust the PICs. A third was the poor design of the reactor lid which warped during operation leading to fugitive emissions.

Here, this work has developed several improvements to upgrade the control strategy. In addition to all the modifications on the reactor mentioned previously, load cells were added to the system to measure the biomass loss and gas usage, providing the information necessary for a detailed carbon balance. Figure 4.1 and Table 4.1 show and explain the measurement instrumentation that integrates into the control system of the reactor.

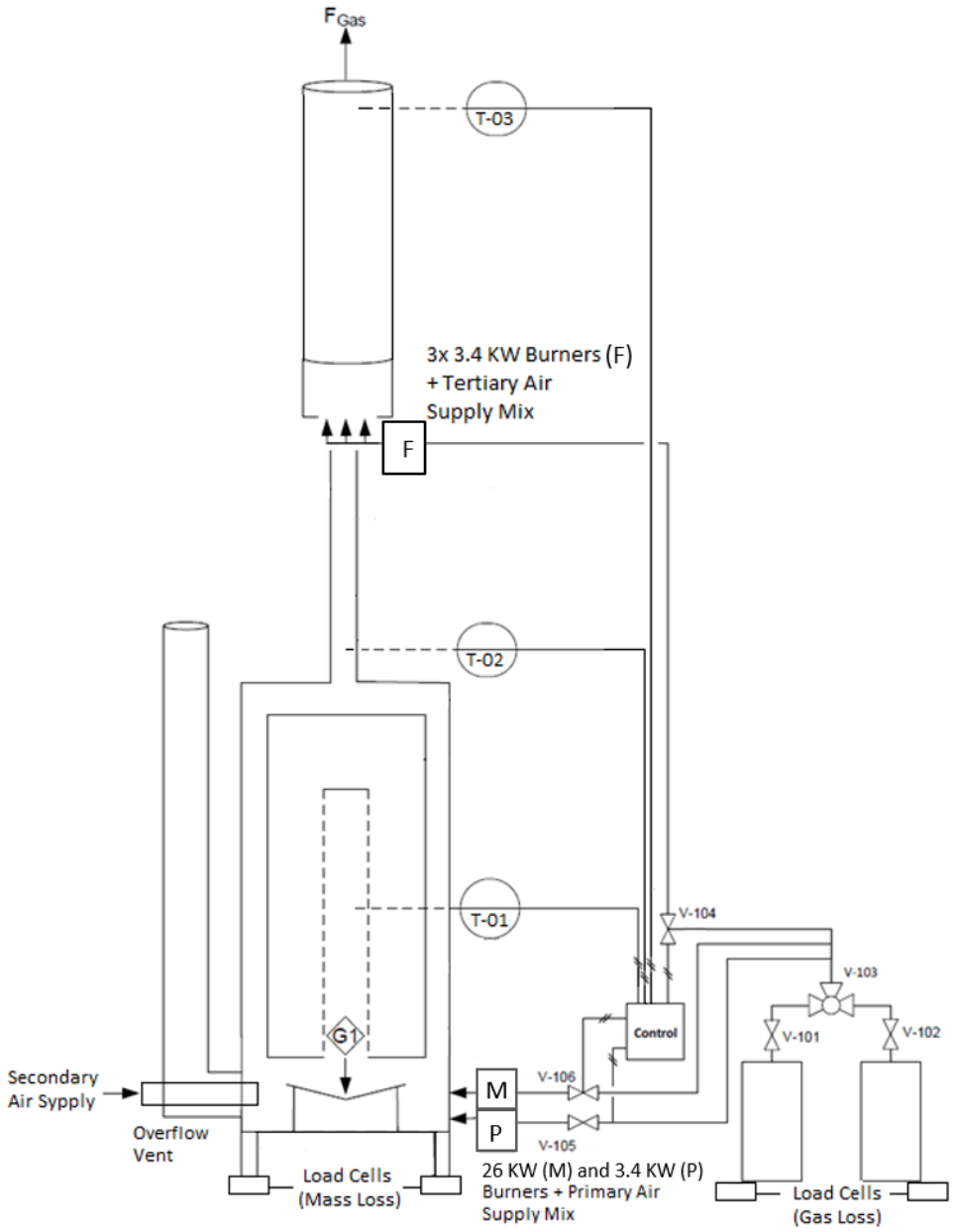

Figure 4.1: Upgraded control strategy design

Table 4.1: Description of the controlling and measurement elements pointed in figure 4.1.

V – 101 / 102 / 103 / 104 / 105 / 106	Gas Valves
T-01	Thermocouple 1 – Inner reactor temperature
T-02	Thermocouple 2 – Flue stack temperature
T-03	Thermocouple 3 – Chimney / Top of flare temperature
Load Cells (reactor mass loss) [up to 500 kg each]	Four (4) load cells were mounted underneath the four corners of the reactor to measure the weight loss of the biomass during reaction

Load Cells (gas loss) [up to 100 kg each]	Four (4) load cells were mounted underneath the LPG gas cylinders frame to measure the gas usage during reaction
G1	Volatiles flow to combustion chamber
M	Main bottom burner of 26 kW
P	Pilot bottom burner of 3.4 kW
F	Flare system burners / Three (3) of 3.4 kW each

4.2. Weight Loss Control

Eight loads cells (Accupoint Static Weigh Module, PT Ltd) were acquired for this project; four with capacity of 500 kg each to measure the mass loss during the reaction, and four with capacity of 100 kg each to measure the LPG gas weight loss. LPG is supplied to the burners from two 90 kg gas cylinders, mounted on a frame. The recorded mass loss is the total loss, so includes LPG used both in the combustion chamber and at the flare. Using load cells on the reactor means the reactor is essentially treated as a giant thermogravimetric analyzer. After wheeling the reactor outside before beginning experiments, it was jacked up, then lowered gently onto four wooden blocks placed below the load cells.

4.3. Combustion chamber burner control

The control of the combustion chamber is to; (i), heat the reactor until pyrolysis begins, and continue heating during pyrolysis; (ii), provide partial ignition of the vapours during pyrolysis; (iii), turn off the main burner when a determined set-point (usually 350°C) is reached; (iv), thereafter, provide additional air to facilitate the partial combustion of pyrolysis vapours depending on the target highest treatment temperature, between 400-700°C, at levels of none, secondary air from main burner, or that plus tertiary external air; (v), maintain the pilot burner throughout pyrolysis to enable partial ignition; and (vi), turn off the pilot burner once the reaction is complete. By following this control strategy, the LPG use will be economized.

In addition, the system is designed to ensure that the annular heating zone never exceeds 1050 ℃, which is the maximum safe operating temperature of Stainless Steel.

The three thermocouples delimitation, which provided the temperature inputs, are described below:

- T-01: This thermocouple is located in the perforated core of the pyrolyser. It measures the temperature of the vapors leaving the pyrolyser and give us a reference of the char temperature being produced (reaction zone temperature).

- T-02: This thermocouple is mounted in the base of the flue stack. It measures the temperature of the gases after heat has been transferred across the wall of the pyrolyser, but before further heat loss occurs as the gases go up the stack. Pyrolysis becomes exothermic when the rate of change of T01 is greater than T02. This begins when T01 exceeds 240°C and is well underway when T01 reaches 350°C. Beyond this, the reaction is assuredly exothermic because T01 exceeds T02.

- T-03: This thermocouple is placed at the top of the chimney. It measures the temperature of the gases after being combusted in the chimney flare zone. A well-performing flare should exceed 750°C for >1.5 seconds to ensure combustion of the particulate and other products of incomplete combustion. It is indicative of the thermal experience of the vapors, rather than directly determining whether all PIC have been combusted.

The temperature inputs were used to control:

1. When T01 reached the set-point (usually 350°C) it triggered the OFF switch for the main bottom burner (26 kW). When this main burner was switched OFF, the default mode meant both the LPG supply was switched OFF and the forced air supply was externally dumped. For HTT targets above 400°C, the forced air supply was not dumped, but instead redirected into the combustion chamber. For the 600 and 700°C HTT chars, extra secondary air was also blown into the chamber, but only when the pyrolysis gases were obviously flammable. These modes of operation will be later in Chapter 5. Apart from the default, the other operations were made manually.

2. When the T03 reached the set-point (adjusted from 850-1050°C) it triggered the downward modulation of the chimney flare burners (3x 3.4 kW).

4.4. Emissions Control

A Testo 350-XL gas analyser was used to primarily monitor the carbon monoxide (CO) levels, but it also has the capability to measure nitric oxide and nitrogen dioxide (NOx), carbon dioxide (CO2), hydrocarbons (CH4 and Nonmethane Organic Compounds (NMOCs)) and hydrogen sulphide (H2S). The gases were sampled at the top of the chimney through a ¼ inch pipe, and then drawn downward using a vacuum pump to the gas analyzer. By sampling at the top of the chimney, the flue gases had not yet dispersed into the atmosphere. Thus, the concentrations are representative of the flare performance in destroying the products of incomplete combustion, in order to meet the emission standards. From these measurements, it was possible to analyze which improvements in the reactor design and operation were required to abate emissions.

Currently, there is no specific standard that limits pyrolysis emissions. However, the United States of America Environmental Protection Agency (EPA) consider that a stack concentration of 2400 ppm of carbon monoxide over a minimum of one-hour sampling time is a limit for a biomass suspension burner which surpasses 3 MW of heat production. Although there are different limits that vary according to the reactor configuration, energy output and type of fuel, this seems to be the most acceptable number to consider in this work. Nevertheless, this limit cannot be considered as an acceptable CO level in the working environment. The New Zealand Worksafe Exposure Limit for operators for CO concentration must not exceed 50 ppm for 1-hour exposure (WorkSafe, 2013).

The 60 kg reactor was operated eight times, a test run and full runs 1 to 7. Each of these progressively targeted certain objectives and included learnings from previous runs. These are detailed below.

5.1 Test run

In order to analyse the mechanism of the heat transfer through the biomass, this experiment was performed where the pyrolysis reaction was stopped early. The stop point was around 250°C (T01) during the heat up phase. The reactor was then left to cool, after which it was opened (figure 5.1).

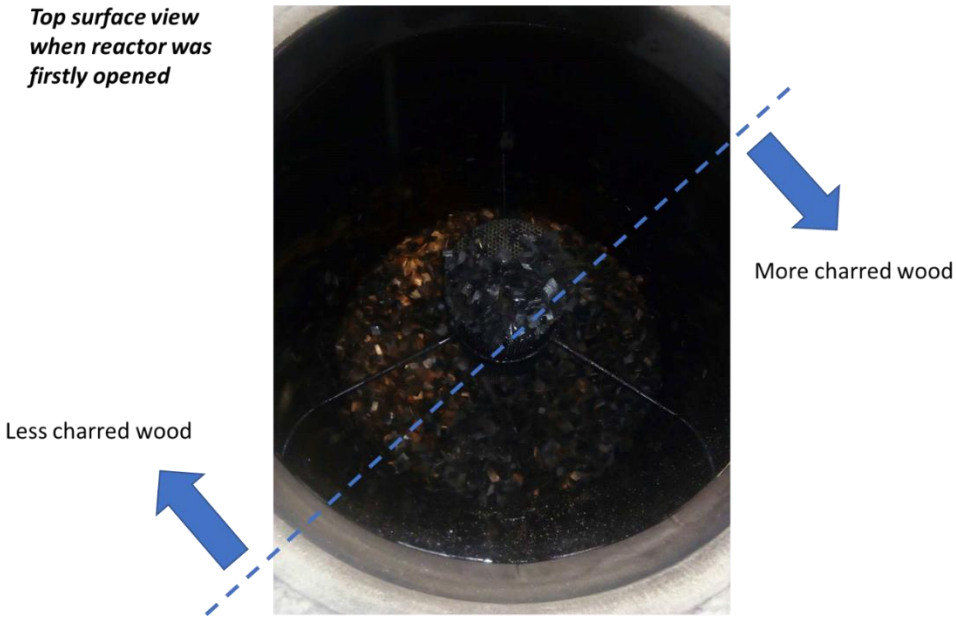

Figure 5.1: Top view of the charred wood chips within the reactor.

When the reactor was first opened, shown in figure 5.1, it was clearly possible to see a difference in charring among the wood chips. The right bottom part, below the dotted line, highlighted in the figure as “more charred wood”, had the greater amount of charred biomass. This was due to the bottom burners being on the opposite side of the chamber, and thus their flames being directed to this side which is directly

underneath this area. As expected, this part of the batch receives more heat and consequently the wood placed in this region gets carbonized first.

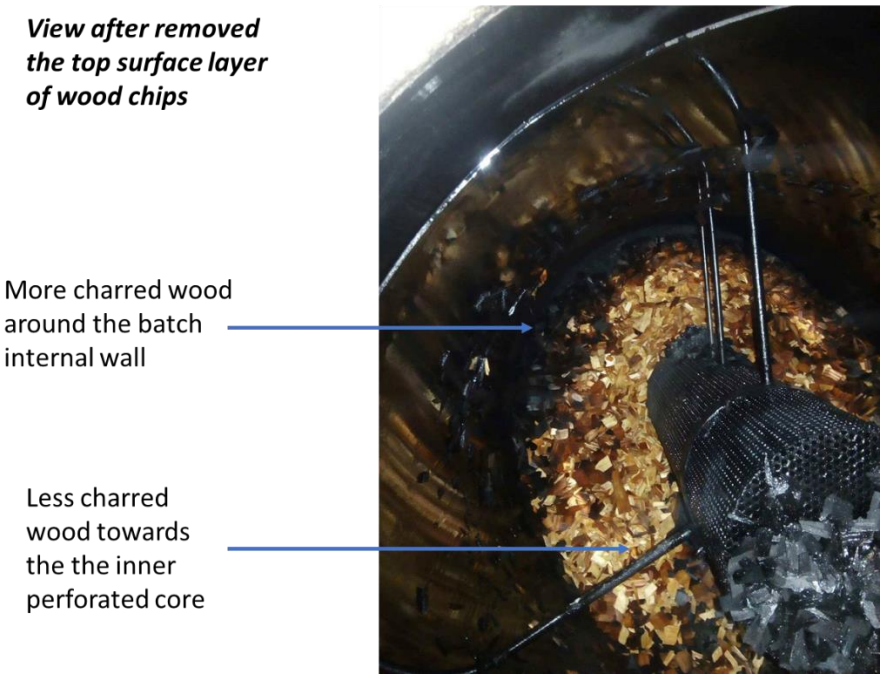

Figure 5.2: View of the wood chips in the reactor for the test run after the top layer of 3 cm had been removed.

After removing the upper superficial layer of wood chips, as shown in figure 5.2, the overall mechanism of heat transfer becomes apparent. Near the internal wall, there was a significantly higher amount of charred wood, while near the inner perforated core the wood chips were far less carbonized. Also, a great amount of tar ended up attached to the more charred wood chips and all around the internal wall and lid.

These observations support the hypothesis of the reactor design (Section 2.5.2.4); that is, heat and mass transfer move in the same direction, from the heated wall to the inner core. The consequence is the gradual advance across the reactor of the pyrolysis reaction front, observed here by stopping the reaction during this time. The presence of tar furthermore supports the hypothesis; that is, the condensable tar phase goes through cycles of volatilization and condensation. Volatilization first occurs when enough heat is present to cause pyrolysis, and

condensation occurs when the volatiles meet the cooler more central woodchips. Re-volatilization occurs when enough heat is present to overcome the latent heat of the liquid tar. In this test trial, the tar was observed among the char and on the walls, rather than in the cooler wood chips, but this is likely due to migration during cool-down, which occurred overnight, where the walls, lid and near-wall particles are the coolest surfaces and so become favoured for condensation. Lastly, it also suggests that this volatilization-condensation cycling increases the residence time within the reactor which assists in secondary reactions, which optimize the char yield. The observations clearly support this increase in residence time.

5.2. Run 2 (400°C char)

This experiment reproduced the main operating strategy of Bridges (2014), giving the temporal changes in mass and temperature shown in Figure 5.3. Bridges strategy involves turning off the main bottom burner when the reactor temperature reaches 350°C (T01) after which the reaction is expected to be mildly exothermic. In Bridges' trials, T01 then gradually rose to between 600-700°C. Since then, the secondary air vents in the bottom combustion zone were sealed (Section 3.3.1). This meant that secondary combustion of the pyrolysis gases did not occur and so secondary heating of the reactor also did not occur. Thus, the maximum temperature attained in the reactor was much lower, at around 400°C. There were several other minor variations from the procedure of Bridges. First, the pilot burner was turned off when the inner reactor temperature reached 410°C (T01). The reason for doing this was to evaluate the response of the reaction zone when the reactor reached 400°C. Second, the flare system was turned off when the chimney-top temperature (T03), which had peaked at 800°C and had been falling since the pilot burner had been turned off, dropped to 630°C after about 4 hours and 40 minutes. The reason for turning the flare off before the end of the experiment was to observe the quantity, color and smell of the smoke and thus to determine whether the reaction was finished. The detail of the operating strategy is given in Table 5.1.

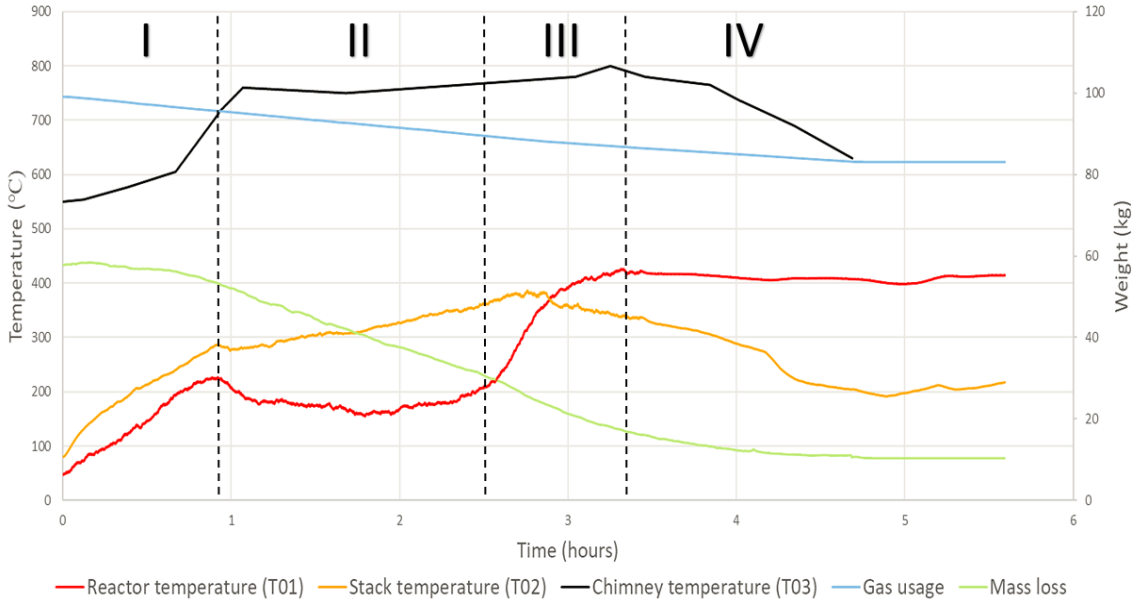

Figure 5.3: Temperature and mass as a function of time for Run 2 (400℃). Temperatures are the centre of the reactor, the bottom of the stack and above the flare. Masses are the reactor mass, showing the loss in mass as wood chips convert to char, and the LPG tanks, showing the fuel use in heating the reactor and augmenting the flare. The vertical dotted lines indicate the non-specific boundaries between stages of operation, I (dehydration), II (endothermic), III (exothermic) and IV (cool-down).

Table 5.1: Run 2 mass measurements of initial wood (air dry basis) and the char at the end of pyrolysis (start of cool-down) and after cool-down. Yield is given on a moisture-free basis.

Wood chips (kg)	Initial moisture content (%w)	Mass loss during pyrolysis (kg)	Char weight after cooling (kg)	Yield after pyrolysis (%)	Yield after cooling (%)	Total gas usage (kg)
57,20	11,80	38,80	3,20	36,45	6,34	16,20

Yield after pyrolysis is calculated as the remaining mass after pyrolysis divided by the wood feedstock on a dry-basis, i.e., (57,20-38,8)/(57,20×(1-0,118)) = 0,3645.

Table 5.2: Operating strategy for Run 2.

• The main burner was turned off at 350°C (T01). This means the LPG flow of the main bottom burner was stopped and its air flow supply was dumped externally to the combustion chamber.

• The pilot burner was turned off at 410°C (T01). This means the LPG and air flow supply to the bottom burners was entirely stopped. • The flare was turned off at 630°C (T03). This means the LPG and air flow supply to the chimney flare system was stopped.

Table 5.3: Major observations for Run 2.

• Pyrolysis progresses through three well-defined stages, I, II and III, characterized respectively by drying, an endothermic phase as the pyrolysis front spreads across the reactor and the reactor temperature is steady, and an exothermic phase when the reactor temperatures increases rapidly. • A great amount of tar was found after the experiment attached to the bottom of the stack and the top of the internal lid. • Between the period from completion of pyrolysis to after cool-down, the char lost a significant amount of mass and contained a lot of ash.

Table 5.1 shows the mass balance results. On a moisture-free basis, a high yield of 36,45% was obtained at the end of pyrolysis, before cool-down, but only 6,05% after cool-down. Other major observations of Run 2 are contained in Table 5.3. On opening the reactor, it was evident that the mass loss was due to continued smoldering of char to ash. For this to happen, air was getting inside the reactor. This required two leaks. First, the seal between the bottom combustion chamber and the reactor, which was a silicon-fibre rope, was not effective, allowing air into the combustion chamber during cool-down. Even when cooling, the still hot reactor creates a thermal updraft and so the bottom chamber will have slightly negative pressure, allowing air ingress if poorly sealed. Second, the reactor lid was most likely not hooked properly into its bayonet fittings, thus allowing short-circuiting of gases through the reactor. If the fitting is poor, this will be the path of least resistance. Air contacting hot char will smolder, forming ash. With these problems in mind, future runs made special effort to ensure these seals were secure. Also, aluminum tape was used to seal other possible gaps,

specifically between the reactor and the top lid and other thermocouple holes (just in case they had unseen cracks into the pyrolysis chamber).

Figure 5.3 shows the temporal change in temperatures and masses for Run 2. Here, the reactor inner temperature (T01) follows the same initial profile for all experiments conducted later in this work. The profile can be divided into three distinct stages, labelled I, II and III. During stage I, all profiles heat up to around 200°C during the first hour of reaction, then decrease to around 160°C. During this time, three processes are occurring; (i), moisture evaporation; (ii), sensible heating; and (iii), primary pyrolysis as first hemicellulose, then cellulose and lignin, are decomposed. It is likely that all three processes are occurring simultaneously. The fact that the temperature reaches 200°C then decreases is interesting and inexplicable. Free water requires a pressure gradient to be driven out of the woodchips, which are up to 20 mm thick, and so needs temperatures well above 100°C. There is no defined boundary between moisture evaporation and the onset of pyrolysis. The latter is indicated by the top flare temperature increasing to over 700°C, between ~40-65 minutes, which indicates that decomposition of the wood has taken off and the volatiles are being burnt at the flare. Stage II begins with the mentioned fall in temperature to 160°C, then remains constant for the next 1,5 hours, as heat spreads from the annular region towards the core as described above (Section 5.1). This stage is called the endothermic phase because the reaction requires heat. The value of 160°C is not necessarily reflective of the temperature at the pyrolysis front but is reflective of the combined effect of wood liquefaction, volatilization and condensation. Stage III begins when the reactor core temperature (T01) starts to increase significantly, representing the beginning of an exothermic phase. It is termed 'exothermic' because the temperature of the reactor is increasing much faster than any other temperature in the system, and certainly represents a change in reaction kinetics.

After turning off the pilot burner at 410°C at about 3 hours and 20 minutes, the reaction neither increased in temperature, nor cooled, but instead remained stable for the remainder of the monitoring time. While this indicates a balance between heat loss and mild exothermicity, it does ask the question 'What causes the mild

exothermicity. The sources of the exothermicity are either pyrolysis or smoldering combustion, the latter due to the above-mentioned problem of short-circuiting gas flow. However, in order for air to get into the reactor, the combustion chamber and the reactor must be at negative gauge pressure. While the ash formation during cool-down means that they must be at negative gauge pressure during cool-down, this is not necessarily the case during pyrolysis, or at least it is ameliorated, due to the high evolution rate of pyrolysis gases and the combustion chamber having forced draft burners. Therefore, while short-circuiting cannot be ruled out, it is less likely, and so it can be concluded that the mild exothermicity is most likely from pyrolysis. The mild exothermicity suggests that secondary reactions are occurring.

Upon opening the reactor, a lot of tar was found in the headspace, on the lid and condensed in the stack. Relevant to this is the low temperature, ~400°C in the reactor (T01) and at the bottom of the stack (T02) tracking downwards from ~390°C to ~280°C between ~2.75 to ~4.25 hours. These lower T2 temperatures have clearly resulted in tar condensation. Furthermore, some tar was found inside the reactor which indicates that wood had liquefied to tar but had not reached high enough temperature to be volatilized. Also found inside the reactor were dark small solids particles, probably soot, that had not been carried away. These observations, together with the high yield, indicate that pyrolysis was incomplete at this nominal highest treatment temperature (HTT) of 400°C.

In relation to the flare temperature (T03), when it was turned off at 630°C at about 4:40 hours, it was still possible to see and smell some pyrolysis gases being emitted. It also shows that the reaction had not finished. Therefore, the flare system should be turned off later when the reactor temperature begins an auto-decrease in temperature, as observed by Bridges (2014) in higher temperature trials.

5.3. Run 3 (450°C char)

In this experiment, heat was provided for a longer period in order to reach a greater (HTT) char compared with Run 2. To do this, the main burner was turned off when the inner reactor temperature reached 400°C (T01) and the pilot burner off at 390°C (T01)

during the later cooling stage at the end of the experiment. Also, the top flare system was kept on throughout the run. The time recordings of temperature and mass are shown in Figure 5.4 and the detail of the operating strategy is contained in Table 5.5. In addition, The Testo 350 (Section 4.4) gas analyzer was used to evaluate the carbon monoxide (CO) concentration of the gases being released at the top of the chimney in order to determine whether the system is capable of completely combusting the pyrolysis gases to meet the emission standard of 2400 ppm of CO (US EPA standard). However, during the experiment, this equipment was not working properly due to condensed water from the sampling line getting into the sample probe. This meant only a few measurements of CO concentration were made.

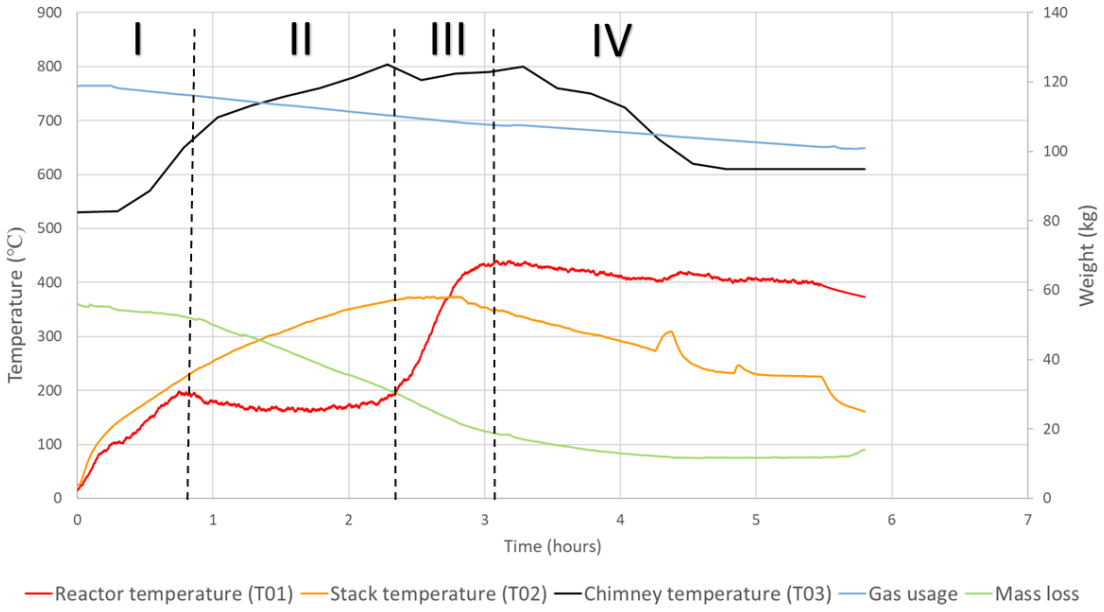

Figure 5.4: Temperature and mass as a function of time for Run 3 (450℃). Temperatures are the centre of the reactor, the bottom of the stack and above the flare. Masses are the reactor mass, showing the loss in mass as wood chips convert to char, and the LPG tanks, showing the fuel use in heating the reactor and augmenting the flare. The vertical dotted lines indicate the non-specific boundaries between stages of operation, I (dehydration), II (endothermic), III (exothermic) and IV (cool-down).

Table 5.4: Run 3 mass measurements of initial wood (air dry basis) and the char at the end of pyrolysis (start of cool-down) and after cool-down. Yield is given in a moisture-free basis.

Wood chips (kg)	Initial moisture content (wt%)	Mass loss during pyrolysis (kg)	Char weight after cooling (kg)	Yield after pyrolysis (%)	Yield after cooling (%)	Total gas usage (kg)
60,89	10,80	41,80	18,84	35,15	34,69	17,60

Yield after pyrolysis is calculated as the remaining mass after pyrolysis divided by the wood feedstock on a dry-basis, i.e., (60,89-41,8)/(60,89×(1-0,108)) = 0,3515.

Table 5.5: Operating strategy for Run 3.

- The main burner is turned off at 400°C (T01). This means the LPG flow of the main bottom burner was stopped and its air flow supply was dumped externally to the combustion chamber.
- Pilot burner off when inner temperature (T01) dropped to 390°C near the end of the experiment. At this point, both the LPG and air flow supply to the bottom burners was entirely stopped.

Table 5.6: Major observations for Run 3.

- Pyrolysis progressed through the same well-defined stages I, II and III seen in the earlier Run 2.
- The temperature of the flare became stable at 610°C after 4:30 hours when the reactor temperature dropped to 400°C and no further mass loss occurred.
- The concentration of carbon monoxide depended on the stage of the pyrolysis and the degree to which the products of incomplete combustion were decomposed
  - Stage I. No CO detected.
  - Stage II. Once T03 exceeded 680°C, the CO concentration was >5.000 ppm, beyond the TESTO analyser limit.
  - Stage III. CO concentration was ca. 100 ppm. During this period, T03 was between 760-700°C.

- Stage IV. Once T01 became steady ca. 400°C, the CO concentration dropped to ca. 50 ppm. During this period, T03 was between 700-650°C.
- Stage IV. Thermocouple T03 continued to drop as the mass loss rate decreases. Below 650°C, the CO concentration dropped to zero.

Table 5.4 shows the mass balance results for Run 3. This experiment pyrolyzed 60,89 kg of wood chips with an average moisture content of 10,8 wt%, resulting in a production of 18,84 kg of char. On a moisture free basis, the yield of char is 35,15% at the end of pyrolysis and 34,69% after cool-down. In contrast to run 2 where the yield was very low due to some air getting inside the reaction zone, the improvements had the desired effect. The internal lid was hooked very strongly into its bayonet fittings and all the possible gaps throughout the reactor were covered by aluminum tape. The overall yield of 35,12% was only slightly lower than for Run 2 at 36,45%. This is expected, both in their similarity and that Run 3 is slightly lower than Run 2 due to its slightly higher HTT.

In general, Run 3 behaved similarly to Run 2. The inner reactor temperature (T01) had the same profile during the first 2:30 hours of experiment, progressing through stages I, II and III in the same way, i.e., drying until the temperature has reached around 200°C, then cooling slightly to an endothermic stage at a constant temperature of about 160°C, before the same rapid increase after 2 hours as the exothermic phase begins. Here, the HTT was around 435°C (T01), which is ~15°C higher than Run 2. The modest gain reflects the extra heat supplied by the main burner which was turned off when T1 reached 400°C instead of 350°C as in Run 2. As the main burner is the principal heat source, it is clear that the reaction is not exothermic enough to generate enough heat to overcome the heat losses of this relatively small system, even when the pilot burner is on all the time. The same reaction conditions essentially prevail and, subsequently, the reactor temperature remains around 400°C for an extended period of time. Therefore, in order to make higher HTT chars, more heat needs to be provided to raise the annular driving zone to well beyond 400°C.

Accidentally, the main burner switched on again when the reactor temperature (T01) cooled down to 400°C, because this was a controller set point. This caused a slight increase in the temperature around 4:15 hours, as the graph shows. However, it did not influence the reactor performance.

The rise and fall of the flare temperature (T03) is indicative of the presence of combustible volatiles in the flue gas. As seen in Run 2, it rises in stages I and II as pyrolysis begins and spreads across the reactor, reaching 800°C here, then remains steady through stage III, before falling when no further mass loss occurs until it stabilized at 610°C. Therefore, 610°C (T03) is an indicative temperature for the flare at the end of the trial, which tells the operator that the pyrolysis reaction has ended.

Carbon monoxide (CO) concentrations were sampled above the flare just below the top of the chimney. They follow a pattern aligned to stages I, II and III. In stage I, the drying stage, no CO was found and the top flare temperature (T03) increased steadily from 530°C to 680°C. In stage II, the endothermic stage, the CO concentration was over 5.000 ppm (i.e., beyond the measurement range of the Testo 350 gas analyzer) and the T03 temperature rose further, from 680°C to 805°C. In stage III, the exothermic stage of rapid increase in reactor temperature (T01), the CO concentration decreased to about 100 ppm while the flare temperature (T03) remained in the high 700s. Once the reactor temperature became stable at ~400°C early in stage IV, the CO concentration reduced to around 50 ppm and the flare temperature continued to decrease from 700 to 650°C. Thereafter, the CO concentration decreased to 0 ppm. These results lead to two conclusions; first, stage II pyrolysis produces more products of incomplete combustion than the flare can combust, which some will be soot particles; and second, in stages III and IV, the flare temperature is indicative of the amount of combustible volatiles present because, as the mass loss rate decreases towards the end of pyrolysis, the flare temperature also decreases. Operationally, the first of these is of concern because these levels of CO exceed the 2400 ppm limit. Without changing the flare burners, three factors could improve flare performance: increasing air supply to the combustion zone, increasing the temperature of the flare combustion by insulating the chimney, and increasing the residence time by extending the height of the flare shroud. These actions were taken in all future experiments.

5.4. Run 4 (600°C char)

The main aim of this run was to make a higher HTT char than in the previous two runs but achieving this by turning off the main combustion zone burner at 350°C, similarly to Run 2, instead of at 400°C, as carried out in Run 3. The motivation for reducing the use of the main 26 kw burner is that the net carbon sequestration of biochar production is less when more fossil fuel LPG is required to drive the process. (Sequestration calculations are carried out in Chapter 6.) To make higher HTT char requires secondary combustion, which is achieved by blowing air into the combustion chamber. This was done by changing the mode of operation of the main burner after it is switched off at 350°C. Previously, when the burner was turned off, the LPG supply was stopped, and the air supply was dumped externally. Now, instead of dumping the air, it is set to continue blowing into the combustion chamber. The pilot burner in the combustion chamber was kept going throughout the trial in order to ignite the volatiles. The hot partially combusted pyrolysis gases then pass through the annulus between the reactor wall and the external wall and so return their heat to drive the pyrolysis. This has the additional benefit of reducing the combustion load on the flare. The details of the operating strategy are given in Table 5.8. The technique was monitored to ensure that it could not lead to overheating of the reactor, which would be a safety risk if it could occur.

Also, to save LPG, the top flare system was turned off during the cool-down stage when the reaction was completely finished. This is indicated by both no further change in mass and the chimney temperature decreasing to 610°C (T03). The time-dependent recordings of temperature and mass are shown in Figure 5.5.

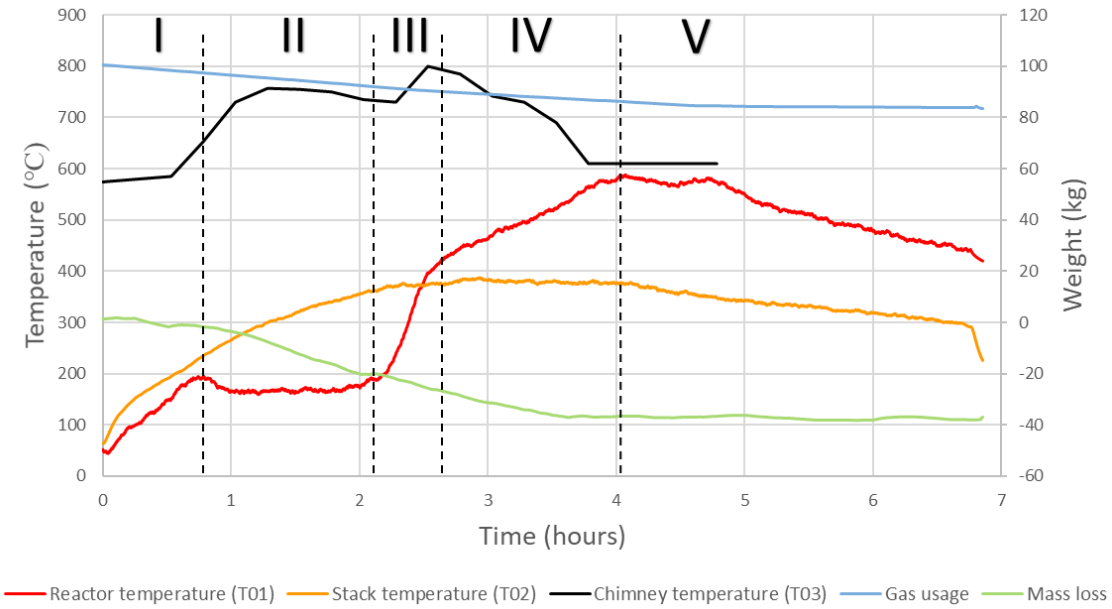

Figure 5.5: Temperature and mass as a function of time for Run 4 (600℃). Temperatures are the centre of the reactor, the bottom of the stack and above the flare. Masses are the reactor mass, showing the loss in mass as wood chips convert to char, and the LPG tanks, showing the fuel use in heating the reactor and augmenting the flare. The vertical dotted lines indicate the non-specific boundaries between stages of operation, I (dehydration), II (endothermic), III (exothermic 1), IV (exothermic 2) and V (cool-down).

Table 5.7: Run 4 mass measurements of initial wood (air dry basis) and the char at the end of pyrolysis (start of cool-down) and after cool-down. Yield is given in a moisture-free basis.

Wood chips (kg)	Initial moisture content	Mass loss during pyrolysis (kg)	Char weight after cooling (kg)	Yield during pyrolysis (%)	Yield after cooling (%)	Total gas usage (kg)
56,83	11,20	39,60	14,08	34,14	27,90	15,80

Yield after pyrolysis is calculated as the remaining mass after pyrolysis divided by the wood feedstock on a dry-basis, i.e., (56,83-39,6)/(56,83×(1-0,112)) = 0,3414.

Table 5.8: Operating strategy for Run 4.

- The main burner was turned off at 350°C. This means the LPG flow was stopped, but the air flow continued to be directed into the combustion chamber and was not dumped externally as occurred in Runs 2 and 3.

• The pilot burner was always on. • The flare was turned off after it had been stable at 610°C for 1 hour (from 3:45 to 4:45 hours in the experiment) and when the reactor temperature started to drop. This means that the LPG flow was stopped, and the air flow was stopped because the blower also turns off.

Table 5.9: Major observations for Run 4.

• Pyrolysis progressed through the well-defined stages I, II and III seen in Runs 2 and 3, but here had an additional stage IV characterized by continued rise in reactor temperature from 400 to 600°C. • Opening air vents in the base of the chimney reduced the CO concentration.

Table 5.7 gives the mass balance for Run 4. In this experiment, 56,83 kg of wood chips with an average moisture content of 11,2% produced char with yields, on a moisture-free basis, of 34,14% at the end of the trial and 27,90% after 24 hours of cool-down. As in the previous runs, great attention was taken to avoid air getting in contact with the hot char. The internal lid was hooked very strongly into its bayonet fittings and all the possible gaps throughout the reactor were covered by aluminum tape. However, some ash could be seen over the char, which means that air was still getting inside the reactor. That said, the first yield follows the expected trend, slightly lower than Runs 2 and 3, due to the higher HTT.

Figure 5.5 shows the temporal changes in temperature and mass for Run 4, and Table 5.9 details the major observations of the experiment. The first 2:30 hours of Run 4 behaved similarly to the previous runs, progressing through stages I, II and III as previously described. However, here, a new stage IV is seen, beginning at 400°C. Instead of the inner reactor temperature (T01) reaching a plateau around 400°C, it kept increasing, albeit at a lower rate, until almost 600°C. This result highlights the effectiveness of blowing air in to promote partial combustion of the pyrolysis gases in the chamber. The fact that stage IV has a lower rate of temperature increase also suggests that the reaction mechanism at higher temperatures is different. After 4

hours and 45 minutes the cooling stage began. Notably, the reactor temperature cooled faster than for Runs 2 and 3, decreasing from 600°C to 400°C over the last two hours of the experiment. This probably relates to the higher HTT, expected to result in a purer char with less volatile matter content (Section 7.1).

The TESTO 350 gas analyzer was again used to measure the carbon monoxide (CO) concentration at the top of the chimney. The results are shown in figure 5.6. The analyzer worked well during the experiment, noting that CO concentrations over 5.000 ppm are beyond the range of the analyser. Samples were taken each 15 minutes, because the gas analyzer had to be recalibrated after each measurement. During stage I (drying phase), the CO concentration was 0 ppm, which was expected as the mass loss is mostly water vapour. It is also likely that small amounts of CO evolved will be absorbed into the water, which is condensed out before the gas analyser. The solubility of CO in water at 18°C is 0,03 g/kg water. Similarly to Run 3, stage II yielded high CO concentrations, beyond the instrument limit of 5.000 ppm, which again indicates that the flare system was not capable of completely combusting the VOCs. This excessive CO concentration persisted through stage III. When the flare temperature (T03) reached 800°C at 2:40 hours, a visibly great amount of smoke was being released. To improve flare combustion, the air vents in the bottom of the chimney were fully opened (see Figure 3.7). When this was done, the CO concentration dropped to 1.500 ppm, within emission limits (<2.400 ppm). While this had the desired effect, adding extra air must be done carefully as the flare also needs to remain above 750°C to ensure destruction of all PICs (Note: PICs are the VOCs plus particulate). Here, the temperature did drop below 750°C at 3:00 hours and so the vents were half-closed. The rapid cooling of the flare suggests that insulating the chimney could help retain heat. Also notable was that, when the flare temperature (T03) cooled from 800°C to 700°C, the CO concentration decreased from 1.500 to 600 ppm, then to 0 ppm when T3 later stabilised at 610°C. This stable temperature, 610°C, indicates that pyrolysis is complete, as observed in Run 3. In conclusion, from Run 3 but emphasized here with more complete CO data, improvements are needed to; (i), insulate the chimney to elevate the flare temperature; (ii), increase the air supply during stage II; (iii), increase the residence time of the gases in the chimney by

increasing the height of the chimney; and (iv), increase the turbulence of the flare combustion. The changes that were made are shown in Figure 3.7.

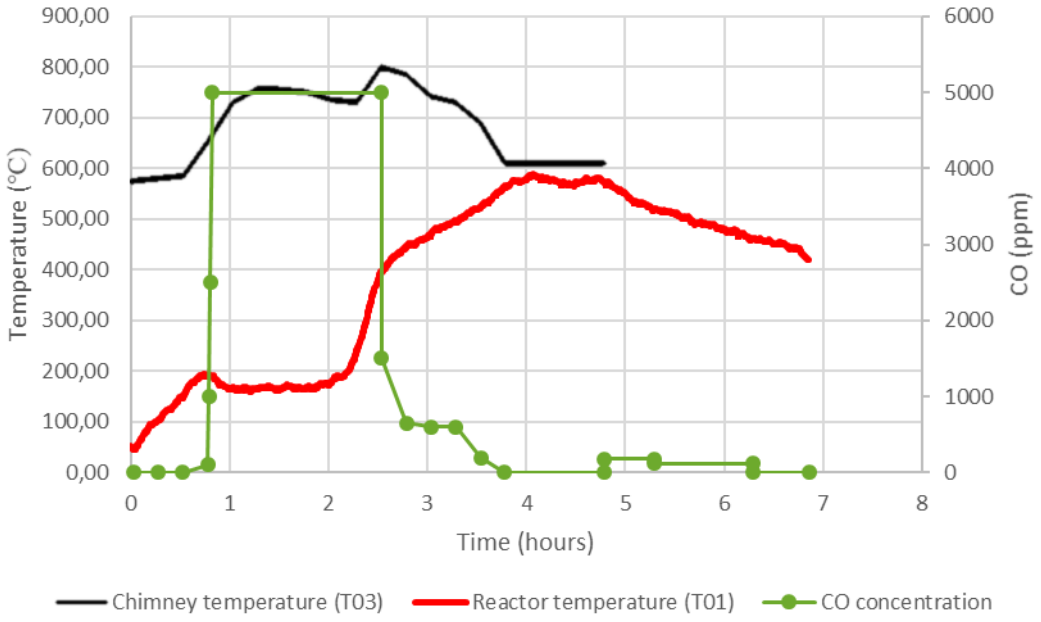

Figure 5.6: CO concentration measured using a TESTO 350 gas analyser. Values of 5.000 represent the measurement limit of the instrument. When the flare temperature reached 800℃ at ~2:40 hours, the tertiary air vents in the base of the chimney were opened. Due to the falling flare temperature, they were half-closed at ~2:50 hours.

5.5. Run 5 (600°C char)

The goals of run 5 were to attain a yet higher HTT char, as well as improve the flare performance. As demonstrated in Run 4, a 600°C HTT char was obtained by supplying air into the chamber combustion zone. However, further increases are possible because Bridges (2014) reached temperatures of char just over 700°C. Two strategies were employed. The main burner was kept on until 450°C (100°C higher than for Run 4) and additional air was provided by inserting an extra tube, carrying air from the main blower, into the chamber through the pressure-relief port (Figure 3.3). The operating strategy is given in Table 5.11. Despite these improvements, these strategies did not provide the extra benefit expected and the HTT was only slightly over 600℃ (Figure 5.7). It showed that higher HTTs are not achieved by

more heating from the main burner, but rather from additional air, and that the arrangement here was ineffective to provide that extra air.

To improve flare performance, the four actions, (i)-(iv), in Section 5.4 above were carried out. Turbulence (iv) was improved by inserting a chicken wire cage into the chimney. It was expected that this chicken wire would not only promote turbulence but would also absorb and radiate heat, helping to keep the top combustion zone hot. However, too much chicken wire was used which created an increased resistance, causing a positive back-pressure in the reactor, resulting in fugitive emissions from between the combustion zone and the bottom of the reactor, and from between the lid and the top of the reactor. This is a health and safety hazard. Therefore, to avoid this back-pressure problem, the chicken wire was removed for future trials. A further operating strategy change was to not turn the flare on until stage 1 drying was complete, indicated by the fall in peak temperature from ~200°C to ~160°C. The motivation for this was to avoid using LPG in the flare when there are no volatiles.

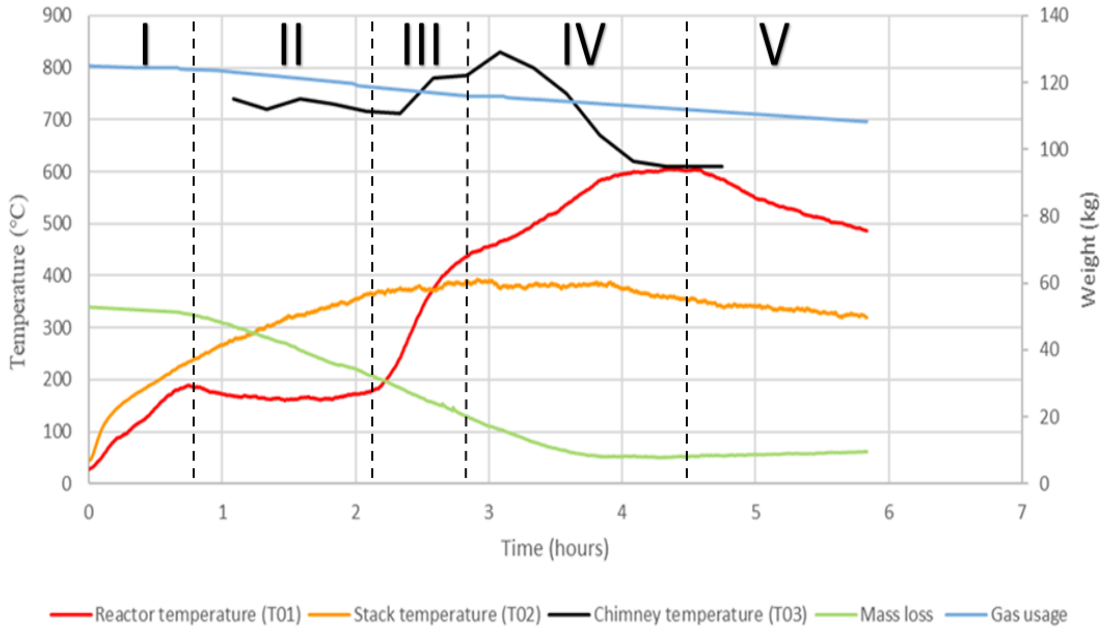

Figure 5.7: Temperature and mass as a function of time for Run 5 (600℃). Temperatures are the centre of the reactor, the bottom of the stack and above the flare. Masses are the reactor mass, showing the loss in mass as wood chips convert to char, and the LPG tanks, showing the fuel use in heating the reactor and augmenting the flare. The vertical dotted lines indicate the non-specific boundaries between stages of operation, I (dehydration), II (endothermic), III (exothermic 1), IV (exothermic 2) and V (cool-down).

Table 5.10: Run 5 mass measurements of initial wood (air dry basis) and the char at the end of pyrolysis (start of cool-down) and after cool-down. Yield is given in a moisture-free basis.

Wood chips (kg)	Initial moisture content (%wt)	Mass loss after pyrolysis (kg)	Char weight after cooling (kg)	Yield after pyrolysis (%)	Yield after cooling (%)	Total gas usage (kg)
56,70	11,50	40,64	4,40	32,00	8,77	13,80

Yield after pyrolysis is calculated as the remaining mass after pyrolysis divided by the wood feedstock on a dry-basis, i.e., (56,70-40,64)/(56,70×(1-0,115)) = 0,3200.

Table 5.11: Operating strategy for Run 5.

- The main burner was turned off at 450°C. This means the LPG flow was stopped and the air flow was directed into the combustion chamber in the manner of Run 4, rather than being dumped as occurred in Runs 2 and 3.
- A new air supply was delivered through a pipe connected to the main blower and injected through the pressure-relief port. The arrangement is shown in side elevation in Figure 4.1. This extra flow was started from the beginning of the experiment, when the bottom burners were first turned on.
- The flare was off for the first 1:10 hours, until the end of stage I where the temperature decreases from the first peak of ~200°C. The motivation here was to avoid using LPG when the flue contains no hydrocarbons needing combustion.

Table 5.12: Major observations for Run 5.

- The flare was turned on after the stage I had peaked at a reactor temperature of 200°C and was dropping to 160°C. At this point, the flue was starting to appear smoky and heavy, but quickly became clear again when the flare started.
- The chicken wire used to increase turbulence in the chimney caused a positive back-pressure and consequently smoke came out from gaps between the combustion chamber and the reactor, and the reactor and the lid.

- The mass loss rate is constant during stage I, increasing steadily through stage II, constant at its peak rate through stage III and falling steadily through stage IV.

Table 5.10 gives the mass balance of Run 5 and Table 5.12 gives the major observations of Run 5. In this experiment, 56,70 kg of wood chips with an average moisture content of 11,50% produced char with yields, on a moisture-free basis, of 32,00% at the end of the trial and 8,77% after 24 hours of cool-down. Clearly, air had short-circuited through the reactors during cool-down. It is possible that this also occurred during the late stages of the experiment, due to the yield of 32,00% being less than 34,14% in Run 4 which had a similar HTT of 600°C. The observed fugitive emissions during pyrolysis also demonstrate that the reactor was not fully sealed, and so provided evidence that air could ingress during the late stages of pyrolysis and cooldown. The chicken wire will have had no effect on this process because, during cool-down, the gas flows are low and the resistance, which is proportional to the square of velocity, is minimal. Therefore, the natural updraft combined with air leaking into the combustion chamber and the reactor lid not being securely notched into the bayonet fittings, caused short-circuiting and the observed ash formation. It must be noted that the lid is notoriously difficult to notch into the bayonet fittings.

The TESTO 350 gas analyser was not used in this experiment as it was sent away for recalibration.

The temporal plots for Run 5 of temperature and mass, shown in figure 5.7, are supported by the mass loss rate, plotted separately in figure 5.8. Run 5 exhibits the same stages I-IV as described for Run 4. During stage I drying, the mass loss rate is stable at 0,04 kg/min, which indicates that the constant temperature increase drives a relatively constant increase in pressure gradient within the wood chips, resulting in the observed constant mass loss rate. During stage II, which is the endothermic reaction phase where the pyrolysis front spreads across the reactor, the mass loss rate increases steadily to its peak at ~ 0,30 kg/min as more and more of the reactor reaches pyrolysis conditions. It then remains relatively constant at 0,30 kg/min though stage III, which is the first exothermic stage. Subsequently, in stage IV, the second

exothermic stage, it decreases steadily to reach zero as no more biomass is available to convert to char at 700°C. With no exothermic reactions taking place, the system begins to naturally cool.

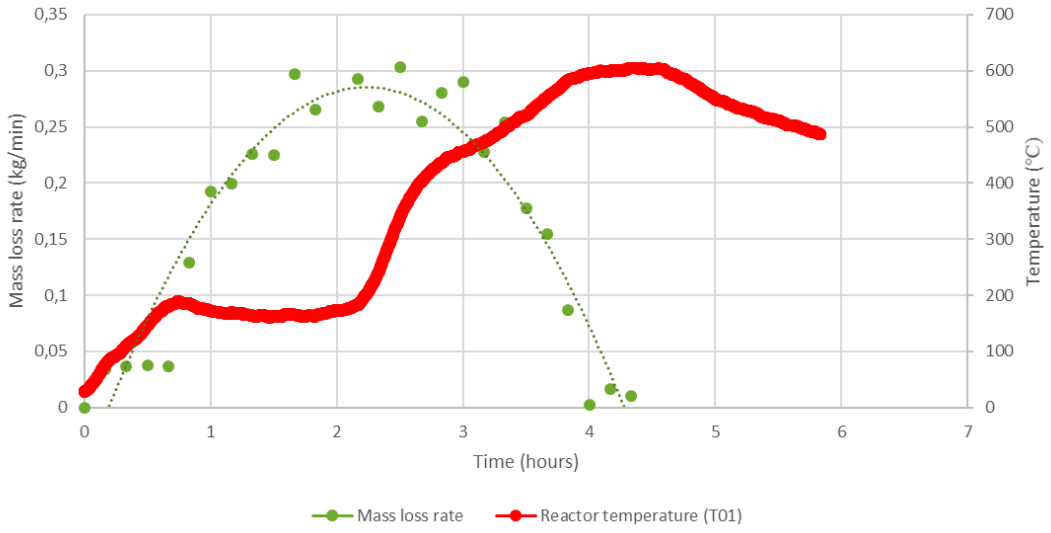

Figure 5.8: Mass loss rate for Run 5. The dotted line is a guide to represent the trend of the loss rate.

5.6. Run 6 (700°C char)

The goals of run 6 were to reach a HTT of 700°C and to improve the burning of the pyrolysis gases, using the least amount of LPG possible. The secondary air strategy of Run 5 was ineffective. Here, another approach was taken, where the pressure-relief vent shown in Figure 4.1 was disconnected to the chamber giving the access port shown in Figure 3.3), providing both an access port for air supply and a view of the combustion chamber. Two operating modes were possible, natural convection and forced convection. Natural convection relied on the system updraft to draw in air. For forced convection, a spare blower was rigged up to provide the supplementary air. As shown in Figure 5.9, the air is blown at the access port rather than injected into it. Also, as carried out in Run 5, when the main burner was turned off at 350°C, the burner air supply was not dumped, but

continued to be directed into the combustion chamber. The detail of the operating strategy is given in Table 5.14.

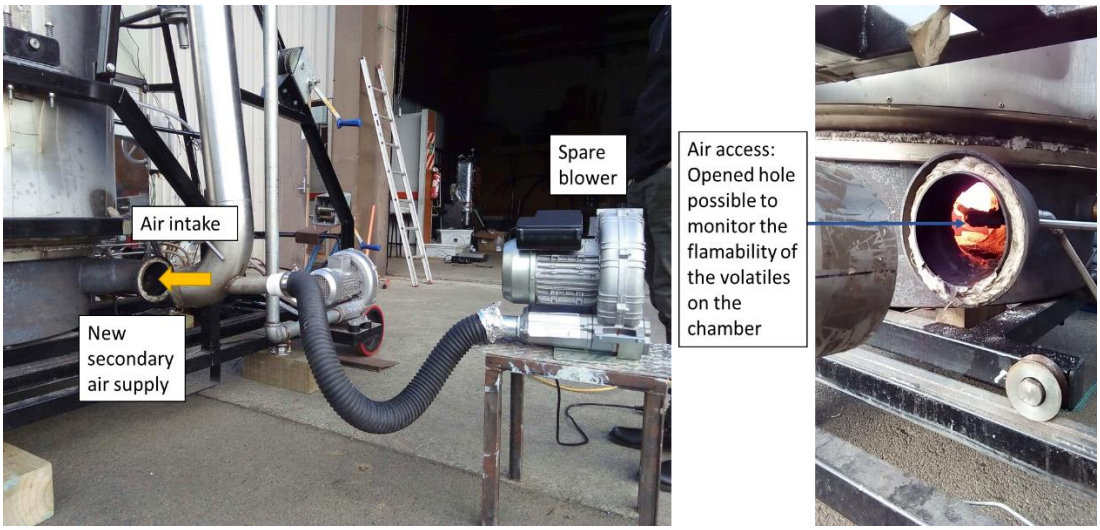

Figure 5.9: Secondary air supply system showing the disconnected pressure-relief stack and rigging of the spare blower to provide air for the forced convection mode of operation. The right figure shows the view through port into the combustion chamber.

Some trial and error experiments were carried out. In natural convection mode, some fluctuating fugitive emissions were observed coming out the access port. In forced convection mode, these were eliminated and significant improvement on the flammability could be seen, with a more expansive flame inside the combustion chamber. It was important here to not add too much air and cause net cooling, and so the temperatures of the inner reactor and the stack (T01 and T02) were monitored carefully. The optimal secondary air flow was found to be 12 m/s, set from a distance of about 40 cm, which visually gave good burning of the volatiles in the chamber, and did not affect the inner and flue stack temperatures (T01 and T02). However, the top flare temperature (T03) decreased from 900°C to around 800°C, which showed that more pyrolysis gases were being burnt in the combustion chamber, decreasing the quantity of gases needing to be combusted in the flare, but not compromising the need to keep the flare above 750°C. So, with these actions, it was concluded that the system was working more efficiently.

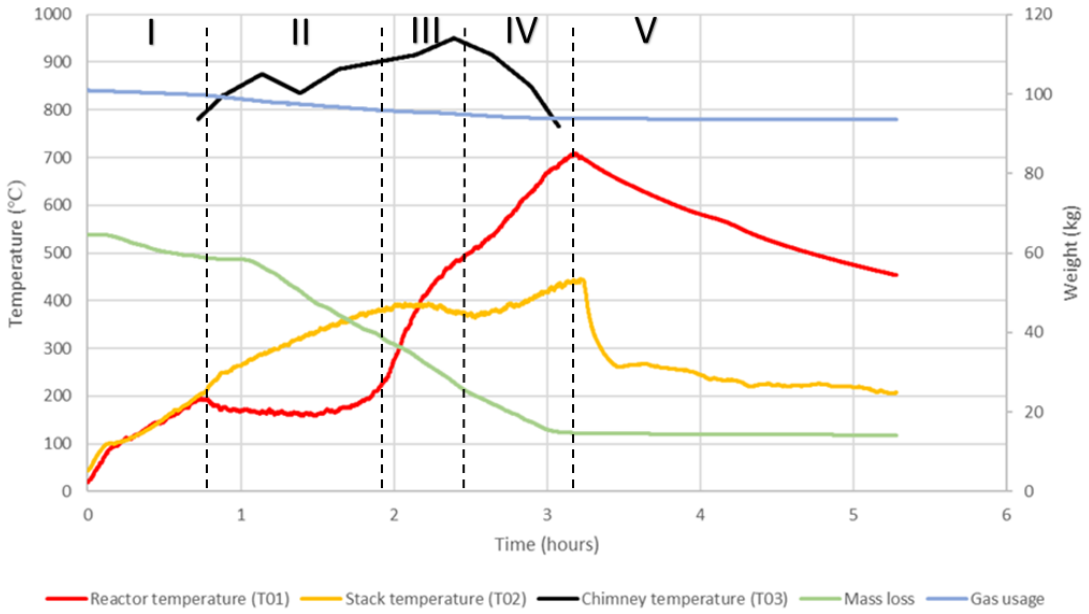

Figure 5.10: Temperature and mass as a function of time for Run 6 (700 ℃). Temperatures are the centre of the reactor, the bottom of the stack and above the flare. Masses are the reactor mass, showing the loss in mass as wood chips convert to char, and the LPG tanks, showing the fuel use in heating the reactor and augmenting the flare. The vertical dotted lines indicate the non-specific boundaries between stages of operation, I (dehydration), II (endothermic), III (exothermic 1), IV (exothermic 2) and V (cool-down).

Table 5.13: Run 6 mass measurements of initial wood (air dry basis) and the char at the end of pyrolysis (start of cool-down) and after cool-down. Yield is given on a moisture-free basis.

Wood chips (kg)	Initial moisture content (%wt)	Mass loss during pyrolysis (kg)	Char weight after cooling (kg)	Yield after pyrolysis (%)	Yield after cooling (%)	Total gas usage (kg)
54,60	11,20	40,20	12,78	29,70	26,55	8,19

Yield after pyrolysis is calculated as the remaining mass after pyrolysis divided by the wood feedstock on a dry-basis, i.e., (54,60-40,20)/(54.60×(1-0,112)) = 0,2970.

Table 5.14: Operating strategy for Run 6.

- The flare was turned on at 190°C (T01).
- The main burner was turned off at 350°C (T01). This means the LPG flow was stopped and the air flow was continued into the combustion chamber, rather than dumped externally.

• A new secondary air intake was created by removing the pressure-relief vent stack. It was operated blowing air into the port at 12 m/s using a spare blower set about 40 cm from the access port. This was continued until 550°C (T01). Thereafter, the spare blower was turned off and port was closed.

Table 5.15: Major observations for Run 6.

• Gas analysis was stymied by condensed water getting into the sampling probe. No results were obtained. • Blowing secondary air into the combustion chamber was an effective way to achieve 700°C HTT char. The optimal secondary air velocity was 12 m/s.

Table 5.13 gives the mass balance for Run 6. In this experiment, 54,60 kg of wood chips with an average moisture content of 11,20% produced char with yields on a moisture-free basis of 29,70% at the end of the trial and 26,55% after 24 hours of cool-down. The 29,70% yield at the end of pyrolysis follows the trend of falling yield for higher HTTs. Some ash formation during cool-down has resulted in further loss of yield, despite best efforts to prevent air ingress during cool-down. It is recommended that the silica rope seal be replaced regularly on the combustion chamber.

The temporal changes in temperature and mass for Run 6 are shown in figure 5.10. The reactor temperature followed the same stages as seen previously, stage I, II, II and IV, but here stage IV was extended as the HTT increased towards 700°C. Therefore, the effect of more heat recirculation is to drive the internal exothermic reaction. The fact that it must be exothermic is apparent from the stack temperature, T02, which is substantially less than the internal reactor temperature. It is noteworthy that at the time the HTT is reached, the stack temperature is some 250°C cooler. This indicates that the main benefit of the secondary combustion in the combustion chamber is not so much to drive the reaction, but rather to prevent cooling. This cooling problem is a feature of small units. Larger industrial systems, with much larger thermal mass of biomass relative to the reactor, will not have this cooling problem. Also noticeable is the increase in T2 above 400°C when the reactor core exceeds 600°C, which indicates that highly flammable gases are released right at the end of pyrolysis. At this

temperature, the gases are expected to be predominantly hydrogen and methane (Wang and Wang, 2009).

The main observations of Run 6 are given in Table 5.15. Unfortunately, the gas analyzer did not work reliably, due to water condensate at the sampling point. Visual inspection of the flue showed that it was clear, without a smoky appearance, which indicates that the system was working efficiently, and emissions were likely to be low, but this could not be confirmed. To avoid the water entering the sampling probe, a water trap was designed and installed on the gas sampling line for Run 7. The water problem is worst during stages III and IV, the exothermic phases, when more combustion was occurring in the flare and water is produced as a product of combustion.

Nevertheless, the main goal of this run was achieved, which was producing a 700°C char. This shows that precise control of the secondary air supply is crucial to drive the recycling of heat to obtain high HTT chars. Another benefit of secondary combustion in the combustion chamber is the reduced load on the flare, which helps to meet emission standards.

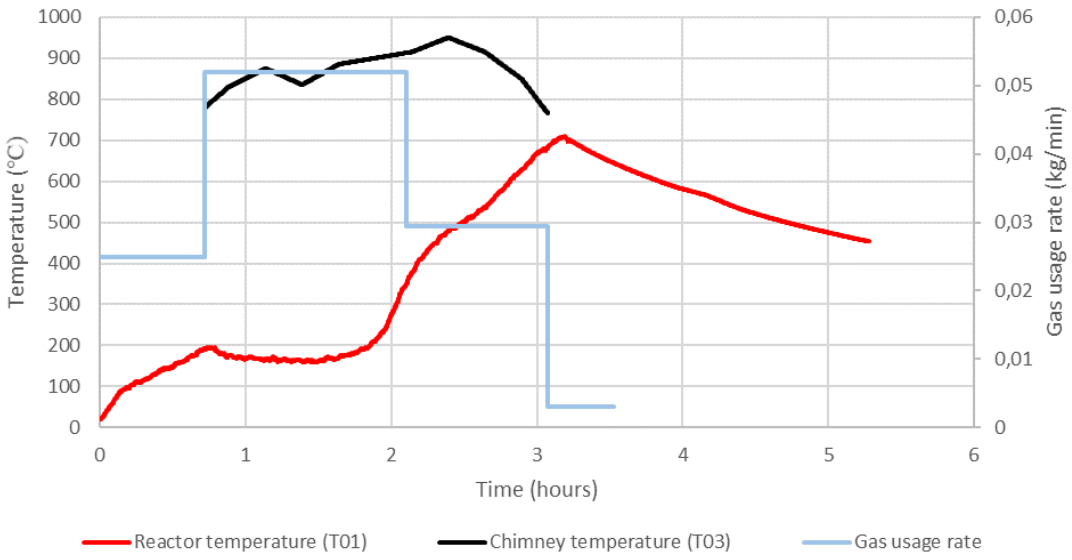

Figure 5.11: LPG usage rate during Run 6. The combustion chamber contains the main burner, 26 kW, and a pilot burner, 3,4 kW. The flare contains three burners, all 3,4 kW.

LPG is a fossil fuel and its use detracts from the overall carbon footprint of the biochar production process, to be discussed in the next chapter. Figure 5.11 shows the LPG usage rate during the experiment, planned as the optimal control strategy for the flare system. At the start of the experiment, only the two combustion chamber burners are on, consuming 0,025 kg LPG/min of LPG. The flare is not needed during this stage I drying phase, as volatiles are not being produced. When the flare is then turned on at the beginning of stage II, the total consumption increases to 0,052 kg LPG/min. When the reactor core reached 350°C (T01), the main burner was turned off, leaving the top flare burners and the pilot bottom burner consuming 0,030 kg/min. Finally, when pyrolysis is complete, i.e., no further mass loss is occurring and the reactor begins to naturally cool, the flare is switched off, leaving only the pilot burner on and the LPG consumption rate drops to 0.003 kg LPG/min. The pilot burner remained on until the system cools down from 700°C to 600°C. The reason for leaving the pilot on was safety, to provide ignition of any gases that may still be released.

5.7. Run 7 (700°C char – optimal strategy)

This was the last experiment of this work. The main goal was to make fine adjustments to the strategy of Run 6 to optimize the system for the recycling of heat and abatement of emissions. Also, it had the objective of collecting reliable emissions data to enable accurate calculation of the carbon footprint of this reactor under the conditions presented in this work.

Again, the pressure-relief stack was disconnected from the chamber to provide a port for trialing different secondary air rates and to visually monitor the flammability of the pyrolysis gases. It was noticed that during stage II, the pyrolysis gases were not flammable enough to combust. The reason is not known but could be speculated to be the combined effect of high inert load of CO2 and water vapour, and a possible adsorptive effect of sooty particulate on available oxygen. To avoid this non-flammability zone, the secondary air was blown into the chamber from the beginning

of stage III, just when the exothermic phase started and the gases were noticeably more flammable. The optimal secondary air speed was around 12 m/s. Also, to facilitate greater combustion of the gases in the flare, the vents of the chimney were left fully open until, towards the end of pyrolysis, they were half closed when the temperature of the chimney dropped under 750°C. The details of the operating strategy are given in Table 5.17.

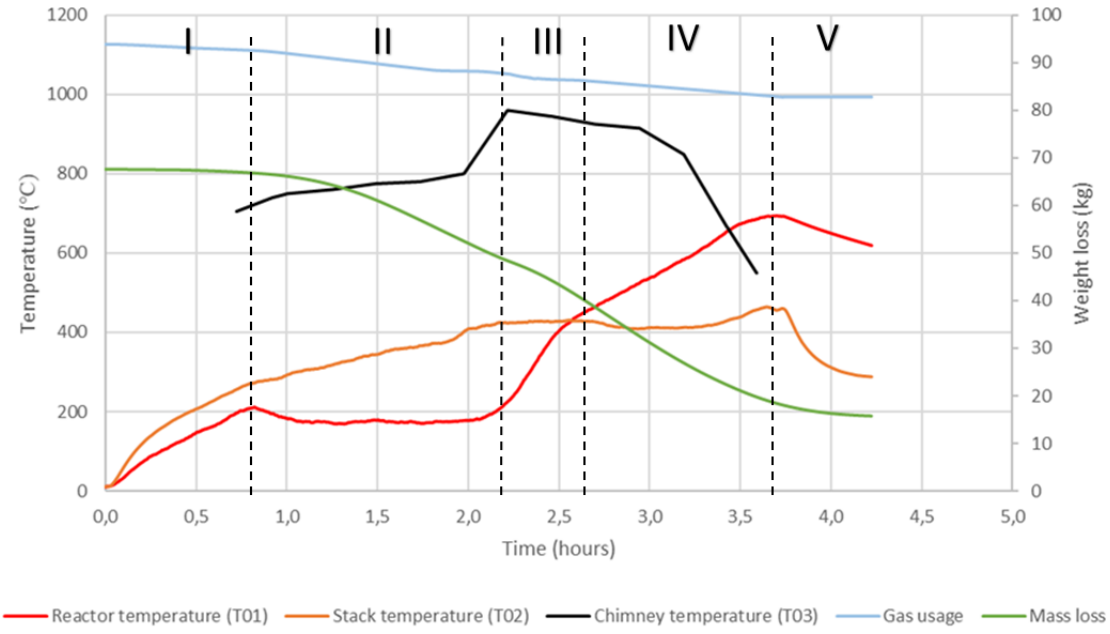

Figure 5.12: Temperature and mass as a function of time for Run 7 (700℃). Temperatures are the centre of the reactor, the bottom of the stack and above the flare. Masses are the reactor mass, showing the loss in mass as wood chips convert to char, and the LPG tanks, showing the fuel use in heating the reactor and augmenting the flare. The vertical dotted lines indicate the non-specific boundaries between stages of operation, I (dehydration), II (endothermic), III (exothermic 1), IV (exothermic 2) and V (cool-down).

Table 5.16: Run 7 mass measurements of initial wood (air dry basis) and the char at the end of pyrolysis (start of cool-down) and after cool-down. Yield is given on a moisture-free basis.

Wood chips (kg)	Initial moisture content (%wt)	Mass loss during pyrolysis (kg)	Char weight after pyrolysis (kg)	Yield after pyrolysis (%)	Yield after cooling (%)	Total gas usage (kg)
51,80	10,20	37,60	14,2	30,53	26,71	10,15

Yield after pyrolysis is calculated as the remaining mass after pyrolysis divided by the wood feedstock on a dry-basis, i.e., (51,80-37,60)/(51,80×(1-0,102)) = 0,3053.

Table 5.17: Operating strategy for Run 7.

- The main burner was turned off at 350°C. This means the LPG flow was stopped and the air flow was continued into the combustion chamber, rather than dumped externally.
- The new secondary air flow, using the spare blower and directed through the pressure-relief port, was started at the onset of stage III, i.e., the exothermic reaction phase (at about 2 hours).
- The new secondary air flow was stopped, subsequent to the HTT being surpassed, when the top chimney temperature (T03) dropped below 600°C.
- The flare was turned on when reactor temperature (T01) started to decrease after stage I (drying phase). The flare was switched off at the end of the experiment, when T1 begins to cool down after surpassing the highest HTT.
- The vents in the base of the chimney, were closed until the flare was switched on, then fully opened. Later, after the HTT had been reached, they were half closed when the top of the chimney temperature (T03) decreased to 750°C.

Table 5.18: Major observations for Run 7.

- The optimal period of secondary air input was found to be during the stages III and IV, due to the better flammability of the volatiles released throughout the exothermic phase. Doing this avoids possible cooling of the system from blowing air into the combustion chamber during stage II, when the volatiles are still not flammable enough.

- The flare is capable of complete combustion of the off-gases in the chimney. It is potentially consuming more LPG than needed for doing so, giving opportunity for further improvement of gas usage.

Table 5.16 shows the mass balance for Run 7. In this experiment, 51,80 kg of wood chips with an average moisture content of 10,2% produced char with yields, on a moisture-free basis, of 30,53% at the end of the pyrolysis and 26,71% after 24 hours of cool-down. The pyrolysis yield was slightly better than Run 6 which had the same 700°C HTT and, as expected, was lower than the earlier runs with lower HTTs. The continued problem with air short-circuiting underlines the need to develop a more effective lid sealing system (the bayonets are hard to engage), and to seal all the gaps around the reactor, with special attention to interface between the combustion chamber and the reactor. These problems are partly related to the research nature of the pyrolyser but, nevertheless, give some guidance about how to design commercial units.

Figure 5.12 gives the temporal change in temperatures and masses for Run 7. The reactor temperature profile (T01) followed the same stages I-IV as described for all the previous runs. Similarly to Run 6, it has an extended stage IV, as the same HTT of 700°C was achieved, and also exhibited the same curious elevation in the stack temperature (T02) during the final stages of pyrolysis.

The Testo 350 gas analyser was used to sample the gases at the top of the flare. Concentrations of CO, NOx and a general hydrocarbon, CxHy were obtained, as shown in Figure 5.13. The generalized hydrocarbon will be mostly methane. In addition to using a water trap, the gas analyser was flushed between samples in order to ensure the sampler was dry and so avoid condensation inside the instrument.

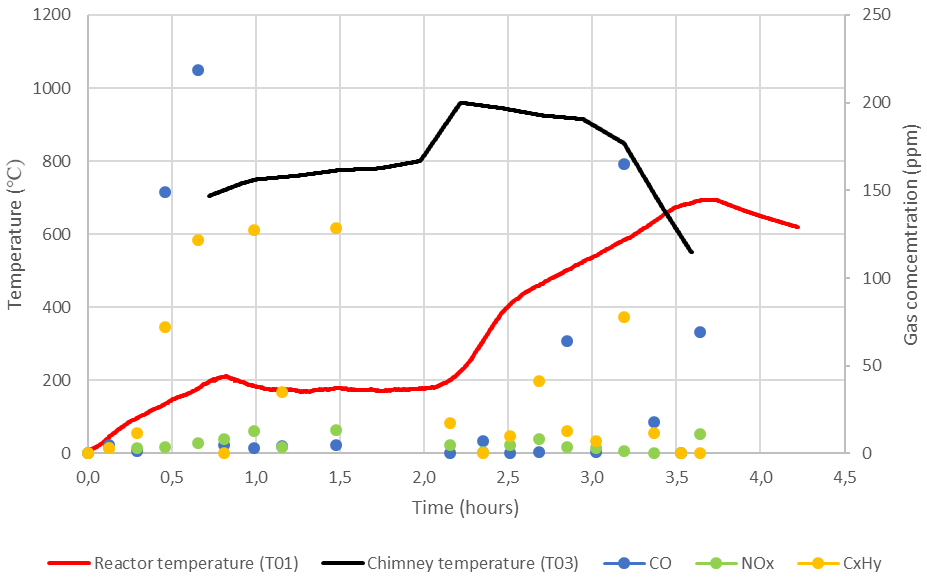

Figure 5.13: Concentrations of carbon monoxide (CO), generalized hydrocarbon (CxHy) and generalized nitrogen oxides (NOx) measured at various times during Run 7 with the reactor (T01) and flare (T03) temperatures shown to indicate the progress of decomposition.

The emissions relate to the operating strategy in Table 5.17. In stage I, the flare is off and initially only drying occurs, but towards the end of this stage, the wood chips nearest the wall begin to pyrolyse and emit products of incomplete combustion (PICs). Consequently, the CO and CxHy concentrations rise until the flare is turned on. During stage II, all burners are on and the vents in the bottom of the chimney are fully open. Hydrocarbon is detected at ~140 ppm, although CO is very low at ~10 ppm, which indicates that the flare is only just managing to effectively combust the PICs. At the onset of stage III, as the reactor temperature begins to rise, secondary air was injected through the pressure-relief port using the spare blower. The benefit of the additional air is reflected in the hydrocarbon concentration, which drops to less than 20 ppm. During stage III, the control set-point of 350°C is reached, and the main burner is switched off, after which its air supply continues to be blown into the combustion chamber. Therefore, only the pilot burner flame is available to cause ignition of the pyrolysis gases; the consequence is a slight increase through stage IV in the CO and hydrocarbon concentrations. At no time, however, do they exceed the stack emission limit of 2.400 ppm set by the US EPA for biomass suspension burners greater than 3 MW. Indeed, they even better the limits for fluidized bed biomass burners of 230 ppm

CO (Federal Register, 2015). Therefore, in conclusion, the operating strategy of Run 7 successfully abates the emissions.

5.8. Chapter 5 - Summary

Chapter 5 has detailed each of the seven trials of the 60 kg Massey pyrolyser. The first of these, the test run, confirmed that the pyrolysis front spreads across the reactor, from the heated wall towards the central perforated core. Runs 2-7 showed that different HTTs were attainable, here nominally 400, 600 and 700°C, by adjusting the operating parameters. They also showed that the new flare system, after modification in this work, is capable of reducing emissions to well within limits as defined by US EPA for suspension burners and indeed betters the limits for fluidized bed biomass burners. Furthermore, Runs 2-7 all followed the same reactor core temperature profile, progressing through four stages, I-IV, followed by cooling. The similarities between these stages are analysed in more detail in Chapter 6, together with proximate and ultimate analyses of the char, and a discussion of the effective of heat transfer within the reactor. Chapter 6 uses the data collected here to determine the net sequestration for biochar manufacture in this reactor. The findings have implications for small-scale biochar production in general.

Chapter 6 - Carbon Balance

The calculations applied in this section aim to provide an accurate carbon balance of the best-case experiment (Run 7). The reason for selecting Run 7 is that the monitoring of the stack gases was complete, which means the carbon footprint can be accurately determined alongside emissions compliance. The calculations are therefore able to be applied to all future trials.

Different methods of carbon footprint analysis were considered. The Massey pyrolyser contains different mass flow sources interacting simultaneously, such as burners, secondary and tertiary air supply, and pyrolysis gases. However, mass is recorded collectively, as the reactor weight change (i.e., loss of biomass) and the LPG tanks weight change (i.e. usage of gas), and air flow is not recorded. Therefore, it is not possible to determine the individual mass inflows. The way around this is to calculate the carbon balance, because air does not contain carbon, and the averaged carbon content of the LPG (mixture of propane and butane) is known, as is the carbon content of the wood. Furthermore, for the purpose of establishing the environmental impact, it is assumed that all carbon leaving the system from wood and LPG is either CO2, CO or CH4, which are recorded by gas analysis where the methane represents the overall hydrocarbon release.

The carbon quantity in the wood and char was obtained from elemental laboratorial analysis (see Chapter 7.1). The net carbon footprint is then the carbon left in the char, minus the carbon used in the LPG and the emitted carbon weighted to its additional global warming potential, that is, its impact additional to that of CO2. This methodology will be explained in the following sections.

6.1. Theoretical calculations

The wood mass added to the reactor, $M_{air\text{-}dried}$ [kg], is air dried and has an oven-dried mass, $M_{oven\text{-}dried}$ [kg]

The moisture content is m_w, the fraction of moisture on an oven-dried basis

$$m_w = \frac{M_{air-dried} - M_{oven-dried}}{M_{oven-dried}} \quad \left[\frac{kg\ water}{kg\ wood}\right]$$

The oven dried wood has an ash content, measured by proximate analysis as the residual on ignition (ROI) (see §7.1)

$$m_{ash,wood} = \frac{M_{residual\ on\ ignition}}{M_{oven-dried}} \quad \left[\frac{kg\ ash}{kg\ wood}\right]$$

Ultimate analysis, using the elemental analyser (see §7.1), gives the fractional amounts of carbon, hydrogen and by difference oxygen in the wood, such that

$$m_{carbon} + m_{hydrogen} + m_{oxygen} + m_{ash} = 1$$

Thus, the mass of carbon in the load charged to the reactor is

$$M_{carbon,wood} = m_{carbon} M_{oven-dried} = m_{carbon}\left(\frac{M_{air-dried}}{1 + m_w}\right) \quad [kg]$$

When running the reactor, LPG is used. This is a 50:50 mixture of propane and butane on a mass basis. These evaporate at slightly different rates so when with a full tank the mix is rich in propane and near empty the mix is rich in butane. However, we assume that the mix is always 50:50. Propane is C3H8, with molecular weight of 44,1 g mol^{-1}. Butane is C4H10 with molecular weight 58,12 g mol^{-1}. For our purposes 44 and 58 are accurate enough. Thus a 50:50 mixture will have a mean molecular weight of 51 and the mass fraction of carbon will be

$$\frac{(3 \times 12 + 4 \times 12)}{(3 \times 12 + 8 + 4 \times 12 + 10)} = 0{,}8235$$

Thus, the amount of carbon used is this fraction of the LPG used

$$C_{LPG} = 0{,}8235 M_{LPG} \quad [kg\ carbon]$$

At the end of pyrolysis, the reactor contains char. The raw measured mass of this char is M_{char}. Proximate analysis measures its volatile matter content (VM). This was done following the procedure described on the international ASTM for Chemical Analysis of Wood Charcoal (see §7.1), which results in

$$m_{VM} + m_{FC} + m_{ash,char} = 1$$

Ultimate analysis by the elemental analyser give the fractions of carbon, hydrogen and oxygen by difference (see §7.1), giving the mass balance

$$m_{carbon,char} + m_{hydrogen,char} + m_{oxygen,char} + m_{ash,char} = 1$$

The carbon remaining in the char is

$$C_{char} = M_{char} m_{carbon,char}$$

Alternately, some use the fixed carbon value; $C_{char} = M_{char} m_{FC}$. They are not the same, but this method is older, before elemental analysers were available. Here we are considering the actual carbon content. However, the elemental analyser also includes the inorganic carbon, which goes into the environment as carbonate and is used for plants growth. Although it is not sequestered carbon, the amount is small and so it still included in this calculation. This assumption is helped by the low ash content of pine wood.

The maximum possible sequestration is the carbon in the char minus the carbon used in the LPG. In this case, all emissions are considered to be CO2 only, i.e., assuming no additional global warming potentials.

$$Seq_{max} = M_{char} m_{carbon,char} - 0{,}8235 M_{LPG} \quad [kg]$$

Or it can be expressed as a sequestration percentage conversion from the biomass carbon

$$Seq_{max}{}' = \frac{M_{char} m_{carbon,char} - 0{,}8235 M_{LPG}}{m_{carbon} M_{oven-dried}} \times 100 \quad [\%]$$

Note that the electrical input of running the blowers is not included in the carbon footprint calculations.

The carbon from the biomass is emitted during pyrolysis. In the perfect scenario, when the flare is operating perfectly, this carbon (and that from the auxiliary fossil fuel) will be emitted as CO2. If any carbon is emitted as anything other than CO2, then it has an additional global warming potential that detracts from the net sequestration of the carbon balance. This also applies to any NOx formed during combustion, and SOx. However, both are negligible in our system, so are not included (SOx because there is only a trace amount of sulphur in pine wood, and NOx because the flare temperature is controlled well below the onset of NOx formation). Here, we considered the most conservative values from the IPCC fifth assessment report (IPCC, 2014) which are GWP = 1 for CO2, GWP = 18,6 for CO and GWP = 84 for CH4, noting that the 20-year horizon figures are used, chosen because 20 years is within the career span of most workers. The Testo 350 gas analyser measurement yields a hydrocarbon concentration (HC). Because the flare is effective in cracking most products of incomplete combustion, the hydrocarbon must be assumed to be methane, carrying the greater GWP. This provides the most conservative calculation.

The effect of CO and CH4 is to produce additional CO2 emissions equivalent to their mass emitted multiplied by (GWP-1). Thus, the net sequestration, in kg, becomes

$$Seq_C = M_{carbon,char} - M_{carbon,LPG} - M_{carbon,CO}(GWP_{CO} - 1) - M_{carbon,CH4}(GWP_{CH4} - 1) \quad [kg]$$

Where M_{CO} and M_{CH4} are the masses of CO and CH4 released over the experiment.

Or, as a sequestration conversion from the biomass carbon

$$\frac{Seq_C}{M_{carbon,wood}} \quad [\%]$$

In order to determine Seq_C , the quantities M_{CO} and M_{CH4} need to be calculated from the gas analyser results which are point measurements of concentration in parts per million of the overall stack gas flowrate. For that, it is necessary to find the total mass flow of the system. Because the air inflow is unknown, this is done with respect to the carbon.

To find the mass flow of the process, the first step is to calculate the mass of carbon in the emissions. From the overall carbon balance

$$M_{carbon,wood} + M_{carbon,LPG} = M_{carbon,char} + M_{carbon,emission}$$

Consequently,

$$M_{carbon,emission} = M_{carbon,wood} + M_{carbon,LPG} - M_{carbon,char} \quad [kg]$$

Then, it needs to be transformed in moles of carbon where the molecular weight $M_{w,carbon}$ is 12 g/mol

$$N_{carbon,emission} = \frac{M_{carbon,emission}}{M_{w,carbon}} 1000 \quad [moles]$$

From that, it can be calculated the total moles of gas released during experiment

$$N_{exhaust} = \frac{N_{carbon,emission}}{n_{carbon,emission}} \quad [moles]$$

Where the mole fraction of carbon in the emission, $n_{carbon,emission}$, is

$$n_{carbon,emission} = \left(\frac{C_{CO2}[\%]}{10^2} + \frac{C_{CO}[ppm]}{10^6} + \frac{C_{CH4}[ppm]}{10^6}\right)[-]$$

The concentration units refer to the gas analyser output for each quantity averaged over the experiment (see §7.6), where the CO2 concentration is a volume fraction, and CO and CH4 are parts per million on a molar basis. Each term, therefore, is mole fraction of each gas: CO2, CO and CH4, which can be described by $n_{CO2,emission}$, $n_{CO,emission}$, and $n_{CH4,emission}$.

Therefore, the total mass of gas leaving the stack over the duration of the experiment is

$$M_{exhaust} = \frac{N_{exhaust} M_{w,gas}}{1000} \quad [kg]$$

Where $M_{w,gas}$ is the average molecular weight of the exhaust gas. The exhaust is a combustion gas, and so an average molecular weight of 32 g/mol can be assumed. Averaged over the experiment, the average stack gas flow is

$$\dot{M}_{exhaust} = \frac{\frac{N_{exhaust} M_{w,gas}}{1000}}{\Delta t_i} \quad \left[\frac{kg}{s}\right]$$

Where Δt_i is the total time of the experiment in seconds. Exhaust gas flow, however, does change within the experiment as the volatiles evolution from the biomass is variable. It is not needed for the mass balance.

The emitted mass of carbon from each gas (CO2, CO and CH4) is

$$M_{carbon,CO2} = n_{CO2,emission} N_{exhaust} \frac{M_{w,carbon}}{1000} \quad [kg]$$

$$M_{carbon,CO} = n_{CO,emission} N_{exhaust} \frac{M_{w,carbon}}{1000} \quad [kg]$$

$$M_{carbon,CH4} = n_{CH4,emission} N_{exhaust} \frac{M_{w,carbon}}{1000} \quad [kg]$$

The impact on the net sequestration of these gases is that which is additional to being emitted as simply CO2. This additionality is defined by GWP-1, so therefore only applies here to CO and CH4. Here, the most conservative values are used, published in the Fifth Assessment Report (AR5) of the United Nations Intergovernmental Panel on Climate Change (IPCC, 2014), which are 18,6 for CO and 84 for CH4, for a 20-year horizon.

In this way, the net sequestration given above is able to be calculated

$$Seq_C = M_{carbon,char} - M_{carbon,LPG} - M_{carbon,CO}(GWP_{CO} - 1) - M_{carbon,CH4}(GWP_{CH4} - 1) \quad [kg]$$

6.2. Carbon footprint of run 7 – Scenario with abatement of emissions

Run 7 loaded 51,8 kg of wood chips with average moisture content of 10,2%, which was converted into 14,2 kg of char (weight before cooling). The elemental analysis of pine wood chips gives an average value of 51,5% of carbon (Bridges, 2014) and the

analysis of the char of run 7 resulted on average to have 94% carbon content (figure 7.1). Also, 10,15 kg of LPG was used.

The average concentration of the greenhouse gases CO2, CO and CH4 measured during experiment were 1.096%, 32 ppm and 51 ppm, respectively.

The maximum sequestration of this experiments is

$$Seq_{max} = M_{char} m_{carbon,char} - 0.8235 M_{LPG} \quad [kg]$$

$$Seq_{max} = (14{,}2)(0{,}94) - (0{,}8235)(10{,}15) = 4{,}99 \ kg$$

The mass of carbon loaded in the reactor is

$$M_{carbon,wood} = m_{carbon} M_{oven-dried} = m_{carbon} \left(\frac{M_{air-dried}}{1 + m_w} \right) \quad [kg]$$

$$M_{carbon,wood} = 0{,}515 \left(\frac{51{,}8}{1 + 0{,}102} \right) = 24{,}2 \ kg$$

Then, the carbon balance gives the mass of carbon contained in the gaseous emissions

$$M_{carbon,wood} + M_{carbon,LPG} = M_{carbon,char} + M_{carbon,emission}$$

$$24{,}2 + (0{,}8235)(10{,}15) = (14{,}2)(0{,}94) + M_{carbon,emission}$$

$$24{,}2 + 8{,}3585 = 13{,}34 + M_{carbon,emission}$$

$$M_{carbon,emission} = 19{,}21 \ kg$$

As moles of carbon, this is

$$N_{carbon,emission} = \frac{M_{carbon,emission}}{M_{w,carbon}} 1000 = \frac{19{,}21}{12} \times 1000$$

$$N_{carbon,emission} = 1.608{,}83 \ moles \ of \ C$$

Knowing that the average off-gases concentration is 1,096% to CO2, 32 ppm to CO and 51 ppm to CH4, putting everything in a percentage scale, it gives

$$n_{carbon,emission} = \frac{1.096}{100} + \frac{32}{10^6} + \frac{51}{10^6} = 0{,}01104 or\ 1{,}104\%$$

From that, the total moles of gas is

$$N_{exhaust} = \frac{1.608{,}83}{0{,}01104} = 145.727{,}35\ moles\ of\ gaseous\ emissions$$

As the molar weight of the combustion gas is about 32, the total mass of gaseous emissions is

$$M_{exhaust} = \frac{N_{exhaust} M_{w,gas}}{1000} \quad [kg]$$

$$M_{exhaust} = \frac{145.727{,}35\ \times 32}{1000} = 4660 \quad [kg]$$

When considered as an average flue gas flowrate, it is

$$\dot{M}_{total\ mass} = \frac{\frac{N_{exhaust} M_{w,gas}}{1000}}{\Delta t_i} \quad \left[\frac{kg}{s}\right]$$

$$\dot{M}_{total\ mass} = \frac{\frac{145.727{,}35\ \times 32}{1000}}{12.600} = 0{,}37 \left[\frac{kg}{s}\right]$$

Thus, it is possible to calculate the contribution of carbon from each gas emitted

$$M_{carbon,CO2} = n_{CO2,emission} N_{exhaust} \frac{M_{w,carbon}}{1000} \quad [kg]$$

$$M_{carbon,CO} = n_{CO,emission} N_{exhaust} \frac{M_{w,carbon}}{1000} \quad [kg]$$

$$M_{carbon,CH4} = n_{CH4,emission} N_{exhaust} \frac{M_{w,carbon}}{1000} \quad [kg]$$

Inserting the values yields

$$M_{carbon,CO} = \frac{32}{10^6} \times 145.727{,}35 \times \frac{12}{1000} = 0{,}056\ kg\ of\ C$$

$$M_{carbon,CH4} = \frac{51}{10^6} \times 145.727{,}35 \times \frac{12}{1000} = 0{,}089\ kg\ of\ C$$

$$M_{carbon,CO2} = \frac{1{,}096}{100} \times 145.727{,}35 \times \frac{12}{1000} = 19{,}17\ kg\ of\ C$$

To calculate the final carbon footprint, it is necessary to consider the GWP potential of each gas. The values are 18.6 for CO and 84 for CH4, in a CO2 equivalent basis, 20 years horizon (IPCC, 2014).

$$M_{GWP\ deduction\ as\ C} = M_{carbon,gas} GWP_{gas}$$

For CO:

$M_{GWP\ deduction,CO\ as\ C} = 0{,}056 \times 18{,}6$ = 1,04 kg of C as CO2 equivalent

For CH4:

$M_{GWP\ deduction,CH4\ as\ C} = 0{,}089 \times 84$ = 7,476 kg of C as CO2 equivalent

As the effect of CO and CH4 is to produce additional CO2 emissions equivalent to (GWP-1), the net sequestration of the system becomes

$$Seq_C = M_{carbon,char} - M_{carbon,LPG} - M_{carbon,CO}(GWP_{CO} - 1) - M_{carbon,CH4}(GWP_{CH4} - 1)$$

$$Seq_C = 13{,}34 - 8{,}3585 - 0{,}056(17.6) - 0{,}089(83) = 13{,}34 - 16{,}73 = -3{,}38\ kgC$$

$$Seq_C = -3{,}38\ kgC$$

The sequestration conversion from the biomass carbon is

$$\frac{Seq_C}{M_{carbon,wood}} = \frac{-3{,}38}{24{,}2} = -0{,}14\ \left[\frac{kgC}{kgC_{wood}}\right] or -\ 14\%$$

This result highlights the difficulty in sequestrating carbon in batch pyrolysis. In run 7, even with the after-burning flare system optimized as described in chapter 5, no carbon sequestration was obtained. The net carbon footprint was – 3,38 kg, which means that while 13,34 kg of carbon was sequestered in the char, an amount, 16,73 kg of CO2eq, left the system. As can be seen, the additional emission effect of the greenhouse gases, CO and CH4, was significant, representing half of the equivalent emission. While their concentrations were well within stack emissions limits, their global warming potential multiplying factor (GWP-1) ensured that they have a large impact on the overall carbon footprint, to the extent that here, despite a good operating strategy, no net sequestration occurred. The next calculations investigate two scenarios, by operating the reactor without the flare, i.e., no emissions abatement, or in the perfect scenario, with total oxidation of all combustion gases to CO2 and H2O.

6.3. Scenario without abatement of emissions

In order to sample the raw emissions when producing biochar in the Massey 60 kg pyrolyser, the flare burners were turned off periodically. In this no abatement scenario (without flaring) the average concentration of each gases was 1,18% for CO2, 5655 ppm for CO and 1707 ppm for CH4 (estimation shown in figure 6.5).

In run7, the flare system worked for 177 minutes. Knowing by measurement that the gas use rate of the three flare burners together is 0,027 kg/min, the amount of gas consumed by the flare system was: 0,027 x 177 = 4,78 kg. This represents the amount of carbon saved if the flare were not operated, and so in this scenario it just needs to be deducted from the total LPG usage.

As the total LPG consumed was 10,15 Kg, the gas consumption without flaring is

$$M_{carbon,LPG,no\ abatement\ scenario} = M_{carbon,LPG} - M_{carbon,LPG,flare}$$

$$M_{carbon,LPG,no\ abat*} = 10{,}15 - 4{,}78 = 5{,}37\ kg$$

The mass of carbon in the gas is

$$M_{carbon,LPG,no\ abat*} = 0.8235 M_{LPG} \quad [kg\ of\ Carbon]$$

$$M_{carbon,LPG,no\ abat*} = (0{,}8235)(5{,}37) = 4{,}42\ kg\ of\ C$$

The maximum sequestration in this scenario is

$$Seq_{max} = M_{char} m_{carbon,char} - M_{carbon,LPG,no\ abat*} \quad [kg\ of\ Carbon]$$

$$Seq_{max} = (14{,}2)(0{,}94) - 4{,}42 = 8{,}93\ kg\ of\ C$$

The mass of carbon in the gaseous emissions is

$$M_{carbon,wood} + M_{carbon,LPG,no\ abat*} = M_{carbon,char} + M_{carbon,emission}$$

$$24{,}2 + 4{,}42 = 13{,}34 + M_{carbon,emission}$$

$$M_{carbon,emission} = 15{,}28\ kg$$

Transforming this to moles of carbon yields

$$N_{carbon,emission} = \frac{M_{carbon,emission}}{M_{w,carbon}} 1000 = \frac{15{,}28}{12} \times 1000$$

$$N_{carbon,emission} = = 1.273{,}33\ moles\ of\ C$$

Knowing that the concentrations are 1.18% for CO2, 5655 ppm for CO and 1707 ppm for CH4, putting everything in a percentage unit, it gives

$$n_{carbon,emission} = \frac{1.18}{100} + \frac{5655}{10^6} + \frac{1707}{10^6} = 0{,}01916\ or\ 1{,}916\%$$

The total moles of gas is

$$N_{exhaust} = \frac{1.273{,}33 \times 100}{1{,}1916} = 106.858{,}85\ moles\ of\ gaseous\ emissions$$

As the molar weight of the combustion gas is assumed to be about 32, the total mass of gaseous emissions is

$$M_{exhaust} = \frac{N_{exhaust} M_{w,gas}}{1000} \quad [kg]$$

$$M_{exhaust} = \frac{106.858{,}85 \times 32}{1000} = 3420 \quad [kg]$$

When considered as an average flue gas flowrate, it is

$$\dot{M}_{total\ mass} = \frac{\frac{N_{exhaust} M_{w,gas}}{1000}}{\Delta t_i} \left[\frac{kg}{s}\right]$$

$$\dot{M}_{total\ mass} = \frac{\frac{106.858{,}85 \times 32}{1000}}{12.600} = 0{,}27 \left[\frac{kg}{s}\right]$$

Thus, it is possible to calculate the contribution of carbon from each gas emitted

$$M_{carbon,CO2} = n_{CO2,emission} N_{exhaust} \frac{M_{w,carbon}}{1000} \quad [kg]$$

$$M_{carbon,CO} = n_{CO,emission} N_{exhaust} \frac{M_{w,carbon}}{1000} \quad [kg]$$

$$M_{carbon,CH4} = n_{CH4,emission} N_{exhaust} \frac{M_{w,carbon}}{1000} \quad [kg]$$

Inserting the values yields

$$M_{carbon,gas} = m_{gas} N_{gas} \frac{M_{w,carbon}}{1000} \left[ppm\ mols\ \frac{kg}{mol} = kg\ of\ Carbon\right]$$

$$M_{carbon,CO} = \frac{5655}{10^6} \times 106.858{,}85 \times \frac{12}{1000} = 7{,}25\ kg\ of\ C$$

$$M_{carbon,CH4} = \frac{1707}{10^6} \times 106.858{,}85 \times \frac{12}{1000} = 2{,}19\ kg\ of\ C$$

$$M_{carbon,CO2} = \frac{1.18}{100} \times 106.858{,}85 \times \frac{12}{1000} = 15{,}13\ kg\ of\ C$$

To calculate the final carbon footprint, it is necessary to consider the GWP potential of each gas, with the values are 18.6 for CO and 84 for CH4, in a CO2 equivalent basis and 20 years horizon (IPCC, 2014).

$$M_{GWP\ deduction\ as\ C} = M_{carbon,gas} GWP_{gas}$$

For CO:

$$M_{GWP\ deduction,CO\ as\ CO2\ eq} = (7{,}25)(18.6) = 134{,}85\ kg\ of\ C\ as\ CO2_{eq}$$

For CH4:

$$M_{GWP\ deduction,CH4\ as\ CO2\ eq} = (2{,}19)(84) = 183{,}96\ kg\ of\ C\ as CO2_{eq}$$

As the effect of CO and CH4 is to produce additional CO2 emissions equivalent to (GWP-1), the net sequestration of the system becomes

$$Seq_C = M_{carbon,char} - M_{carbon,LPG} - M_{carbon,CO}(GWP_{CO} - 1) - M_{carbon,CH4}(GWP_{CH4} - 1)$$

$$Seq_C = 13{,}34 - 4{,}42 - (7{,}25)(17.6) - (2{,}19)(83) = 13{,}34 - 4{,}42 - 148{,}2 - 210{,}8 = -300\ kgC$$

$$Seq_C = -300\ kg\ of\ Carbon$$

Or as a sequestration conversion from the biomass carbon

$$\frac{Seq_C}{m_{carbon}M_{oven-dried}} = \frac{-300}{24{,}2} = -12{,}4\left[\frac{kgC}{kgC_{wood}}\right] or -1.240\,\%$$

As expected, this scenario without abatement resulted in much higher negative net sequestration. This means that no carbon sequestration occurred; rather, more carbon (as CO2 equivalent emissions) left the system than got sequestered in the char. The net carbon footprint was – 300 kg, which means that 13,34 kg of carbon was sequestered in the char, but 313,34 kg of carbon (from LPG use and as additional CO2 equivalent emission) left the system. Another way of representing it is the ratio of net carbon sequestration over the carbon in the biomass, here being – 1.240%. It means that net sequestration value represents 1.240% of the mass of carbon inputted in the system via biomass (pine wood chips)

6.4. Zero net sequestration scenario

Another interesting scenario to analyses is when the net carbon sequestration equals to zero. To do so, the amount of carbon sequestered in the char must be the same as the additional CO2 equivalent amount of carbon emitted from CO and CH4 plus the amount of carbon used by burning LPG. This is a way of determining the allowable emission limits while achieving a zero-carbon footprint. The formula for zero net sequestration is given below.

$$Seq_C = M_{carbon,char} - M_{carbon,LPG} - M_{carbon,CO}(GWP_{CO} - 1) - M_{carbon,CH4}(GWP_{CH4} - 1) = 0$$

Rearranging,

$$M_{carbon,CO}(GWP_{CO} - 1) + M_{carbon,CH4}(GWP_{CH4} - 1) = M_{carbon,char} - M_{carbon,LPG}$$

Appling the GWP values of CO and CH4, it becomes

$$17.6M_{carbon,CO} + 83M_{carbon,CH4} = M_{carbon,char} - M_{carbon,LPG}$$

As $[Seq_{max} = M_{carbon,char} - M_{carbon,LPG} = 4{,}99\ kg]$ is the maximum carbon sequestration in our experiment (see §6.2), the balance becomes

$$17.6M_{carbon,CO} + 83M_{carbon,CH4} = 4{,}99$$

Where the terms represent the additional global warming effect of the emissions as equivalent CO2

$$17.6M_{carbon,CO} = M_{carbon,CO\ as\ CO2\ eq}$$

$$83M_{carbon,CH4} = M_{carbon,CH4\ as\ CO2\ eq}$$

The analysis from this point depends on the concentration of each harmful gas (CO and CH4). If no CH4 is present, the maximum permissible amount of CO is 0,284 kg, corresponding to the concentration of 85 ppm. Similarly, if no CO is present, the maximum permissible concentration of CH4 is 0,060 kg, corresponding to the concentration of 18,8 ppm.

Table 6.1 explores further scenarios where concentrations of CO and CH4 change proportionally to their GWP values, in order to achieve zero carbon footprint.

Table 6.1. Emission levels of CO and CH4 needed to achieve zero carbon footprint in Run 7 based on defined CO:CH4 ratios. The concentrations are averaged over the time of Run 7.

No.	CO:CH4	CO [ppm]	CH4 [ppm]
1	1:0	85	0
2	0:1	0	18,8
3	1:1	15,4	15,4

Under the circumstances of run 7, net carbon sequestration turns to positive when average concentration of CO and CH4 after flaring is less than 15,4 ppm.

Knowing that CO and CH4 concentration throughout pyrolysis are unlikely to be stable and equal, in order to avoid turning the net carbon sequestration to negative, their fluctuation have to follow an opposite movement based on the proportion of their GWP values, which is 18,6 for CO and 84 for CH4 (IPCC, 2014). It means that, when their average concentration is stable at 15,4 ppm, each ppm increases of CH4, for example, need to be compensated by 4,52 ppm decreases for CO, and vice versa.

The key result of this analysis is the low ppm values in Table 6.1. They are the limiting permissible emissions for each gas under each ratio scenario, and are clearly far lower than the US EPA limit of 2400 ppm CO for biomass suspension burners or 230 ppm CO for fluidized bed burners.

Chapter 7 - Results and discussion

This chapter first gives the laboratory analyses of the char produced in selected experiments, which are then needed to discuss some relevant issues arising from this work. These include the effect of the system design and operating strategy on the dynamics of heat and mass transfer, the char quality and the emissions compliance. It then discusses the environmental implications for small and larger scale pyrolysis.

7.1. Proximate and elemental analysis of the char

Proximate and ultimate analyses were undertaken only on runs 3, 4, 5 and 6, due to the recurring problem of air ingress during cooldown in the other experiments, resulting in ash production. As an exception here, run 5 had significant loss of yield and ash production during cooldown. These selected experiments still presented good quality of char, without noticeable amount of ash over the char surface.

The sample points of the char were strategically placed in different spots throughout the reactor, to ensure homogeneity in laboratory analysis. Four (4) collection points were selected: two (2) placed 20 cm from the batch wall but 50 cm away vertically from each other, and two (2) 10 cm from to the inner core but also 50 cm away vertically from each other. The lower sampling points were 40 cm away from the bottom of the reactor. For ultimate analysis, the samples were mixed together, ground, from which three samples were taken for analysis.

Proximate analysis followed the international ASTM E 871 and 872 for Chemical Analysis of Wood Charcoal (procedure detailed in the methodology section, chapter 3, item 3.1), and ultimate analysis was conducted on the Elementar Analysensysteme GmbH (Hanau, Germany) vario MACRO cube, using the procedure detailed in Ripberger (2015).

Table 7.1: Proximate and elemental analysis of the chars from runs 3, 4, 5 and 6, which represent pyrolysis temperature of 450, 600, 600 and 700°C, respectively. Four (4) samples of each run were utilized for moisture content and volatile matter analysis, and three (3) samples to ultimate (elemental) analysis. Average values shown in the bottom tables.

			Moisture Content			Volatile Matter			Elemental Analysis		
run	Temp	sample	before (g)	after (g)	moisture	total (g)	loss (g)	VM (%)	N (%)	C (%)	H (%)
3	450°C	3.1	1.0100	0.9603	4.92%	1.0206	0.2198	21.53	0.40	79.66	4.37
		3.2	1.0247	0.9741	4.94%	1.0897	0.2670	24.50	0.30	79.69	4.62
		3.3	1.0118	0.9623	4.89%	1.0108	0.2146	21.23	0.39	80.21	4.54
		3.4	1.0212	0.9705	4.96%	1.0018	0.2284	22.80			
4	600°C	4.1	1.0104	0.9649	4.50%	1.0808	0.0570	5.27	0.60	90.35	1.44
		4.2	1.0206	0.9727	4.69%	1.0223	0.0599	5.86	0.64	90.45	1.26
		4.3	1.0156	0.9706	4.43%	1.117	0.0690	6.18	0.58	90.68	1.16
		4.4	1.0118	0.9675	4.38%	1.0986	0.0595	5.42			
5	600°C	5.1	1.0115	0.9135	9.69%	1.111	0.0944	8.50	0.60	83.90	1.54
		5.2	1.0127	0.9147	9.68%	1.213	0.0998	8.23	0.50	84.58	1.24
		5.3	1.0180	0.9201	9.62%	1.087	0.0801	7.37	0.48	83.97	1.25
		5.5	1.0212	0.9244	9.48%	1.0385	0.0910	8.76			
6	700°C	6.1	1.0062	0.9878	1.83%	1.3299	0.0575	4.32	1.07	93.97	0.10
		6.2	1.0018	0.9801	2.17%	1.1213	0.0471	4.20	1.13	93.18	0.01
		6.3	1.0123	0.9928	1.93%	1.0875	0.0453	4.17	1.23	94.70	0.03
		6.4	1.0098	0.9900	1.96%	1.0279	0.0400	3.89			

		Average moisture content	Average volatile matter	Average elemental analysis		
run	3	4.92 ± 0.04	22.53 ± 1.97	0.36 ± 0.06	79.86 ± 0.35	4.51 ± 0.14
run	4	4.5 ± 0.19	5.68 ± 0.5	0.61 ± 0.03	90.49 ± 0.19	1.29 ± 0.15
run	5	9.62 ± 0.14	8.214 ± 0.84	0.53 ± 0.07	84.15 ± 0.43	1.34 ± 0.2
run	6	1.97 ± 0.21	4.14 ± 0.28	1.14 ± 0.09	93.95 ± 0.77	0.05 ± 0.05

The expected trend, as pyrolysis temperature increases, is for char volatile matter to decrease, carbon content to increase and the H/C ratio to decrease. Moisture content is expected to decrease with increasing pyrolysis temperature, because it depends on the hydrophobicity of the char surface which increases with pyrolysis temperature, its equilibrium with humid air and the time of exposure before being placed in the drying oven. Runs 3, 4 and 6 follow this trend, but run 5 did not. Run 5 was also particularly different to run 4, which had the same pyrolysis temperature. The major operational difference between run 5 and the others was the use of a chicken wire cage in the chimney, which caused a back-pressure in the reactor (resulting in fugitive emissions and so was removed for later trials). This possibly affected the kinetics of pyrolysis and certainly seems to have resulted in a profound change in the surface properties of the char, causing the higher equilibrium moisture content after cooling. It is well known that pyrolysis in higher pressure systems increase char yield (Mok & Antal, 1983), caused by the greater extent of secondary reactions due to the closer proximity of volatiles and remaining char which catalyses those reactions. This does not seem to be the effect seen here where run 5 has, in addition to a greater equilibrium moisture content, a higher

volatile matter content and lower carbon content in its char. To explore this further, the yield needs discussing.

Table 7.2 calculates the overall carbon yield (the fraction of carbon in the wood that ends up in the char) by multiplying the mass yield at the end of the experiment with the ultimate analysis carbon content. No trend is evident here due to the confounding effect of an unknown and small amount of air passage through the reactor due to the poorly secured lid (as discussed in Chapter 5). Run 3 is the best result with the least decrease in mass yield. Run 5 is the worst with yield after cooling of only 8,77%. To consider here is that the analyses in table 7.1 above were on the char collected after cooldown, and so the results may be affected by ashing. However, despite this, the proximate and ultimate analyses do not appear to have been significantly affected. This is likely to be due to the nature of ashing, which occurs by surface oxidation, whereas the tests were carried out on samples of char particles. Sampling selected surviving particles: these were ground which diluted the ashing effect. Thus, it can be concluded that the proximate and ultimate analyses probably reflect the properties of the char at the end of each experiment before cooldown. However, the ashing effect (which probably occurred to some minor extent during the late stages of the experiment when the volatile evolution rate was low) does confound the overall carbon yields given in the right column of table 7.2.

Table 7.2: Yields for runs 3, 4, 5 and 6.

Run	HTT (°C)	Mass yield at the end of the experiment (%)	Mass yield after cooling (%)	Carbon content of cooled char (%)	Carbon yield (%)
3	450	35,15	34,69	79,86	28,07
4	600	34,14	27,90	90,49	30,89
5	600	32,00	8,77	84,15	26,92
6	700	29,70	26,55	93,95	27,90

Returning to run 5, the reason for its anomalous properties are not clear: it produced a char with higher volatile matter content, lower carbon content and higher equilibrium moisture content. As noted above, its only notable difference, apart from the extent of ashing during cooldown, was the system pressure, which was higher than the other trials due to the chicken wire cage creating a resistance in the chimney. Speculating, it is possible the slightly higher reactor pressure lowered the pressure gradient across individual particles, resulting in a slightly longer residence time of evolved volatiles within particles. These internal secondary reactions may have promoted repolymerisation, forming heavier tars, which remained in the char due to having higher boiling points. While this is speculation, it is clear that the char is different which suggests that the balance of the different types of secondary reactions changed (see figure 2.9 for the types of reaction).

A last interesting feature of the ultimate analysis is the reduction in hydrogen content from 600 to 700°C, where hydrogen concentration drops expressively. It aligns with the observation in runs 6 and 7, evidenced by the increase of stack temperature (T02), and so is probably the exothermic evolution of hydrogen gas.

7.2. Analysis of the pyrolysis stages

One disadvantage when controlling batch pyrolysis systems is the uncontrolled gas evolution, ranging from zero to a high rate then later decreasing to almost zero again as pyrolysis reaches its end point. Complicating this is the composition change, ranging from inflammable to flammable (Wang & Wang, 2009). Figure 7.1 shows the estimated predominance of CO2, CO, CxHy and H2 among the stages of pyrolysis defined here. It indicates the flammability of the off-gases in each phase and is an important indicator for the secondary air input rate needed to combust the volatiles and particulate.

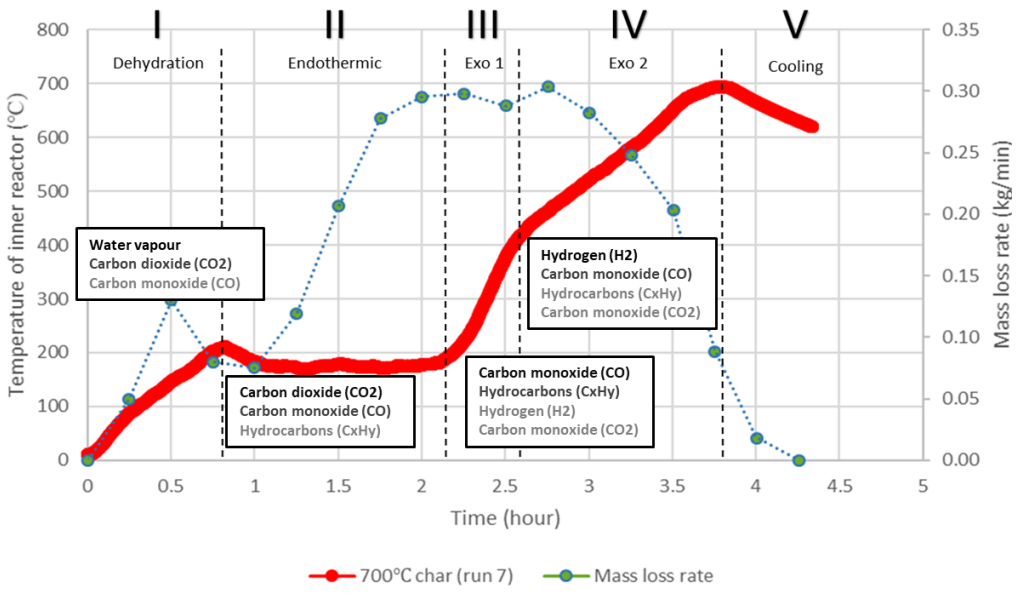

Figure 7.1: Stages of pyrolysis based on the inner reactor temperature (T01) profile, under the circumstances of this work experiments. The estimated predominance of CO2, CO, CxHy and H2 in each phase of pyrolysis is shown in the white blocks in order of dominance using the composition trends found by Wang and Wang (2009). The gases at the top of the blocks are estimated to have a higher concentration than those at the bottom.

When the flare is operating without pyrolysis gases, which occurs at the very end of the experiments, the flare temperature is close to 610°C (see Fig 5.4, 5.5 and 5.7). Thus, any elevation of the flare temperature is indicative of the flammability of the volatile-particulate mixture. This is indicative because the true effect is somewhat confounded by the opening and closing of air vents at the flare burners and the use of a secondary air injection into the combustion chamber.

In Run 7, a second observation of flammability was possible in the combustion chamber, through the explosion vent porthole into which a secondary air flow was blown. Temperature at the flare is an indicator of the pyrolysis gas flammability. Despite considerable mass loss occurring during phase II, the flare temperature during this phase increased from 700°C to 800°C until 2 hrs after which is quickly rose to its peak at about 970°C. This indicates some flammability in phase II which is followed by considerably more flammability in phase III. However, in phase II, the visual observation in the combustion chamber showed that the forced draft burners had a flame, but that no secondary flames were visible from the pyrolysis

gases. Later in phases III and IV, secondary flames were present. To consider the reason why phase II did not produce secondary flames, it is important to understand how the gas composition changes. Here, CO2 is the dominant gas which is non-flammable. Water vapour is also a reaction product, but some water may also be present from continued drying after the arbitrary end of phase I. It is likely that CO, which is flammable, is either present below its flammability limit (LFL 0.12 vol% in air) or is adsorbed onto the high available surface area of the tarry volatiles and particulate, a so does not combust on its own. The presence of this high surface area will also adsorb any free oxygen that enters as excess air with the forced draft burners, or as secondary air blown through the port (which is a small amount, to avoid creating a positive pressure in the chamber). Thus, the mixture in the combustion zone is too lean in oxygen to combust. At the flare, the outcome is different, because the tarry volatiles and particulate are flammable, when a large excess of air is supplied. Complete combustion is achieved when the temperature is elevated, nominally to above 750°C, but the pyrolysis gases cannot achieve this on their own. For this reason, the flare was modified in a number of ways: use of LPG burners for augmented combustion, providing a windshield with extended height to provide residence time and insulating it to retain heat, and by using modulated air inlet ports to provide the combustion air (Section 3.3.5).

As noted in Section 5.1, phase II is characteristised by the core temperature of the reactor remaining below 200°C while the pyrolysis front advances steadily across the reactor. Once this is completed, the reactor becomes exothermic (phase III) and its core temperature rapidly rises to overtake the annulus temperature at ~2.6 hours, after which exothermic pyrolysis continues (phase IV) until there is no longer any fuel to convert to char. During phases III and IV, a secondary flame is seen in the combustion zone, indicating that the pyrolysis gases are flammable and within the flammability limits. This combustion is partial, however, as it only results in a small lowering of the stack temperature, where the flare temperature is still elevated above 900°C; however, as phase IV proceeds the evolution rate of pyrolysis gases decreases

and so the flare temperature also decreases. A late increase in stack temperature occurs as due to the probably exothermic generation of hydrogen after 3.5 hours (see figure 7.2 below).

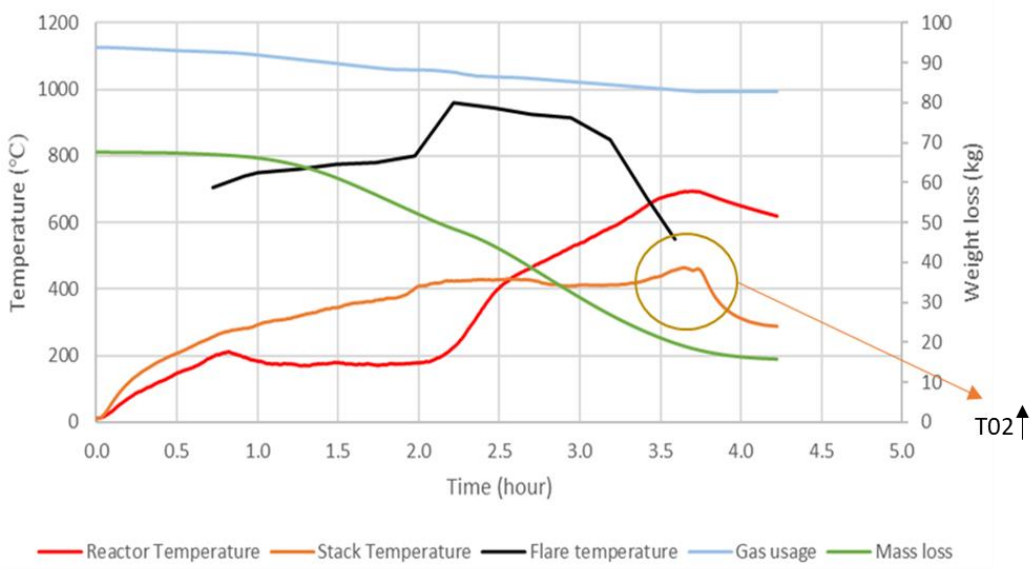

Figure 7.2: Rise on stack temperature (T02) after 3,5 hours due to increase on hydrogen production from latest stages of pyrolysis.

These results highlight the problem of flammability of pyrolysis volatiles and particulate. The high evolution of these makes supplying enough air a design and control challenge. Furthermore, reaching the temperature necessary to ensure complete destruction requires augmentation with a highly flammable fuel. Doing so, as chapter 6 highlights, reduces the carbon footprint for the process.

7.3. Analysis of the heat transfer efficiency of the reactor

The test run, described in chapter 5.1, established that the charring advances across the reactor from the outer wall towards the core. All later trials showed that this 'advancing front' (Phase II) stage lasts about 1.5 hours. This outcome occurs because the Massey biochar reactor is designed to have transference of heat and mass in the same direction, starting from the wall, which is heated by hot gases travelling up the

annulus between the reactor and the outer wall. The initial heating is by conduction and radiation to the particles against the heated wall. However, subsequent heat transfer in the bed is convective, dominated by the convective mass transport of first steam then volatiles, along a decreasing pressure gradient towards the core. It is greatly facilitated by cycles of condensation and revolatilisation, first of water vapour, then of volatiles.

Such heat transfer behavior was studied by Caco (2017); however, his work did not include a condensation temperature for the tarry vapours, because this is not a recognized quantity due to the vast array of compounds that constitute these tarry vapours. Nevertheless, these results suggest that an aggregate condensation temperature does occur as, during this 'advancing front' (Phase II) period, the reactor core temperature was constant in all trials, at below 200°C.

Pyrolysis is clearly endothermic in this phase, as demonstrated in figure 7.3, where the difference continues to increase between the temperature of the (base of the) stack and the core of the reactor. The increasing temperature difference translates to an increasing heat input, which results in a rising mass loss rate (Fig 7.1) over most of phase II.

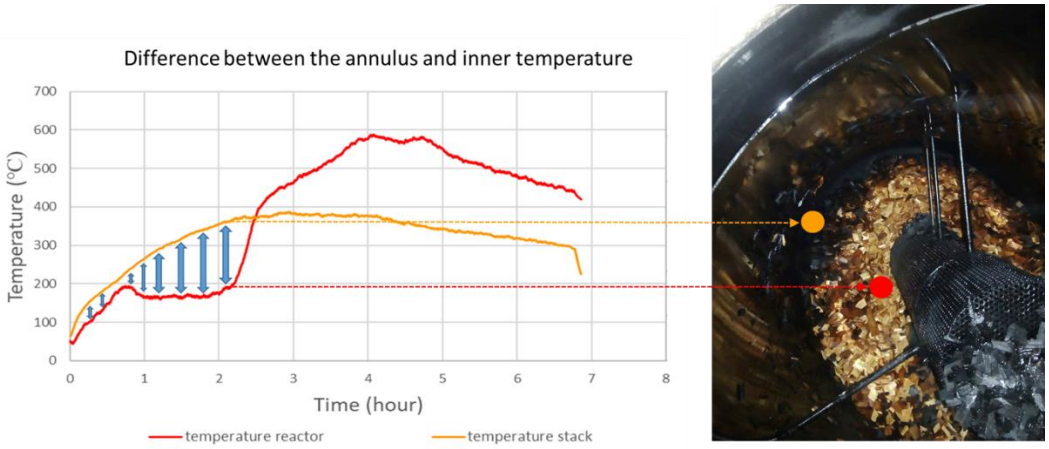

Figure 7.3: Difference on temperature and decomposition stages of the wood chips in a non-complete pyrolysis experiment. Red and yellow lines represent the evolution of the inner reactor (T01) and stack (T02) temperatures, respectively. The maximum difference of temperature between T01 and T02 is around 2 hours of experiment, highlighted by the doted lines, and the wood charring stages of each zone is pointed in the picture.

Once the 'advancing front' reaches the core after 2 hours of experiment, an abrupt increase of the core temperature (T01) occurs, described here as the beginning of phase III (see Fig 5.12). This signifies a transition to an exothermic reaction regime because the reactor temperature increases at a much faster rate than the stack and indeed surpasses it part way into phase III. Thereafter, the reactor core temperature depends on the mode of operation used to achieve the various HHTs (highest treatment temperatures) between 400-700°C, which will be compared in the following section.

7.4. Analyzes of pyrolysis temperature evolution of 400, 600 and 700°C chars

An important focus of this work was to develop different strategies to run the Massey reactor, enabling pyrolysis to target specific qualities of char. To achieve this, the burners and secondary air supply are controlled to influence the heat input to the reactor and the tertiary air supply (at the flare) is controlled to mitigate emissions. In effecting these controls, it is also important to optimize gas usage. As chapter 5 details, this level of versatility was achieved and so represents a great advantage over conventional batch systems, which produces a single outcome.

Figure 7.4 compares the evolution of the inner temperature (T01) of the pyrolyser in the three biochar HTT scenarios attained in this work (400, 600 and 700°C).

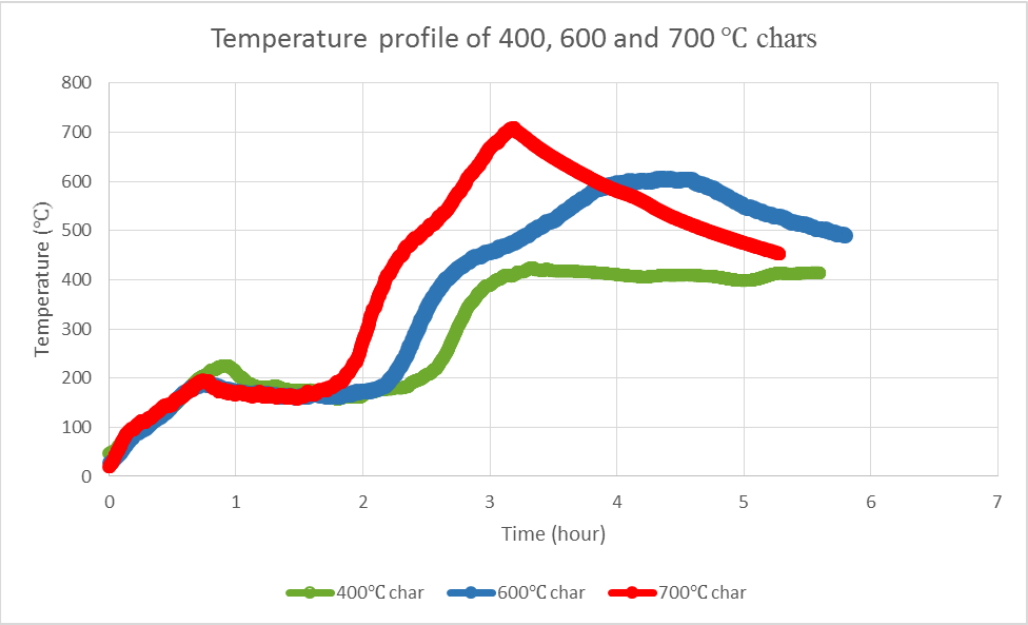

Figure 7.4: Comparison of the inner reactor temperature (T01) progress overtime during pyrolysis of the 400, 600 and 700°C highest treatment temperature (HTT), corresponding to run 2, 4 and 6, respectively.

Comparing the progress of the temperatures (T01) in the three different HTT pyrolysis, they all had very similar behavior, as explained, until the first exothermic stage (III). However, the rate of increase in phase III is different, with the 700°C pyrolysis being the fastest. This relates to the operating strategy when targeting a higher HTT, where more off-gases are burnt in the combustion chamber and also providing more heat back to the process.

At the transition from phase III to IV, the main difference is the temperature stasis of the 400°C treatment. As 400°C HTT strategy does not continue to blow air into the chamber after that the main bottom burner is turned off, the absence of air to combust the pyrolysis gases restricts the recycling of heat and thus the heat loss from the system equals the heat generated, noting that the temperature remains at just over 400°C for some time before it starts to cool down. The higher temperature trials, 600 and 700°C HTTs, exhibited further exothermic reactions, represented by phase IV. As their operating strategy applied secondary air to combust volatiles in the chamber, it released extra heat to drive pyrolysis over 400°C. The difference between them was the speed that T01 increased. Inner

reactor temperature (T01) of 700°C pyrolysis on the stage IV increased faster due to extra air blown into the chamber by the spare blower connected to the reactor. It allowed more combustion to occur and consequently the reaction to been driven more intensely, which resulted in a higher temperature of char, likely able to reach 700°C due to hydrogen (H2) production and combustion after 600°C.

In the higher temperature trials, this exothermic regime appears to transition to a second mechanism, signaled by the abrupt change in slope of the increasing core temperature. This second slope seems to maintain itself throughout phase IV, even as the mass loss rate begins to steadily decrease, indicating that the exothermicity is also steadily increasing.

7.5. Analyzes of emission scenarios of run 7

In run 7, the gases, after been combusted by the flare, were sampled each 15 minutes, giving the real time concentration of CO2, CO, CH4. (The actual measurement is hydrocarbon, CxHy, which will be dominated by methane, CH4, and is referred to as CH4 for the remainder of the discussion.) Samples were also taken with the flare LPG burners turned off to obtain the emissions without abatement. As the purpose of these measurements was to calculate the carbon footprint of Massey pyrolyser, only the carbon content of the gases was considered. Oxides of nitrogen, even if slightly present in the flue gas, carry a high GWP values. They were not considered in the emission scenarios because their concentration during sampling was both variable and low. There are two main reasons for this. First, the nitrogen content of pine wood is lower than other organic biomas types used for biochar production, and second, the temperature of the flare is significantly below the range expected to form NOx from reaction with nitrogen gas.

A few samples were disregarded as unreliable due to water condensation inside the pipe collector. This problem was solved by both the installation of a water trap in run 7 and by drying the analyser pistol before sampling. The two measurement scenarios,

without abatement (LPG burners are off) and with abatement (LPG burners are on), are discussed below.

Figure 7.5 shows the concentration of CO and CH4 in the flue gas without abatement. The average concentration of CO was 5655 ppm and CH4 was 1707 ppm, and their peak concentration was 15000 and 4000 ppm, respectively, at around the beginning of stage IV. The emissions are low during phase I drying, as expected. Carbon monoxide is the first to rise sharply at the onset to phase II, then doubles over the duration of phase II as the charring front advances across the reactor, then more than doubles again during the exothermic phase III, before dropping steadily then sharply over the duration of phase IV. Only by the late stages of phase IV, did the CO concentration decrease below the US EPA stack emissions limit of 2400 ppm for biomass suspension burners (Federal Register, 2015). Methane, the indicator for hydrocarbon, is initially negligible at the onset of phase II, but increases steadily of phase II, then sharply over phase III and peaks mid-way through phase IV, before dropping to a negligible value. The later rise and peak of the methane is expected (Wang and Wang, 2009). These results support the conclusions about the endo- and exothermicity of the system. During the first two hours of reaction (phases I and II), which have been recognised as endothermic, CO and CH4 production is relatively low which does not favour flammability and so pyrolysis is endothermic, needing to be driven by the combustion zone LPG burners. Phases II and IV are exothermic and have significantly higher combustible gas production, which provides a positive feedback to the operation of the reactor. The heat released, if combusted in the combustion zone underneath the reactor, can be recycled into the system and provide a saving of LPG.

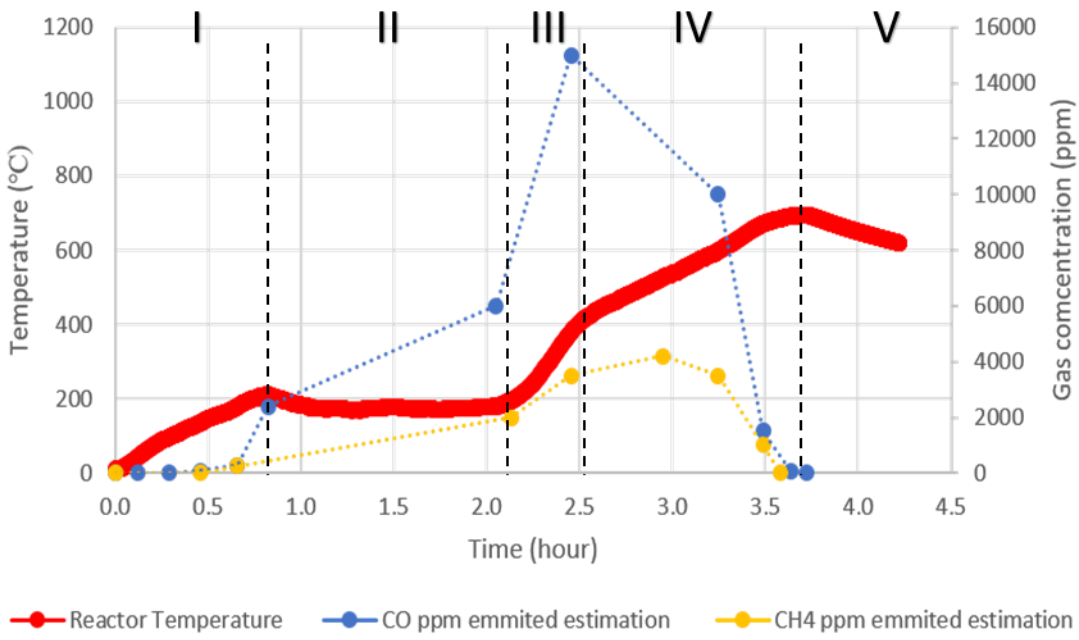

Figure 7.5: Estimation of CO and CH4 emissions without flaring in the Massey pyrolyser. The solid points represent the sampling results when flare was off and the dotted lines give the trend of gas concentration evolution throughout pyrolysis.

Figure 7.6 shows the average concentration of CO and CH4 abatted by flaring in each stage of pyrolysis. The average values between stages were used to facilitate the calculation of the total average gases concentration used in the carbon balance, chapter 5. When the flare system turned on around 45 minutes, the CO concentration dropped instantly to almost zero and remained under 50 ppm until pyrolysis was finished. The CH4 concentration did not show an abrupt decrease when the flare was turned on; instead, it stayed well under 100 ppm for the entire time of reaction. The experiment-time average concentration was 32 ppm for CO and 51 ppm for CH4. Comparing this with the concentration values of CO and CH4 in the scenario without abatement shows that the new flare and chimney system were very capable of mitigating emissions. These are well below the 2400 ppm US EPA limits of 2.400 ppm CO in a biomass suspension burner and 230 ppm in a biomass fluidized bed burner (Federal Register, 2015). The CH4 concentration was steadier during pyrolysis than CO. Its slight increase during exothermic stages was due to an operational change where the main burner in the combustion had been turned off, leaving only the pilot burner is

ON. Less partial combustion here means the CO concentration entering the flare is slightly higher, which carries through to a slight increase in the post-flare measurement (see Chapter 5.7).

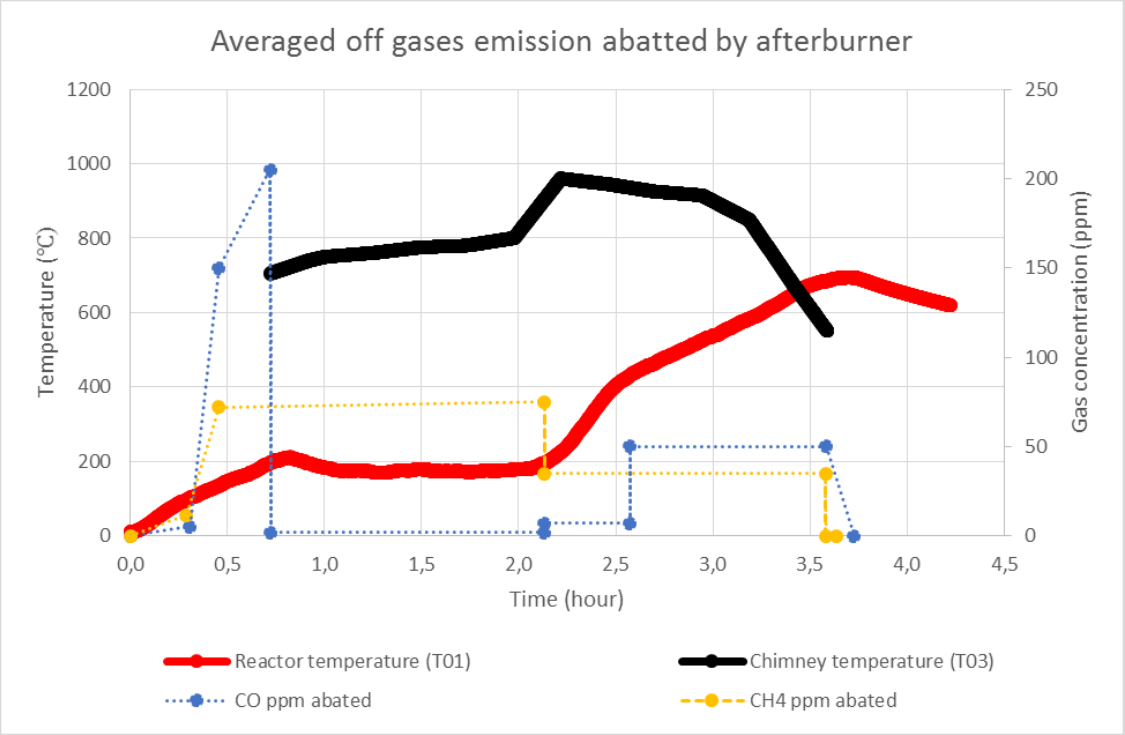

Figure 7.6: Average concentration of CO and CH4 in the scenario with abatement of emission, during the different stages of pyrolysis.

Figure 7.7 combines the three scenarios for CO emissions from run 7: [1] no abatement; [2] abatement by flaring; and [3] mitigation of CO emission at the EPA standard of 2400 ppm. Scenario 3 represents a hypothetical mitigation of CO emission at 2400 ppm. These levels were used in the calculations of chapter 6 to determine the system carbon footprint for different emissions scenarios. The figure shows just how effectively the Massey pyrolyser abated the emissions.

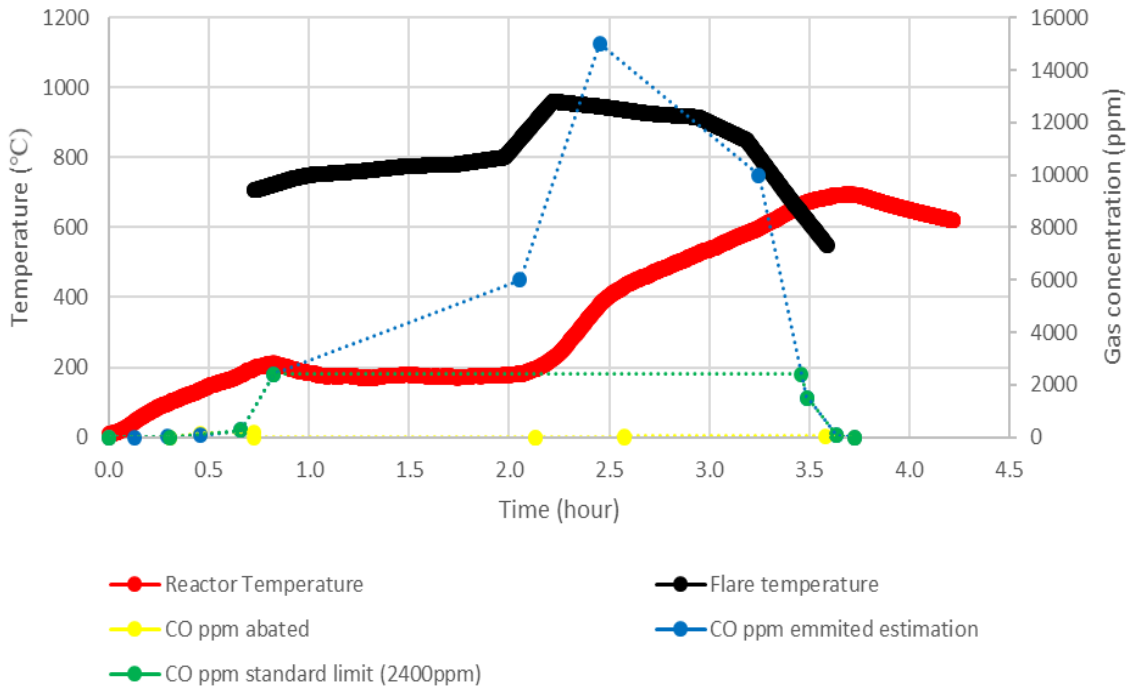

Figure 7.7: Three emission scenarios for CO: [1] no abatement (estimation of raw emission); [2] abatement (by flaring); and [3] abatement at the EPA standard of 2400 ppm. The estimated variation of CO concentration among the scenarios and during pyrolysis is represented by the dotted lines.

Carbon dioxide is one of the products of complete combustion. Water is the other. Here, CO2 was measured during run 7 for the two scenarios, with and without flaring.

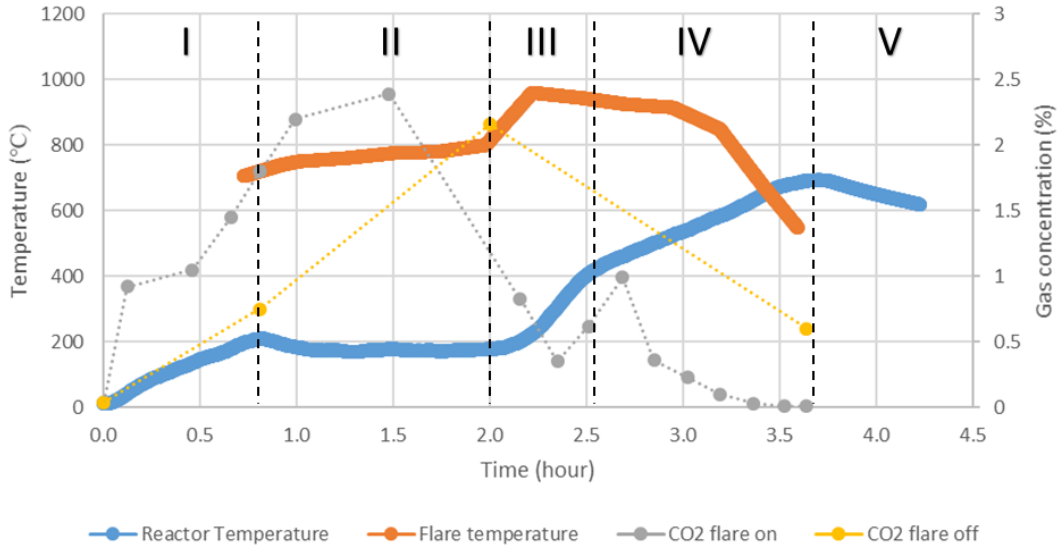

Figure 7.8: Two scenarios for CO2 concentration: [1] with flaring of pyrolysis gases; [2] without flaring. The estimated variation of CO2 concentration among the scenarios and during pyrolysis is represented by the dotted lines.

When the flare system is working, the CO2 concentration is an aggregate of the complete combustion of: the pyrolysis gases, the particulate, and the LPG used both in the combustion chamber and in the flare. Its concentration is high in phase II, probably reflecting the higher particulate loading during this phase. Particulate levels were not measured, but visually the flare was a black and smoky when the flare was off. The lower CO2 levels in phase III and early in phase IV, occurred during the time of peak mass loss rate (see fig. 7.2). They probably reflect the lower particulate loading during this stage, and two other effects: the lower CO2 contribution from the main burner in the combustion zone which was turned off early in phase III, and the secondary air inputted into the combustion zone beginning from the start of phase III. These changed the final mass flow of the system, diluting the gases sampled in the chimney. The tail in phase IV reflects the reduced mass loss rate for the system and the final turning off of the LPG pilot burner in the combustion chamber and the flare burners.

Three CO2 measurements were made when the flare system was off. The first, at the phase I-II boundary reflects that pyrolysis is producing CO2 alongside CO and so is low. The second and third readings are elevated which reflect the absence of

dilution by both the flare forced draft burners (and the air that the forced draft draws) and main burner in the combustion chamber, all of which have been turned off.

In summary, the trends in carbon dioxide concentration are expected, as explained above. They were not used in the carbon footprint calculations; rather, all biomass and LPG carbon in the exhaust gases were assumed to be combusted directly to CO2 except the CO and CH4, as measured. It was these that were used to determine the carbon footprint.

7.6. Comparison of raw emissions from Massey pyrolyser and the literature

In order to compare the raw emissions (without abatement) of Massey pyrolyser with other types of kilns, data of emission from biochar production were collected from the literature. A study developed by Pennise et al (2001) is the most cited in this field, and compares values of the products of incomplete combustion (PIC´s) emissions from different types of kilns (traditional earth mounds and brick kilns) in Kenya and Brazil. Similar comparisons are made by Sparrevik et al (2015). Figure 7.9 summarises the CO2, CO and CH4 emission rates of biochar production from wood in different conventional types of kilns, as described in Pennise et al (2001) and Sparrevik et al (2015), and compares with emissions of Massey pyrolyser. The kilns compared in figure 7.9 are Kenyan Earth Mound, Adam retort and Massey pyrolyser. The unit is grams of pollutant per kilograms of char produced.

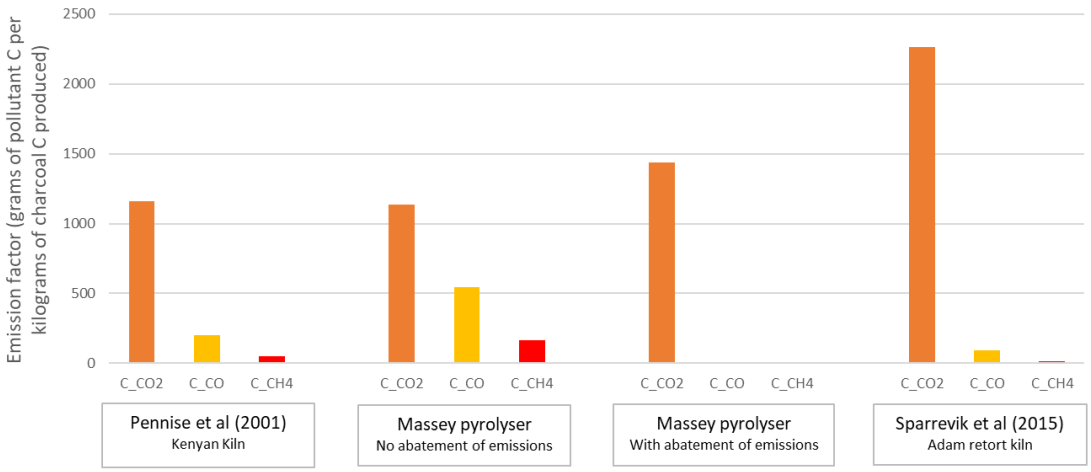

Figure 7.9: Comparison of CO2, CO and CH4 carbon emission from Massey pyrolyser and other types of kilns, per kg of C_char produced. The values of Pennise et al (2001) is for the Kenyan Earth Mound kiln (EM2) used for pyrolyse Eucalyptus (see their Table 6b), and values of Sparrevik et al (2015) is for the Adam retort kiln used for pyrolyse Pine Wood (see their table 4).

With abatement, the Massey pyrolyser is far superior to the other kiln types. Without abatement, the Massey pyrolyser results are within range of the other systems, although appears to show higher emissions of PIC´s than other retort kilns. The reason can only be speculated because insufficient operational data is available in these references. However, the Massey pyrolyser may present higher CO and CH4 emissions because it is more efficient than conventional kilns without air ingress, which means that more pyrolysis is occurring in the wood rather than combustion. Less efficient kilns will consequently produce more CO2 as seen in these results. The above results demonstrate that emissions management systems are needed on biochar pyrolysis systems to avoid release of PICs. Furthermore, this thesis shows how this can be achieved.

7.7. Analyzes of the global warming potential (GWP) of Massey pyrolyser

The global warming potential is analysed here with respect to the biochar production step. It does not consider the harvest, transport, storage, redistribution and long-term soil effects on the GWP. Here, at production in the Massey

pyrolyser, the GWP is estimated by applying the global warming potential values of CO and CH4 emitted. Other greenhouse gases, such as oxides of nitrogen and sulfur, are not considered due to their non-significant concentration. The GWP values used for CO and CH4 are 18,6 and 84, respectively (20-year horizon, IPCC, 2014).

Figure 7.10 compares carbon emission rate in both scenarios, with and without abatement, and gives an idea of the impact on environment of Massey pyrolyser. The unit is grams of carbon (as CO2 equivalent) in the gas per kilograms of char produced.

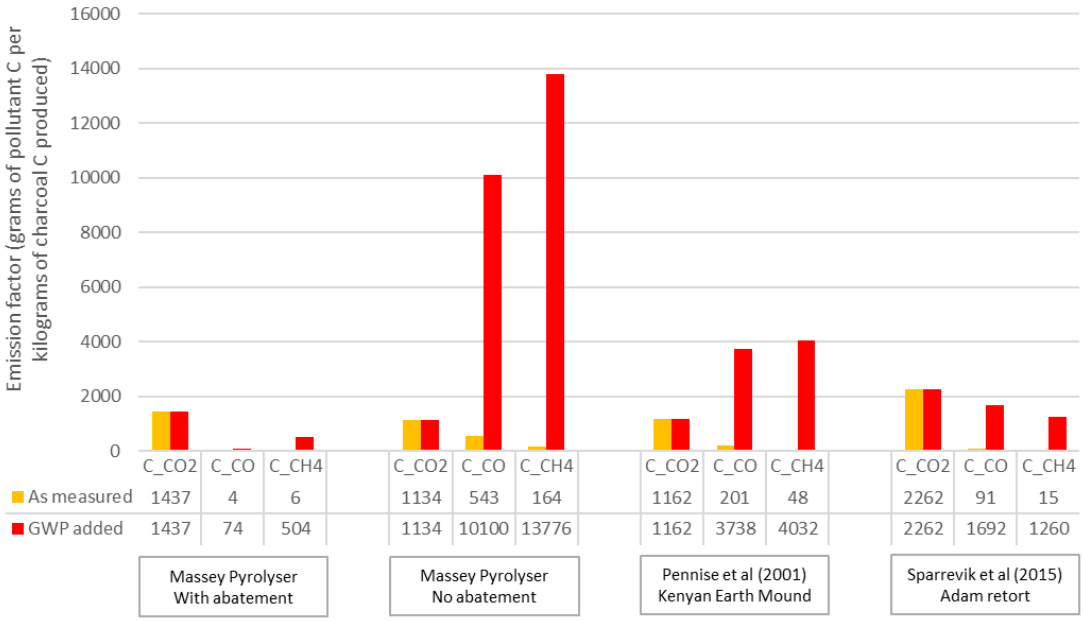

Figure 7.10: Comparison of the emission factor for CO2, CO and CH4 carbon emission from the Massey pyrolyser, Kenyan Earth Mound and Adam retort kilns, per kg of char carbon produced. Orange bars represent the rate of emission without adding the GWP values for the gases. The red bars represent the carbon equivalent production of each gas. The numbers below the bars are the production rate of each gas. The 20 year global warming potential horizon is used in these calculations.

It can be clearly seen that biochar reactors without abatement of the products of incomplete combustion have a serious environmental impact due to the high GWPs of CO and CH4. In the Massey pyrolyser, with no abatement of emissions, i.e., no flaring of pyrolysis gases, the CO emission has an emission factor of 10.100, meaning that per

kilogram of carbon remaining in the char, the emission of CO when multiplied by its global warming potential is responsible for the atmospheric emission of ~10 kg of carbon, which is 36 kg of CO2. This is a tremendous amount. For the hydrocarbon, interpreted as methane, the emission factor is even worse. The figure shows that even a tiny production of CH4 multiplies to a significant equivalent CO2 emission. The other kilns have less environmental impact than the 'no abatement' scenario because they involve some combustion of the pyrolysis gases. Nevertheless, they are nowhere near as good as the Massey pyrolyser when the flare is providing full abatement of emissions.

This analysis shows that emissions abatement is an absolute necessity if biochar production aims to achieve a neutral carbon footprint. As the calculations in chapter 6 showed, run 7 did not quite achieve this, having no net carbon sequestration. As discussed earlier, improvement to the operating strategy and scale-up are expected to produce a net sequestration result, albeit small. This work has implications for the operational performance of all biochar systems, and a need to balance the use of the biochar with the environmental impact of its production.

Chapter 8 – Conclusions

The work has shown that the carbon footprint of small-scale biochar reactors are significantly sensitive to GHG emissions, where non-CO2 emissionsneed to be eliminated by an afterburner flaring system. Furthermore, the system here required the afterburners to be augmented with fossil fuel (LPG) to reach temperatures of *ca*. 750°C necessary to destroy the products of incomplete combustion. This is because the pyrolysis gases are not flammable enough to reach this this temperature on their own. The experiments demonstrate the real challenge to mitigating these pyrolysis emissions in batch systems, which are characterised by uncontrolled gas release and dynamically changing gas composition. The conclusions below are arranged into the operational strategies for achieving different highest treatment temperatures (HTTs) of biochar (8.1), the strategies for operation of the flare system (8.2) and those concerning the carbon footprint and effect of emissions abatement (8.3). Finally, some recommendations for improvement are given.

8.1. Strategies for producing different temperature of chars in Massey pyrolyser

The optimal strategy for producing char in the Massey pyrolyser is to have the main burner ON until the inner temperature of the reactor (T1) reaches 350°C and the pilot burner ON until the char starts to cool down at the end of the batch. With the main burner ON until 350°C allows pyrolysis to progress through phase I, II and into phase III, and deliver a minimum of 400°C (HTT) char. In order to attain higher temperatures without using the main burner for longer, secondary air is blown into the combustion chamber. More secondary air produces higher HTT chars. However, too much air can cool down the system, which is not desirable. In this context, the optimal input rate of secondary air was determined during experiments. With these strategies explained in chapter five, the HTT was able to be manipulated between 400 and 700°C, which covers the range of biochar production generally found in the literature.

8.2. The optimization of the flare system

The flare system was improved significantly during the experiments. The chimney extension of 1,5 meters and its thermal insulation with fiber glass wool provided a much better condition for combustion, due to the higher residence time of the gases and the hotter combustion zone, both of which are determinants to achieve complete combustion of the products of incomplete combustion (750℃, 1.5 s residence time).

The vents located around the wind shield play a key role to guarantee a reliable burning. There is a right moment to partially or fully open. This facilitates combustion when the pyrolysis gas flow is high while also avoiding cooling when their flow is low. Opening and closing is based on the chimney temperature (T03). The vents are fully opened when T03 exceeds 780℃, partially opened when T03 ranges from 750 to 780℃ and closed when T03 is under 750℃.

Moreover, to save LPG usage, the flare system is not needed until phase II, the endothermic 'advancing front' stage, begins. Also, the flare is not needed once the pyrolysis reaction is complete and the reactor has begun to naturally cool, signifying the end of exothermic reactions. At this stage, the rate of gas production is negligible as evidenced by the near-zero mass rate of change of the reactor. With further investigation, it may be possible to shut the system down slightly before this. However, if the goal is optimizing carbon sequestration, then it is important to have it working until the very end of pyrolysis, to avoid any extra release of CO and CH4.

8.3. Emissions and carbon footprint

Achieving complete combustion in small-scale batch systems is not straightforward because of the great range of flowrates and flue compositions. This work showed the challenge of abating emissions in a small-scale biochar reactor. From all adaptations on Massey pyrolyser, CO and CH4 average concentration dropped from 5655 and 1707 ppm (system without flaring), to 32 and 51 ppm,

respectively. Despite this dramatic improvement, it still did not deliver a positive carbon footprint (net sequestration).

The main issue is fuel consumption to start the process by providing heating and to drive the flare to abate the emissions. LPG is a rich source of carbon, and so it becomes a parameter of limitation. Emissions need to be abated as much as possible, while using the least possible LPG fuel.

In determining the carbon footprint in the most conservative way, this work used the 20-year horizon global warming potential (GWP) values for carbon as CO2 equivalent from CO and CH4, which are 18,6 and 84, respectively (AR5, IPCC, 2014). When emissions are abated, the Massey pyrolyser achieved a net sequestration of – 3,38 kg or a net fraction of – 14 % (kg C/kg C in biomass). This showed that even with very good abatement, no net sequestration was obtained. In contrast, when no abatement occurs, the net carbon sequestration is – 300 kg or a net fraction is – 1.240 % (kg C/kg C in biomass). This result highlights the potential impact on the environment that small scale biochar systems can have when they do not have afterburning systems.

8.4. Design and operational recommendations for the Pyrolyser

Finally, some recommendations for the design and operation of the pyrolyser are given.

1. Several improvements were identified that are likely to elevate the Massey pyrolyser to having net sequestration. First, the LPG supply was from two 80 kg LPG tanks which supplied the two combustion chamber burners and the three flare burners. At full capacity, the demand was higher than the maximum rate of LPG evaporation within the tanks, such that the LPG gas supply was leaner in fuel to air ratio than it should have been. This would have lowered the temperature of the flame and thus affected the heating efficiency. A suggested improvement is to add another two LPG tanks and separate the gas supply to the flares from the gas supply to the combustion chamber. Together,

this will mean that the demand side will be more adequately met, and should result in better heating and reduced LPG consumption, due to the shorter time required to reach each desired highest treatment temperature (HTT) for the chars.

2. LPG usage could be also optimized by better controlling the gas flow in the afterburners. Once its gas supply is manageable, during phase II where less off-gases are produced, the top flare system at the chimney could produce less flame, saving LPG and improving the final carbon footprint.
3. The reactor needs to be properly sealed in order to avoid any fugitive emissions during pyrolysis and air intake after pyrolysis. Critical areas are between chamber and reactor, both lids (internal and external) and thermocouples access ports.

Antal Jr., M. J., Croiset, E., Dai, X., DeAlmeida, C., Mok, W. S.-L., Norberg, N., Al Majthoub, M. (1996). High-yield biomass charcoal. *Energy & Fuels, 10*(3), 652-658.

Antal Jr., M. J., & Grønli, M. (2003). The art, science, and technology of charcoal production. *Industrial & Engineering Chemistry Research, 42*(8), 1619-1640.

Antal Jr., M. J., & Mok, W. S. L. (1990). Review of Methods for Improving the Yield of Charcoal. *Energy & Fuels, 4*(3), 221-228.

Arntzen, C. J. (1994). Wood Properties. In J. E. Winandy (Ed.), *Encyclopedia of Agricultural Science* (Vol. 4, pp. 549-561). Orlando: Academic Press.

Baldock, J. A., & Smernik, R. J. (2002). Chemical composition and bioavailability of thermally altered Pinus resinosa (Red pine) wood. *Organic Geochemistry, 33*(9), 1093-1109.

Bezanson, A. (n.d.). Pyrolysis and Torrefaction of Biomass. Retrieved 15/03/2018, from http://poisson.me.dal.ca/site2/courses/mech4840/Pyrolysis%20&%20Torrefaction%20of%20Biomass.pdf

Blackwell, P., Riethmuller, G., & Collins, M. (2009). Biochar Application to Soil. In J. Lehmann & S. Joseph (Eds.), *Biochar for Environmental Management : Science and Technology* (pp. 207-226). London, GBR: Earthscan.

Borba, B. S. M. C., Lucena, A. F. P., Rathmann, R., Costa, I. V. L., Nogueira, L. P. P., Rochedo, P. R. R., Schaeffer, R. (2012). Energy-related climate change mitigation in Brazil: Potential, abatement costs and associated policies. *Energy Policy, 49*, 430-441. doi:10.1016/j.enpol.2012.06.040

Brewer, C. E., Unger, R., Schmidt-Rohr, K., & Brown, R. C. (2011). Criteria to select biochars for field studies based on biochar chemical properties. BioEnergy Research, 4(4), 312-323.

Bridges, R. (2013) Design and characterisation of an 'Open Source' pyrolyser for biochar production. Massey University, Palmerston North, New Zealand.

Bridgwater, A. V. (2003). Renewable fuels and chemicals by thermal processing of biomass. *Chemical Engineering Journal, 91*(2–3), 87-102.

Brownsort, P. A. (2009). *Biomass pyrolysis processes: Review of scope, control and variability*. United Kingdom Biochar Research Centre, London, v. 1, p. 1-39..

Caco, N. (2017). Pilot scale pyrolyser: Compliance and mechanistic modeling. Massey University, Palmerston North, New Zealand.

Camps, M., Jones, J. R., Condron, L. M., Clough, T. J. (2016). Research and application of biochar in new zealand. In *Agricultural & Environmental Applications of Biochar. Advances & Barriers.* (pp. 423-444). Madison, USA. Soil Science Society of America, Special Publication 63. doi: 10.2136/sssaspecpub63.2014.0051

Cimò, G. (2014). Characterization of chemical and physical properties of biochar for energy purposes and environmental restoration. University of Parlermo, Palermo, Italy.

Chun, Y., Sheng, G., Chiou, G. T., & Xing, B. (2004). Compositions and sorptive properties of crop residue-derived chars. *Environmental Science and Technology, 38*(17), 4649-4655.

Creutzig, F., Ravindranath, N. H., Berndes, G., Bolwig, S., Bright, R., Cherubini, F., Masera, O. (2015). Bioenergy and climate change mitigation: An assessment. *GCB Bioenergy, 7*(5), 916-944. doi:10.1111/gcbb.12205

Dari, B., Nair, V. D., Harris, W. G., Nair, P. K. R., Sollenberger, L., & Mylavarapu, R. (2016). Relative influence of soil- vs. biochar properties on soil phosphorus retention. *Geoderma, 280*, 82-87. doi:10.1016/j.geoderma.2016.06.018

Demirbas, A., & Arin, G. (2002). An overview of biomass pyrolysis. *Energy sources, 24*(5), 471-482.

Di Blasi, C. (2008). Modeling chemical and physical processes of wood and biomass pyrolysis. *Progress in Energy and Combustion Science, 34*(1), 47-90.

Elyounssi, K., Blin, J., & Halim, M. (2010). High-yield charcoal production by two-step pyrolysis. *Journal of Analytical and Applied Pyrolysis, 87*(1), 138-143.

Fantozzi, F., Colantoni, S., Bartocci, P., & Desideri, U. (2007a). Rotary kiln slow pyrolysis for syngas and char production from biomass and waste - Part I: Working envelope of the reactor. *Journal of Engineering for Gas Turbines and Power, 129*(4), 901-907.

Fantozzi, F., Colantoni, S., Bartocci, P., & Desideri, U. (2007b). Rotary kiln slow pyrolysis for syngas and char production from biomass and waste - Part II: Introducing product yields in the energy balance. *Journal of Engineering for Gas Turbines and Power, 129*(4), 908-913.

FAO (Food and Agriculture Organization of the United Nations). (2017). The charcoal transition: greening the charcoal value chain to mitigate climate change and improve local Livelihoods, by J. van Dam. Rome: FAO.

Federal Register (2015). 80 224 Part II EPA 40 CFR Part 63. National Emission Standards for Hazardous Air Pollutants for Major Sources: Industrial, Commercial, and Institutional Boiler and Process Heater; Final Rule. November 20th. Available at https://www.gpo.gov/fdsys/pkg/FR-2015-11-20/pdf/2015-29186.pdf

Field, J. L., Keske, C. M. H., Birch, G. L., DeFoort, M. W., & Cotrufo, M. F. (2013). Distributed biochar and bioenergy coproduction: A regionally specific case study of environmental benefits and economic impacts. *GCB Bioenergy, 5*(2), 177-191. doi:10.1111/gcbb.12032

Fuss, S., Jones, C. D., Kraxner, F., Peters, G. P., Smith, P., Tavoni, M., Yamagata, Y. (2016). Research priorities for negative emissions. *Environmental Research Letters, 11*(11), 115007. doi:10.1088/1748-9326/11/11/115007 123

Gaskin, J. W., Steiner, C., Harris, K., Das, K. C., & Bibens, B. (2008). Effect of low-temperature pyrolysis conditions on biochar for agricultural use. *Transactions of the ASABE, 51*(6), 2061-2069.

Glaser, B., Haumaier, L., Guggenberger, G., & Zech, W. (2001). The'Terra Preta'phenomenon: a model for sustainable agriculture in the humid tropics. *Naturwissenschaften, 88*(1), 37-41.

Grieco, E., & Baldi, G. (2011). Analysis and modelling of wood pyrolysis. *Chemical Engineering Science, 66*(4), 650-660.

Guo, J., & Lua, A. C. (1998). Characterization of chars pyrolyzed from oil palm stones for the preparation of activated carbons. *Journal of Analytical and Applied Pyrolysis, 46*(2), 113-125.

H.-Y. Cai, A. J. G., I. N. Chatzakis, J.-Y. Lim, D. R. Dugwell and R. Kandiyoti. (1996). Combustion reactivity and morphological change in coal chars: effect of pyrolysis temperature, heating rate and pressure. *Fuel, 75*(1). doi:0016-2361(94)00192-1

Hayward, M. (2011). Biochar Formulation and Application to Soil Opportunities: NZ Context. Palmerston North, New Zealand.

Imam, T., & Capareda, S. (2012). Characterization of bio-oil, syn-gas and bio-char from switchgrass pyrolysis at various temperatures. *Journal of Analytical and Applied Pyrolysis, 93*(0), 170-177. doi: 10.1016/j.jaap.2011.11.010

International Biochar Initiative. (2012). Standardized Product Definition and Product Testing Guidelines for Biochar that is used in Soil. Retrieved Revision number 0.8, fromhttp://www.biocharinternational.org/sites/default/files/Guidelines_for_Biochar_That_Is_Used_in_Soil_Final.pdf

IPCC AR4 WG3 (2007), Metz, B.; Davidson, O.R.; Bosch, P.R.; Dave, R.; Meyer, L.A. (eds.). Climate Change 2007: Mitigation of Climate Change, Contribution of Working Group III to the Fourth Assessment Report of the Intergovernmental Panel on Climate Change, Cambridge University Press, ISBN 978-0-521-88011-4 (pb: 978-0-521-70598-1).

Jeffery, S., Verheijen, F. G. A., Kammann, C., & Abalos, D. (2016). Biochar effects on methane emissions from soils: A meta-analysis. *Soil Biology and Biochemistry, 101*, 251-258. doi:10.1016/j.soilbio.2016.07.021

Jones, J. R., Caco, N., Bridges, R., Ripberger, G., & Paterson, A. H. J. (2016, September). Batch pyrolysis for biochar manufacture: the compromise between emissions compliance and global warming potential. Paper presented at the Proceedings of the Chemeca conference, Adelaide.

Karhu, K., Mattila, T., Bergström, I., & Regina, K. (2011). Biochar addition to agricultural soil increased CH4 uptake and water holding capacity – Results from a short-term pilot field study. *Agriculture, Ecosystems & Environment, 140*(1-2), 309-313. doi:10.1016/j.agee.2010.12.005

Keller, K., McInerney, D., & Bradford, D. F. (2008). Carbon dioxide sequestration: how much and when? *Climatic Change, 88*(3-4), 267-291. 124

Krey, V., Luderer, G., Clarke, L., & Kriegler, E. (2013). Getting from here to there – Energy technology transformation pathways in the EMF27 scenarios. *Climatic Change, 123*(3-4), 369-382. doi:10.1007/s10584-013-0947-5

Lehmann, J., Czimczik, C., Laird, D., & Sohi, S. (2009). Stability of Biochar in the Soil. In J. Lehmann & S. Joseph (Eds.), *Biochar for Environmental Management : Science and Technology* (pp. 183-206). London, GBR: Earthscan.

Lehmann, J., Gaunt, J., & Rondon, M. (2006). Bio-char Sequestration in Terrestrial Ecosystems – A Review. *Mitigation and Adaptation Strategies for Global Change, 11*(2), 403-427. doi:10.1007/s11027-005-9006-5

Lehmann, J., & Joseph, S. (2009). Biochar for environmental management: An Introduction.

Mason, D. M., & Gandhi, K. (1980). Formulas for Calculating the Heating Value of Coal and Coal Char: Development, Test and Uses. *ACS Division of Fuel Chemistry, Preprints, 25*(3), 235-245.

McKendry, P. (2002). Energy production from biomass (part 1): overview of biomass. *Bioresource Technology, 83*(1), 37-46.

Miller, R. S., & Bellan, J. (1997). A Generalised Biomass Pyrolysis Model Based on Superimposed Cellulose, Hemicellulose and Lignin Kinetics. *Combustion Science and Technology, 126*, 97-137.

Mohan, D., Pittman Jr, C. U., & Steele, P. H. (2006). Pyrolysis of wood/biomass for bio-oil: A critical review. *Energy and Fuels, 20*(3), 848-889.

Mok, W. S. L., Antal Jr, M. J., Szabo, P., Varhegyi, G., & Zelei, B. (1992). Formation of charcoal from biomass in a sealed reactor. *Industrial and Engineering Chemistry Research, 31*(4), 1162-1166.

Mok, W. S. L., & Antal, M. J. (1983). Effects of Pressure on Biomass Pyrolysis. 2. Heats of Reaction of Cellulose Pyrolysis. *Thermochimica Acta, 68*(2-3), 165-186.

Neves, D., Thunman, H., Matos, A., Tarelho, L., & Gómez-Barea, A. (2011). Characterization and prediction of biomass pyrolysis products. *Progress in Energy and Combustion Science, 37*(5), 611-630. 125

Novak. (2009). Characterisation of Designer Biochar Produced at Different Temperatures and their Effects on a Loamy Sand *Annals of Environmental Science, 3*, 195-206.

Oasmaa, A., Peacocke, C., Gust, S., Meier, D., & McLellan, R. (2005). Norms and standards for pyrolysis liquids. End-user requirements and specifications. *Energy and Fuels, 19*(5), 2155-2163.

Onay, O. (2007). Influence of pyrolysis temperature and heating rate on the production of bio-oil and char from safflower seed by pyrolysis, using a well-swept fixed-bed reactor. *Fuel Processing Technology, 88*(5), 523-531.

Pennise, D., Smith, K., Kithinji, J., Emilia Rezende, M., Jardim Raad, T., Zhang, J., & Fan, C. (2001). Emissions of greenhouse gases and other airbone pollutants from charcoal making in Kenya and Brazil. *Journal of Geophysical Research, 106*. doi: 24143-24156. 10.1029/2000JD000041.

Preston, C. M., & Schmidt, M. W. I. (2006). Black (pyrogenic) carbon: A synthesis of current knowledge and uncertainties with special consideration of boreal regions. *Biogeosciences, 3*(4), 397-420.

Ragland, K. W., Aerts, D. J., & Baker, A. J. (1991). Properties of wood for combustion analysis. *Bioresource Technology, 37*(2), 161-168. doi: 10.1016/0960-8524(91)90205-x

Rath, J., Wolfinger, M. G., Steiner, G., Krammer, G., Barontini, F., & Cozzani, V. (2003). Heat of wood pyrolysis. *Fuel, 82*(1), 81-91.

Ripberger, Georg D; Jones, Jim R; Paterson, AHJ and Holt, Robert. (2015). Is it possible to produce biochar at different highest treatment temperatures in the pyrolysis range? - The exothermic nature of pyrolysis. In: Asia Pacific Confederation of Chemical Engineering Congress 2015: APCChE 2015, incorporating CHEMECA 2015. Melbourne: Engineers Australia, 2015: 1950-1957.

Sánchez, M. E., Lindao, E., Margaleff, D., Martínez, O., & Morán, A. (2009). Pyrolysis of agricultural residues from rape and sunflowers: Production and characterization of bio-fuels and biochar soil management. *Journal of Analytical and Applied Pyrolysis, 85*(1–2), 142-144.

Schimmelpfennig, S., & Glaser, B. (2012). One Step Forward toward Characterization: Some Important Material Properties to Distinguish Biochars. *J. Environ. Qual., 41*(4), 1001-1013. doi: 10.2134/jeq2011.0146

Shafizadeh, F., & Chin, P. P. S. (1976). Thermal Deterioration of Wood. *Abstracts of Papers of the American Chemical Society, 172*(SEP3), 37-37.

Singh, B., Singh, B. P., & Cowie, A. L. (2010). Characterisation and evaluation of biochars for their application as a soil amendment. *Australian Journal of Soil Research, 48*(6-7), 516-525.

Smith, P. (2016). Soil carbon sequestration and biochar as negative emission technologies. *Glob Chang Biol, 22*(3), 1315-1324. doi:10.1111/gcb.13178

Sparrevik, M., Adam, C., Martinsen, V., Jubaedah, & Cornelissen, G. (2015). Emissions of gases and particles from charcoal/biochar production in rural areas using medium-sized traditional and improved "retort" kilns. *Biomass and Bioenergy, 72(65-73).* doi: 10.1016/j.biombioe.2014.11.016.

Suzuki, M. (2015). Identifying roles of international institutions in clean energy technology innovation and diffusion in the developing countries: Matching barriers with roles of the institutions. Journal of Cleaner Production, 98, 229-240. doi:10.1016/j.jclepro.2014.08.070

Suzuki, M., Kanie, N., & Iguchi, M. (2016). New approaches for transitions to low fossil carbon societies: Promoting opportunities for effective development, diffusion and implementation of technologies, policies and strategies. Journal of Cleaner Production, 128, 1-5. doi:10.1016/j.jclepro.2016.04.087